

# Top Quark Mass, Parton Showers, and UV Subtraction

**Dissertation**

zur Erlangung des akademischen Grades  
Doctor rerum naturalium  
(Dr. rer. nat.)



vorgelegt

dem Fachbereich für Physik, Mathematik und Informatik  
der Johannes Gutenberg-Universität Mainz

**Robin David Baumeister**

geboren am 9. Januar 1992 in Bad Soden am Taunus

Mainz, den 3. März 2020

Robin David Baumeister  
Institut für Physik  
WA THEP  
Johannes Gutenberg-Universität Mainz  
Staudingerweg 7  
55128 Mainz

D77 / Dissertation der Johannes Gutenberg-Universität Mainz

*Für Jana.*



**ABSTRACT.** Increasing the accuracy of theoretical predictions is an ongoing task in today's high energy physics. In this thesis, we investigate two different aspects that are part of the theoretical modelling of collider events.

In the first part of this thesis, we focus on the parton shower and particularly the role of the top quark mass in the parton shower simulation. Therefore, we analyze the dependence of the peak position of the thrust distribution on the shower cutoff value. Thrust is an observable that is highly sensitive to the mass of the top quark. For our analysis, we use the dipole parton shower algorithm. We compare the outcome of our parton shower simulations to a relation of the dependence from analytic computations. These calculations are based on soft-collinear effective theory and the coherent branching formalism. We show that the result of the parton shower simulations and the analytic computation are in good agreement.

The second part of the thesis is dedicated to fixed-order calculations concerning the field of scattering amplitudes. For processes with more than two particles in the final state, one is particularly interested in computational methods that are suited for automation. One promising approach is found in loop-tree duality combined with numerical loop integration. In the loop-tree duality method at next-to-next-to-leading order, one encounters two-loop diagrams that have a one-loop self-energy insertion on one of the internal lines of the outer loop. This leads to Feynman integrals with raised propagators, i.e. propagators with higher powers. For calculations in the loop-tree duality approach, one needs to calculate the residue for the case that a raised propagator goes on-shell. This calculation involves the calculation of derivatives and is, hence, process-dependent. We show that it is possible to construct ultraviolet counterterms at the integrand level that make the residues vanish in the on-shell scheme. This relocates the problem of raised propagators to a process-independent part of the calculation. Additionally, we provide suitable forms of these counterterms for scalar  $\phi^3$ -theory and QCD.



**ZUSAMMENFASSUNG.** Eine Aufgabe der modernen Hochenergiephysik ist, die Genauigkeit theoretischer Vorhersagen zu erhöhen. In dieser Dissertation untersuchen wir zwei unterschiedliche Aspekte der theoretischen Modellierung von Collider-Events.

Im ersten Teil der Thesis konzentrieren wir uns auf den Partonshower, insbesondere auf die Rolle der Masse des Top-Quarks in Partonshower-Simulationen. Hierfür analysieren wir die Abhängigkeit der Lage des Maximums der Thrust-Verteilung vom Wert des Showercutoffs. Thrust ist eine Observable, die stark von der Masse des Top-Quarks abhängt. Für unsere Analyse verwenden wir den Dipole-Partonshower-Algorithmus. Wir vergleichen das Resultat unserer Partonshower-Simulationen mit einer analytisch hergeleiteten Formel für die Beziehung zwischen dem Wert des Thrust-Maximums und dem Showercutoff. Die analytische Betrachtung basiert auf der Soft-Collinear-Effective-Theory und dem Coherent-Branching-Formalismus. Wir zeigen, dass das Ergebnis unserer Partonshower-Simulationen mit den Vorhersagen der analytischen Herangehensweise übereinstimmt.

Im zweiten Teil der Thesis widmen wir uns Fixed-Order-Berechnungen im Bereich der Streuamplituden. Für Prozesse mit mehr als zwei Teilchen im Endzustand ist man vorallem an Methoden interessiert, die sich automatisieren lassen. Einen vielversprechenden Ansatz bietet Loop-Tree-Duality kombiniert mit numerischer Loop-Integration. In der Loop-Tree-Duality-Methode in nächst-zunächstführender Ordnung begegnen einem Zwei-Loop-Diagramme, bei denen ein Ein-Loop-Selbstenergiendiagramm auf einer internen Linie des äußeren Loops eingefügt ist. Dies führt zu Feynmanintegralen mit erhöhten Propagatoren, also Propagatoren mit höheren Exponenten. Für Berechnungen im Loop-Tree-Duality-Approach ist es notwendig, die Residuen für den Fall zu berechnen, dass ein erhöhter Propagator on-shell geht. Hierbei müssen Ableitungen berechnet werden. Außerdem ist die Berechnung vom betrachteten Prozess abhängig. Wir zeigen, dass es möglich ist, Ultraviolett-Counterterme auf der Ebene des Integranden zu konstruieren, die die Residuen im On-Shell-Schema verschwinden lassen. Diese Vorgehensweise verlagert das Problem der erhöhten Propagatoren in einen prozessunabhängigen Teil der Berechnung. Zusätzlich bieten wir explizite Darstellungen der Counterterme für die skalare  $\phi^3$ -Theorie und QCD.





## Contents

<b>Part 1. Introduction and Basics</b>	<b>1</b>
Chapter 1. Introduction	3
Chapter 2. Quantum Chromodynamics	7
2.1. The Color Group $SU(3)$	8
2.2. The Lagrangian of Quantum Chromodynamics	10
2.3. Feynman Rules	12
2.4. Perturbative QCD	15
2.5. Mass Renormalization	20
<b>Part 2. The Top Quark Mass in Parton Showers</b>	<b>31</b>
Chapter 3. NLO Computations and Dipole Subtraction	33
3.1. The Structure of NLO Computations	34
3.2. Dipole Subtraction – General Overview	37
3.3. Dipole for Colorless Initial State	41
Chapter 4. Parton Showers	49
4.1. From Evolution Equation to Parton Branching	50
4.2. The Dipole Parton Shower	56
Chapter 5. The Top Quark Mass in the Dipole Shower	63
5.1. General Considerations	64
5.2. Analytic Computations	68
5.3. Analyses and Results	78
<b>Part 3. UV Subtraction Terms for Self-Energy Corrections</b>	<b>85</b>
Chapter 6. UV Subtraction Terms at One-Loop	87
6.1. Motivation and a Toy Example	88
6.2. Subtraction Terms for $\phi^3$ -Theory	93

6.3. Subtraction Terms for QCD	101
<b>Part 4. Conclusions and Outlook</b>	<b>109</b>
Chapter 7. Conclusions and Outlook	111
<b>Part 5. Appendix</b>	<b>117</b>
Appendix A. Quantum Chromodynamics	119
A.1. QCD Feynman Rules	119
A.2. Formulae for the Implementation of $\alpha_s$	120
Appendix B. Parton Showers	123
B.1. Lorentz Transformations	123
Bibliography	125

## **Part 1**

# **Introduction and Basics**



## CHAPTER 1

### Introduction

In a world where the precision of experiments in high energy physics is steadily increasing, the continual improvement of theoretical predictions becomes inevitable. One example of the big machines that produce huge amounts of experimental data, that need to be analyzed, is the Large Hadron Collider (LHC) at CERN.

These collider experiments are not only important for the search of new physics but particularly for the validation of existing theories and the examination of their fundamental parameters.

The Standard Model (SM) of particle physics is the current state-of-the-art quantum field theory (QFT) when it comes to describing the fundamental particles and their interactions. The SM is based upon the gauge groups  $SU_c(3)$ ,  $SU_L(2)$ , and  $U_Y(1)$ , where the corresponding charges are the color charge, the weak isospin, and the weak hypercharge, respectively.

The weak interaction and the theory of electromagnetism, quantum electrodynamics (QED), can be summarized in the theory of the electroweak interaction with the underlying gauge group  $SU_L(2) \times U_Y(1)$ . On the other hand, the QFT that describes the strong interaction of quarks and gluons is called quantum chromodynamics (QCD). QCD is a renormalizable non-abelian gauge theory that is based upon the gauge group  $SU(3)$ . In this thesis, we mostly focus on events involving QCD.

Using the fundamentals of QFT, it is possible to compute hard scattering events via Feynman diagrams, using perturbation theory. However, in practice, this approach is limited to a small number of particles in the final state. This does not fully represent the situation found in particle colliders. In the “real world” of the experiment, the hard scattering is just the beginning.

The particles that are produced in the hard event radiate additional particles that may form jets. Additionally, confinement states that color charged particles cannot individually exist in nature but only in bound hadronic states.

Lastly, the hadrons themselves may decay. The resulting particles and jets are measured in the detector of the experiment.

It is up to the theorist to model the described behavior inside the collider experiment in order to make useful predictions. As already mentioned, the hard scattering event can be calculated using fixed-order perturbation theory. After this computation, the parton shower is applied. The parton shower algorithm provides a way to model the radiation of soft and collinear particles off the final-state particles from the hard event.

After the parton shower evolution from the scale of the hard event down to a cutoff scale, hadronization and decay models can be applied. Additionally, the involved particles can be clustered to jets for a more accurate description of the situation inside the detector. There exist computer programs that generate events based on all of these steps. They are called Monte Carlo (MC) event generators. Some of the most commonly used general-purpose event generators are HERWIG [1–4], PYTHIA [5, 6], and SHERPA [7, 8].

The outcome of an MC event generator forms the basis of the template method that makes use of the theoretical predictions to obtain knowledge of parameters of the SM from experimental data.

One of the fundamental parameters of the SM, for whose measurement direct reconstruction via the template method is used, is the mass of the top quark  $m_t$ . With a mass of around 173 GeV, the top quark is by far the heaviest elementary particle in the SM. As such, the knowledge of the value of its mass has a huge impact on our understanding of the SM.

However, until today, the connection between the top mass parameter obtained from direct reconstruction using an MC event generator and the quantum field theoretical top quark mass inside a renormalization scheme is not sufficiently understood. In this context, an important question to ask is how the top quark mass inside a specific MC generator depends on certain parameters of the implemented parton shower simulation.

A first step in this direction has been made in [9]. Here, they analyzed the cutoff dependence of an observable that is highly sensitive to the top quark mass.

We address this question in Chapter 5. There, we analyze the dependence of the peak position of the thrust observable on the value of the shower cutoff. For the parton shower simulations we use an implementation of the so-called dipole shower [10].

We compare our findings to the analytical predictions of [9] and find them to be in good agreement. From this analysis, it is possible to deduce information about the cutoff dependence of the top quark mass.

Considering fixed-order calculations, the urge for high precision predictions requires next-to-next-to-leading order (NNLO) calculations. When the number of final-state particles exceeds two, one is interested in methods that can be automated. One promising approach is the so-called loop-tree duality combined with numerical loop integration.

One problem that arises in this method is the calculation of higher order residues that involves derivatives. This situation occurs for two-loop diagrams with a self-energy insertion on an internal line. We show that this problem can be solved by constructing a counterterm on an integrand level that makes the residue vanish.

This thesis is organized as follows:

In the next chapter, we recapitulate some important features of QCD that are essential for the understanding of the studies carried out in Part 2 and 3. These concepts include the QCD Lagrangian and the derivation of Feynman rules from it, the fundamentals of perturbative QCD, and renormalization.

In Chapter 3, we consider the Catani–Seymour dipole subtraction method that is used to cancel infrared (IR) divergences in next-to-leading order (NLO) computations. The basis of this subtraction scheme is formed by dipoles that also build the foundation of the parton shower algorithm based on Catani–Seymour dipoles.

The general ideas behind the concept of parton showers are subject of Chapter 4. Additionally, we describe the main features and the practical implementation of the parton shower algorithm based on Catani–Seymour dipoles.

Chapter 5 is dedicated to the role of the top quark mass in high energy physics in general and particularly its role in a parton shower. We start with a section on general properties of the top quark mass and the subtleties of its determination. This is followed by an overview of the analytic computations carried out in [9], quantifying a relation between the peak position of the thrust observable and the value of the cutoff parameter in parton shower simulations.

In Section 5.3, we present our analysis of the thrust peak position's dependence on the shower cutoff, using an implementation of the dipole shower. Additionally, we show our results, that agree with the analytic computations.

In Chapter 6 we provide a solution for the problem of raised propagators due to self-energy insertions in the loop-tree duality approach. This problem is accompanied with the calculation of higher order residues. We show that it is possible to find a counterterm to the one-loop self-energy insertion on the integrand level that makes the residue vanish. In addition, we provide a representation of these counterterms for scalar  $\phi^3$ -theory and QCD. The results of this chapter have been published in [11].

In the appendix we provide the Feynman rules for QCD, a set of formulae that are needed for the implementation of the running coupling of QCD and Lorentz transformations that are essential for the dipole shower algorithm.

We note that we use natural units for all calculations throughout this thesis, setting  $\hbar = c = 1$ .



## CHAPTER 2

# Quantum Chromodynamics

## Contents

---

<b>2.1. The Color Group <math>SU(3)</math></b>	<b>8</b>
<b>2.2. The Lagrangian of Quantum Chromodynamics</b>	<b>10</b>
<b>2.3. Feynman Rules</b>	<b>12</b>
2.3.1. Feynman Rule for the Propagator	12
2.3.2. Feynman Rules for the Vertices	13
2.3.3. Feynman Rules for $\phi^3$ -Theory	14
2.3.4. Feynman Rules for QCD	15
<b>2.4. Perturbative QCD</b>	<b>15</b>
2.4.1. QCD Beta Function	16
2.4.2. Observables in Perturbative QCD	17
<b>2.5. Mass Renormalization</b>	<b>20</b>
2.5.1. The Quark Self-Energy	21
2.5.2. Renormalization	25
2.5.3. Renormalization Schemes	26
2.5.4. Pole Mass Renormalon Ambiguity	29

---

In the following sections, we give a summary of the aspects of QCD that are essential for later discussions. We start with the description of the color group  $SU(3)$ , followed by the Lagrangian of QCD. After that, we give a short interlude on how to derive Feynman rules for a theory given the corresponding Lagrangian. This leads to the important topic of perturbative QCD where the Feynman rules are used to derive mathematical formulations for the calculation of scattering amplitudes from Feynman diagrams. Last but not least, the task of renormalization, especially mass renormalization, will be covered which will play a crucial role in the second part of this thesis.

There are many excellent textbooks on QCD. Wide parts of this chapter follow the descriptions in [12–14], and we recommend these books for a more detailed description of the topics covered in this chapter.

### 2.1. THE COLOR GROUP $SU(3)$

All hadronic matter consists of quarks. QCD is the theory of quarks and the associated gauge boson, the gluon. The SM contains six different kinds of quarks and their corresponding antiparticles. The different kinds are also referred to as *flavors*. The individual flavors differ in their masses, electric charge, isospin, and other quantum numbers. A list of the six different quark flavors and some of their properties can be found in Table 2.1.

Name	Symbol	Charge (e)	Mass
Up	u	+2/3	$\sim 2.16$ MeV
Down	d	-1/3	$\sim 4.67$ MeV
Charm	c	+2/3	$\sim 1.27$ GeV
Strange	s	-1/3	$\sim 93$ MeV
Top	t	+2/3	$\sim 172.9$ GeV
Bottom	b	-1/3	$\sim 4.18$ GeV

TABLE 2.1. The six quark flavors with electric charges and masses [15]. The masses of the light quarks (u, d, s) are estimates of the current quark masses in the  $\overline{\text{MS}}$  scheme at  $\mu \approx 2$  GeV. The c and b masses are given in the  $\overline{\text{MS}}$  scheme. The top quark mass is the mass obtained from direct reconstruction.

In addition, every quark carries another degree of freedom, the color index  $a = 1, 2, 3$ .

In QED, the quantum field theory of the electromagnetic force, the corresponding gauge boson, i.e. the photon, does not carry any electric charge. In contrast, the gauge boson of QCD, the gluon, carries a color charge. Therefore, gluons can interact with other gluons. The color charge of a gluon is composed of a combination of the three colors and their corresponding anticolors. From group theory, it follows that the combination of the two color triplets lead to a color singlet and a color octet. Hence, a gluon can carry one of eight different types of color charge. This coincides with the underlying structure of the  $SU(3)$  color group of QCD.

The generators  $t^A$  of the fundamental representation of  $SU(3)$  are chosen to be proportional to the Gell-Mann matrices  $\lambda^A$ :

$$(2.1) \quad t^A = \frac{1}{2} \lambda^A, \quad \text{with } A = 1, \dots, 8.$$

Notice that there are eight generators corresponding to the eight colors a gluon can carry.

Let us denote the matrices of the adjoint representation by  $T^A$ . Their definition is given by

$$(2.2) \quad (T^A)^{BC} := -i f^{ABC}$$

Then, the following relations for the commutators of the generating matrices hold

$$(2.3) \quad \begin{aligned} [t^A, t^B] &= i f^{ABC} t^C, \\ [T^A, T^B] &= i f^{ABC} T^C, \end{aligned}$$

where  $i$  denotes the imaginary unit and  $f^{ABC}$  ( $A, B, C = 1, \dots, 8$ ) the antisymmetric structure constants of  $SU(3)$ . Since  $f^{ABC} \neq 0$ , the generators  $t^A$  form a non-abelian Lie algebra.

The choice of the generators yields the normalization

$$(2.4) \quad \text{Tr}(t^A t^B) = \frac{1}{2} \delta^{AB}.$$

Additionally, we find some useful relations for the color algebra involving the Casimir operators  $C_F$ ,  $C_A$ , and  $T_R$ :

$$(2.5) \quad \sum_A t_{ab}^A t_{bc}^A = C_F \delta_{ac},$$

with  $C_F = (N_c^2 - 1)/(2N_c)$  for the general group  $SU(N_c)$ . Hence, we have  $C_F = 4/3$  for  $SU(3)$ . The color-factor  $C_F$  is associated with a quark emitting a gluon.

$$(2.6) \quad \text{Tr}(T^C T^D) = \sum_{A,B} f^{ABC} f^{ABD} = C_A \delta^{CD},$$

with  $C_A = N_c = 3$ , which can be associated with a gluon emitting another gluon.

Finally,

$$(2.7) \quad t_{ab}^A t_{ba}^B = T_R \delta^{AB},$$

where  $T_R = 1/2$  is associated with the splitting of a gluon into a pair of a quark and an antiquark.

After this short excursion to the group theoretical foundations of QCD in the form of the special unitarity group  $SU(3)$ , we have a look at the physical aspects of QCD, i.e. its Lagrangian, and how to derive Feynman rules from it.

## 2.2. THE LAGRANGIAN OF QUANTUM CHROMODYNAMICS

The gauge theory that is based on the Lie group  $SU(N)$ , without fermions, is Yang–Mills theory. Hence, it is the preferred theory to describe the interactions of the elementary particles in the SM.

Let us start with the Lagrangian for the gauge field of QCD ( $SU(3)$ ), i.e. the gluon field. Remember that we use the conventions of (2.3) and (2.4) for the color matrices. We denote the gluon field by  $A_\mu^A(x)$ .

Then, the Yang–Mills Lagrange density for the gluon field reads

$$(2.8) \quad \mathcal{L}_G = -\frac{1}{4} F_{\mu\nu}^A F^{A,\mu\nu},$$

with the field strength tensor

$$(2.9) \quad F_{\mu\nu}^A = [\partial_\mu A_\nu^A - \partial_\nu A_\mu^A - g_s f^{ABC} A_\mu^B A_\nu^C],$$

where  $g_s$  is the coupling of the strong interaction.

In addition to the Lagrangian for the gluon field (2.8), we need a term to describe the fields of the different quarks. The corresponding Lagrange density is given by

$$(2.10) \quad \mathcal{L}_Q = \sum_{\text{flavors}} \bar{q}_a (i\not{D} - m_q)_{ab} q_b.$$

The slashed notation of  $\not{D}$  is an abbreviation for  $\gamma_\mu D^\mu$ , where  $\gamma_\mu$  are the gamma matrices, satisfying the anticommutation relations

$$(2.11) \quad \{\gamma^\mu, \gamma^\nu\} = 2g^{\mu\nu},$$

with the metric tensor  $g^{\mu\nu} = \text{diag}(1, -1, -1, -1)$ .

The covariant derivative in (2.10) is given by

$$(2.12) \quad (D_\mu)_{ab} = \partial_\mu \delta_{ab} + i g_s (t^C A_\mu^C)_{ab}.$$

The QCD Lagrangian is invariant under the transformation

$$(2.13) \quad t^A A_\mu^A(x) \rightarrow U(x) \left( t^A A_\mu^A(x) + \frac{i}{g_s} \right) U^\dagger(x),$$

with

$$(2.14) \quad U(x) = \exp(-i t^A \theta_A(x)).$$

If one wants to compute Feynman rules for the QCD Lagrangian, it is required to perform gauge fixing. This step is necessary because of the invariance of the Lagrangian under gauge transformations (2.13). The calculations of the gauge-fixing can be found in Section 2.3 of [16]. Here, we want to present the resulting gauge-fixing term in covariant gauge which needs to be added to the Lagrangian

$$(2.15) \quad \mathcal{L}_{\text{GF}} = -\frac{1}{2\xi} (\partial^\mu A_\mu^A)(\partial^\nu A_\nu^A).$$

One is free to choose the gauge-fixing parameter  $\xi$  in order to fix the gauge. A common choice is the Feynman gauge, corresponding to  $\xi = 1$ , which will be used mostly throughout this thesis.

Lastly, there is another term which has to be added to the QCD Lagrangian: the Lagrangian of the Fadeev–Popov ghosts which is given by

$$(2.16) \quad \mathcal{L}_{\text{FP}} = (\partial_\mu \bar{c}^A)(\delta^{AC} \partial_\mu + g_s f^{ABC} A_\mu^B) c^C.$$

Here,  $c^A$  and  $\bar{c}^A$  are the Fadeev–Popov ghosts and antighosts. The Fadeev–Popov terms are necessary because the integration over all paths in the path integral formalism leads to a double counting of paths that are equivalent in terms of gauge ambiguities. To counter these multiple countings, the Fadeev–Popov ghosts have to be introduced. Since these are virtual particles that arise in loops, i.e. unphysical particles that do not exist in nature, the Fadeev–Popov term is only relevant beyond tree-level.

Putting the pieces together, we find the full Lagrangian of QCD as

$$(2.17) \quad \begin{aligned} \mathcal{L}_{\text{QCD}} = & -\frac{1}{4} F_{\mu\nu}^A F^{A,\mu\nu} + \sum_{\text{flavors}} \bar{q}_a (i\not{D} - m_q)_{ab} q_b \\ & - \frac{1}{2\xi} (\partial^\mu A_\mu^A)(\partial^\nu A_\nu^A) + (\partial_\mu \bar{c}^A)(\delta^{AC} \partial_\mu + g_s f^{ABC} A_\mu^B) c^C. \end{aligned}$$

Using this Lagrange density, we are able to derive the Feynman rules for quantum chromodynamics.

### 2.3. FEYNMAN RULES

In this section, we present a recipe to derive the Feynman rules for a theory given its Lagrange density. The depiction of the Feynman rule derivation closely follows Section 2.4 of [16]. We will only give a useful recipe for deriving the Feynman rules and do not cover the exact method of how to derive the recipe itself. These crucial details are part of most textbooks on QFT as for example [13, 14].

The first step towards the derivation of Feynman rules for a given Lagrangian is to order its terms by the number of fields. We can, then, write the Lagrangian as a sum of terms, each having the same number of fields as

$$(2.18) \quad \mathcal{L} = \mathcal{L}^{(2)} + \mathcal{L}^{(3)} + \mathcal{L}^{(4)} + \dots$$

The superscripts denote the number of fields in the corresponding term of the Lagrangian. A physical Lagrangian does not contain terms with just one or even no field. In addition, we have to assume that every field vanishes at infinity such that the boundary terms in partial integration are zero.

#### 2.3.1. Feynman Rule for the Propagator

From the first term in (2.18), i.e. the one that is bilinear in the fields, the Feynman rule for the propagator can be derived. First, the term has to be ordered such that it has the form

$$(2.19) \quad \mathcal{L}^{(2)}(x) = \frac{1}{2} \phi_i(x) P_{ij}(x) \phi_j.$$

Here,  $P_{ij}$  is a real operator that is symmetric and invertable. Note that it can also contain derivatives. In this case, we consider real boson fields  $\phi_i$ , but the statements are also true for other fields, e.g. gauge fields or fermion fields.

Next, we define the inverse of  $P_{ij}$  by

$$(2.20) \quad \sum_j P_{ij}(x) P_{jk}^{-1}(x-y) = \delta_{ik} \delta^4(x-y).$$

The Fourier transform of the inverse is given by

$$(2.21) \quad P_{ij}^{-1}(x) = \int \frac{d^4p}{(2\pi)^4} e^{-ip \cdot x} \tilde{P}_{ij}^{-1}(p).$$

Finally, we obtain the propagator by the Fourier transform of the inverse transformed to momentum space with a prefactor  $i$

$$(2.22) \quad \Delta_F(p)_{ij} = i\tilde{P}_{ij}^{-1}(p).$$

### 2.3.2. Feynman Rules for the Vertices

The Feynman rules for the vertices describe the interaction between different particles. To derive the Feynman rules, we start by ordering the interaction term in a way similar to (2.19)

$$(2.23) \quad \mathcal{L}^{(n)}(x) = O_{i_1 \dots i_n}(\partial_1, \dots, \partial_n) \phi_{i_1}(x) \dots \phi_{i_n}(x),$$

where  $O$  is an operator that may also contain derivatives.

The notation for the partial derivative,  $\partial_j$ , means that it is only applied to the  $j$ -th field  $\phi_{i_j}(x)$ .

Using the formulae for the Fourier transforms of each field

$$(2.24) \quad \begin{aligned} \phi_i(x) &= \int \frac{d^D p}{(2\pi)^D} e^{-ip \cdot x} \tilde{\phi}_i(p), \\ \tilde{\phi}_i(p) &= \int d^D x e^{ip \cdot x} \phi_i(x), \end{aligned}$$

with  $p$  an incoming momentum, we can rewrite the interaction term (2.23) as

$$(2.25) \quad \begin{aligned} \mathcal{L}^{(n)}(x) &= \int \frac{d^D p_1}{(2\pi)^D} \dots \int \frac{d^D p_n}{(2\pi)^D} e^{-i(p_1 + \dots + p_n) \cdot x} \\ &\quad \times O_{i_1 \dots i_n}(-ip_1, \dots, -ip_n) \tilde{\phi}_{i_1}(p_1) \dots \tilde{\phi}_{i_n}(p_n). \end{aligned}$$

Replacing  $p_j$  by  $-p_j$ , i.e. switching from incoming to outgoing momenta, we obtain the vertex as

$$(2.26) \quad V = i \sum_{\text{permutations}} (-1)^{P_F} O_{i_1 \dots i_n}(ip_1, \dots, ip_n).$$

In this vertex, all momenta are outgoing. With the sum over all permutations, we mean all permutations of momenta and indices of identical particles.  $P_F$  gives the number of permutations over identical fermions. Thus, the whole vertex gets an overall minus sign for an odd number of fermion permutations.

2.3.3. *Feynman Rules for  $\phi^3$ -Theory*

As a simple example, we want to apply the recipe to  $\phi^3$ -theory to derive its Feynman rules. The Lagrangian of  $\phi^3$ -theory, without counterterms, reads

$$(2.27) \quad \mathcal{L} = \frac{1}{2}(\partial_\mu\phi)(\partial^\mu\phi) - \frac{1}{2}m^2\phi^2 + \frac{1}{3!}\lambda\phi^3.$$

The part of the Lagrangian bilinear in the fields can be written as in (2.19)

$$(2.28) \quad \mathcal{L}^{(2)}(x) = -\frac{1}{2}\phi(x)(\partial_\mu\partial^\mu + m^2)\phi(x).$$

Hence, we find

$$(2.29) \quad P(x) = -(\partial_\mu\partial^\mu + m^2),$$

and with (2.20)

$$(2.30) \quad P(x)P^{-1}(x-y) = -(\partial_\mu\partial^\mu + m^2)P^{-1}(x-y) \stackrel{!}{=} \delta^4(x-y).$$

Applying the Fourier transform to both sides, with  $\partial_\mu \rightarrow -ip_\mu$ , for both sides we obtain

$$(2.31) \quad \int \frac{d^4p}{(2\pi)^4} e^{-ip\cdot(x-y)}(p^2 - m^2) \tilde{P}^{-1}(p) \stackrel{!}{=} \int \frac{d^4p}{(2\pi)^4} e^{-ip\cdot(x-y)}.$$

The propagator is, therefore, given by

$$(2.32) \quad \Delta_F(p) = i\tilde{P}^{-1}(p) = \frac{i}{p^2 - m^2 + i\varepsilon}.$$

Here, the term  $i\varepsilon$  is a shortcut that is commonly used to imply the time ordering of the two-point function (see for example [13]).

For the interaction part of the Lagrangian we have

$$(2.33) \quad \mathcal{L}^{(3)} = \frac{1}{3!}\lambda\phi^3,$$

and, hence,

$$(2.34) \quad O(\partial_\mu) = O(-ip_\mu) = \frac{1}{3!}\lambda.$$

Using (2.26), we find the Feynman rule for the vertex

$$(2.35) \quad V = i \sum_{\text{permutations}} \frac{1}{3!}\lambda = i\lambda.$$



## 2.3.4. Feynman Rules for QCD

As an example, we present the derivation of the Feynman rule for the gluon propagator. The full set of Feynman rules for QCD can be found in Appendix A.1.

Recall from (2.17) that the part of the Lagrangian bilinear in the gluon fields  $A_\mu^A(x)$  reads

$$(2.36) \quad \mathcal{L}_{\text{gluons}}^{(2)} = \frac{1}{2} A_\mu^A(x) \left[ \partial_\rho \partial^\rho g^{\mu\nu} \delta^{AB} - \left(1 - \frac{1}{\xi}\right) \partial^\mu \partial^\nu \delta^{AB} \right] A_\nu^B.$$

Thus, the operator  $P(x)$  is given by

$$(2.37) \quad P^{\mu\nu,AB}(x) = \partial_\rho \partial^\rho g^{\mu\nu} \delta^{AB} - \left(1 - \frac{1}{\xi}\right) \partial^\mu \partial^\nu \delta^{AB}.$$

Consulting (2.20), we find

$$(2.38) \quad \left[ \partial_\rho \partial^\rho g^{\mu\sigma} \delta^{AC} - \left(1 - \frac{1}{\xi}\right) \partial^\mu \partial^\sigma \delta^{AC} \right] (P^{-1})_{\sigma\nu}^{CB}(x-y) \stackrel{!}{=} g^\mu{}_\nu \delta^{AB} \delta^4(x-y),$$

which has to be transformed to momentum space. The Fourier transformation on both sides yields

$$(2.39) \quad \int \frac{d^4 p}{(2\pi)^4} e^{-i p \cdot (x-y)} \left[ -p^2 g^{\mu\sigma} \delta^{AC} + \left(1 - \frac{1}{\xi}\right) p^\mu p^\sigma \delta^{AC} \right] \\ \times (P^{-1})_{\sigma\nu}^{CB}(p) \stackrel{!}{=} \int \frac{d^4 p}{(2\pi)^4} e^{-i p \cdot (x-y)} g^\mu{}_\nu \delta^{AB}.$$

Comparing both sides gives us the propagator for the gluon (2.22)

$$(2.40) \quad \Delta_F(p)_{\mu\nu}^{AB} = i (P^{-1})_{\mu\nu}^{AB}(p) = \frac{i}{p^2} \left( -g_{\mu\nu} + (1 - \xi) \frac{p_\mu p_\nu}{p^2} \right) \delta^{AB}.$$

## 2.4. PERTURBATIVE QCD

Using the QCD Feynman rules derived in Section 2.3, we are now able to calculate predictions for observables using perturbative expansions in the coupling  $g_s$ , or rather  $\alpha_s := \frac{g_s^2}{4\pi}$ .

### 2.4.1. QCD Beta Function

Before we start with the basics of perturbative computations in QCD, let us take a closer look at the strong coupling  $\alpha_s(\mu)$ , i.e. its corresponding beta function, and the concept of asymptotic freedom. Notice that the coupling depends on an unphysical renormalization scale  $\mu$ .

The fact that the beta function of a non-abelian gauge theory can be negative was first shown by Politzer, Wilczek, and Gross [17–19]. Since the gauge group of QCD,  $SU(3)$ , is non-abelian (see Section 2.1), the statement of negativity, in fact, holds for the beta function of QCD.

The renormalization group equation (RGE) of  $\alpha_s(\mu)$  with respect to the renormalization scale  $\mu$  defines the QCD beta function:

$$(2.41) \quad \beta(\alpha_s(\mu)) := \frac{d\alpha_s(\mu)}{d \log(\mu)} = -2\alpha_s(\mu) \sum_{n=0}^{\infty} \beta_n \left( \frac{\alpha_s(\mu)}{4\pi} \right)^{n+1}.$$

The coefficients  $\beta_n$  are known up to five-loop order [20–24]. The first three coefficients read

$$(2.42) \quad \begin{aligned} \beta_0 &= \frac{11}{3}C_A - \frac{3}{4}T_R n_f, \\ \beta_1 &= \frac{34}{3}C_A^2 - \frac{20}{3}C_A T_R n_f - 4C_F T_R n_f, \\ \beta_2 &= \frac{325}{54}n_f^2 - \frac{5033}{18}n_f + \frac{2857}{2}, \end{aligned}$$

with the number of active quark flavors  $n_f$  and the Casimir operators  $C_F$ ,  $C_A$ , and  $T_R$  known from Section 2.1. The two missing coefficients  $\beta_3$  and  $\beta_4$  can be found in [22].

The minus sign on the right-hand side of (2.41) indicates that the value of the strong coupling decreases when going to higher energies. This is contrary to the behavior of the QED coupling which increases for higher energies. Theories with this property are called infrared free. Theories with the opposite behavior, such as QCD, are called asymptotically free.

The term asymptotic freedom arises from the fact that the strong coupling goes to zero for short distances, i.e. for high energies. At low energies,  $\alpha_s$  is so strong that the partons of QCD, i.e. quarks and gluons, cannot be observed as single particles but as bound states, so-called hadrons. This behavior of quarks and gluons at low energies is known as color confinement.

Asymptotic freedom allows us to calculate observables in QCD perturbatively at high energies way above the QCD scale  $\Lambda_{\text{QCD}}$ , i.e. the location of the Landau pole of the running of the strong coupling. In the  $\overline{\text{MS}}$  scheme (cf. Section 2.5) its world average values at four-loop order are

$$(2.43) \quad \begin{aligned} \Lambda_{\text{QCD}}^{(6)} &= (89 \pm 6) \text{ MeV}, \\ \Lambda_{\text{QCD}}^{(5)} &= (210 \pm 14) \text{ MeV}, \\ \Lambda_{\text{QCD}}^{(4)} &= (292 \pm 16) \text{ MeV}, \\ \Lambda_{\text{QCD}}^{(3)} &= (332 \pm 17) \text{ MeV}, \end{aligned}$$

where the superscript denotes the number  $n_f$  of active quark flavors [15].

Knowing the QCD scale, there exists a solution to the renormalization group equation (2.41) at one-loop order

$$(2.44) \quad \alpha_s(\mu) = \frac{2\pi}{\beta_0} \frac{1}{\log\left(\frac{\mu}{\Lambda_{\text{QCD}}}\right)}.$$

If a solution for the RGE at higher orders is desired, a perturbative expansion around the leading-order solution provides a good approximation (cf. [13] p. 528). Additionally, an expansion of  $\alpha_s(\mu)$  around a reference value at some fixed scale  $\mu_0$ , e.g. the Z-Boson's mass  $m_Z$ , can be used. This is particularly helpful for an implementation into a computer program. A plot for two different approximating implementations for the running of the strong coupling at first order can be found in Figure 2.1. For the corresponding formulae, see Appendix A.2. For the implementation of  $\alpha_s(\mu)$  in Figure 2.1, we used the mass of the Z-Boson,  $m_Z = 91.1876$  GeV, as reference scale with the corresponding value of the strong coupling,  $\alpha_s(m_Z) = 0.118$ . It is apparent that the two implementations differ in their asymptotic behavior when approaching  $\mu = 0$ . The ratio of the two implementations is depicted in the lower panel of Figure 2.1. However, this has no major implications on our analyses throughout this thesis. In practice, the RGE can be solved numerically at a fixed order for exact results.

#### 2.4.2. Observables in Perturbative QCD

Using the strong coupling constant, we can compute observables through their perturbative expansion in  $\alpha_s$ . Before looking at observables, let us start with some remarks on calculating cross sections. Asymptotic freedom allows us to

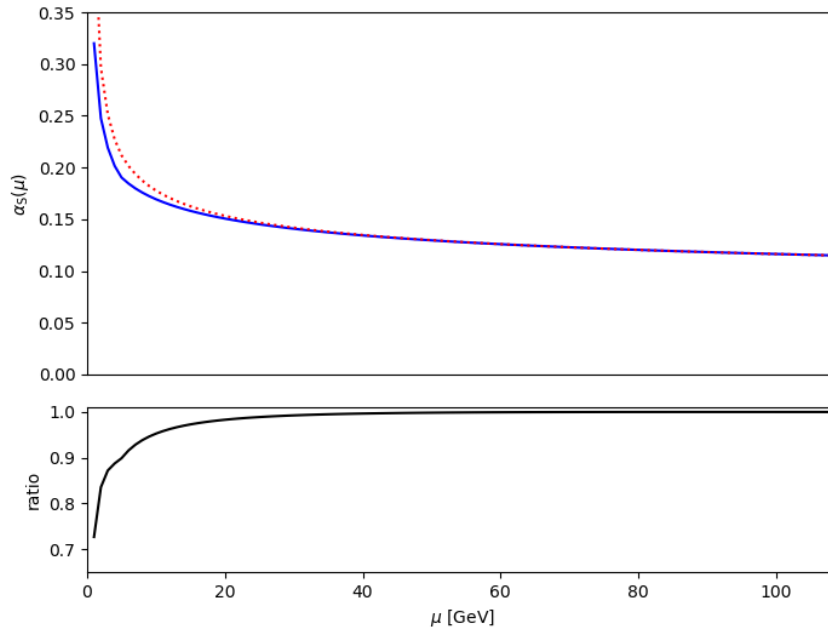


FIGURE 2.1. The running of the strong coupling  $\alpha_s(\mu)$  at two-loop order for two different approximations (upper figure). The blue solid line represents an implementation of (A.1), while we used (A.4) for plotting the dotted red line. The lower panel shows the ratio of both implementations

calculate a certain process in QCD perturbatively, i.e. use a series in  $\alpha_s$  where each term corresponds to a set of Feynman diagrams.

In most cases, the leading order (LO), or Born level, amplitude can be calculated using tree-level diagrams. One-loop diagrams together with real corrections provide the formulae for NLO computations (cf. Section 3.1). Summing up all partial amplitudes of all orders would provide the exact result for a certain process. Since this is not feasible, for it would take infinite computing time, state-of-the-art calculations rarely go beyond NNLO accuracy. Another complication that arises when going to higher orders, besides the rapidly increasing number of diagrams, are infrared divergences (see Section 3.1).

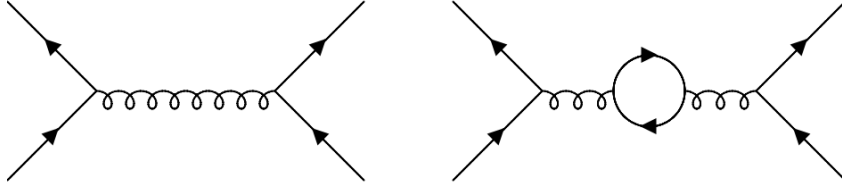


FIGURE 2.2. Examples of a tree-level diagram (left) and a one-loop diagram (right) for a  $2 \rightarrow 2$  scattering process.

Speaking of a typical QCD observable  $O(y)$ , dependent on a variable  $y$ , we encounter a perturbative expansion of the form

$$(2.45) \quad O(y) = \sum_{n=1} \left( \frac{\alpha_s}{2\pi} \right)^n A_n(y),$$

with

$$(2.46) \quad A_n(y) = \sum_{j=0}^{2n} a_{nj} \log^j(y) + \text{power corrections}.$$

Here,  $a_{nj}$  are the coefficients of the expansion of  $O(y)$ . Considering only the first two orders yields

$$(2.47) \quad O(y) = \frac{\alpha_s}{2\pi} A_1(y) + \left( \frac{\alpha_s}{2\pi} \right)^2 A_2(y) + \mathcal{O}(\alpha_s^3),$$

with

$$(2.48) \quad \begin{aligned} A_1(y) &= a_{10} + a_{11} \log(y) + a_{12} \log^2(y), \\ A_2(y) &= a_{20} + a_{21} \log(y) + a_{22} \log^2(y) + a_{23} \log^3(y) + a_{24} \log^4(y). \end{aligned}$$

It is obvious that for small  $y$  we encounter large logarithms. It follows that, although  $\alpha_s$  is small, we have

$$(2.49) \quad \alpha_s \log^2(y) \not\ll 1,$$

and, therefore, our perturbative expansion is spoiled. One way to deal with these large logarithms in the series expansion of the observable is resummation. The Borel transform provides one possibility for the resummation of asymptotic expansions.

Given a power series

$$(2.50) \quad f(\alpha_s) = \sum_{n=1}^{\infty} c_n \alpha_s^n,$$

the corresponding Borel transform is defined by

$$(2.51) \quad B[f](t) := \sum_{n=0}^{\infty} c_{n+1} \frac{t^n}{n!}.$$

The Borel integral is defined as

$$(2.52) \quad \int_0^{\infty} dt e^{-t/\alpha_s} B[f](t),$$

and has the following properties:

- (1) It has the same series expansion as  $f(\alpha_s)$ .
- (2) It provides the exact result under certain conditions.

An example where the Borel resummation does not work is the conversion of the top quark mass from the pole mass scheme to the  $\overline{\text{MS}}$  mass scheme (see Section 2.5). In this case, an ambiguity of order  $\Lambda_{\text{QCD}}$  arises, which is also known as the renormalon ambiguity of the top quark mass [25–29].

## 2.5. MASS RENORMALIZATION

Let us conclude the chapter on QCD basics with a brief discussion of the renormalization of QCD, especially the renormalization of the quark mass.

First, we introduce the renormalization of the quark mass, the coupling, and the field strength into the QCD Lagrangian (2.17) as

$$(2.53) \quad \begin{aligned} \mathcal{L} = & -\frac{1}{4} Z_3 (\partial_\mu A_\nu^A - \partial_\nu A_\mu^A)^2 + Z_2 \bar{q}_a (i\not{\partial} - Z_m m_R)_{ab} q_b - Z_{3c} \bar{c}^A \square c^A \\ & - g_R Z_{A^3} f^{ABC} (\partial_\mu A_\nu^A) A_\mu^B A_\nu^C - \frac{1}{4} g_R^2 Z_{A^4} (f^{EAB} A_\mu^A A_\nu^B) (f^{ECD} A_\mu^C A_\nu^D) \\ & + g_R Z_1 A_\mu^A \bar{q}_a \gamma^\mu t_{ab}^A q_b + g_R Z_{1c} f^{ABC} (\partial_\mu \bar{c}^A) A_\mu^B c^C. \end{aligned}$$

Here, we implicitly sum over the different quark flavors. The renormalization constant for a quark field is denoted by  $Z_2$ , the one for the gluon field by  $Z_3$ , and the one for a ghost field by  $Z_{3c}$ . In addition, the renormalization constant for the mass of a quark is denoted by  $Z_m$ .

The renormalized coupling  $g_R$  appears in four different terms of the Lagrangian. Therefore, it comes with the four renormalization constants  $Z_1$ ,  $Z_{A^3}$ ,  $Z_{A^4}$ , and

$Z_{1c}$ , corresponding to the quark-gluon vertex, the three-gluon-vertex, the four-gluon vertex, and the ghost-gluon vertex, respectively.

The renormalization constants  $Z_a$ , with  $a \in \{1, 1c, 2, 3, 3c, m, A^3, A^4\}$ , can be written as a series in  $\alpha_s$ :

$$(2.54) \quad Z_a = 1 + \sum_{n=1}^{\infty} Z_a^{(n)} \left( \frac{\alpha_s}{4\pi} \right)^n.$$

The counterterms  $\delta_a$  at one-loop order are, then, defined by

$$(2.55) \quad \delta_a := Z_a^{(1)} \frac{\alpha_s}{4\pi}.$$

### 2.5.1. The Quark Self-Energy

We start with the explicit computation of the quark self-energy graph at one loop, pictured in Figure 2.3, to determine the counterterms for the quark field and the quark mass.

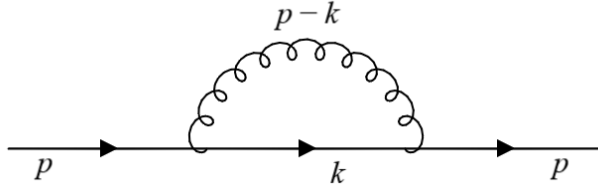


FIGURE 2.3. The quark self-energy graph.

Using the QCD Feynman rules of Appendix A.1, we find

$$(2.56) \quad \begin{aligned} i\Sigma_2^{ab}(\not{p}) &= C_F \delta^{ab} (ig_s)^2 \int \frac{d^4k}{(2\pi)^4} \gamma^\mu \frac{i(\not{k} + m)}{k^2 - m^2 + i\epsilon} \gamma^\nu \frac{-ig_{\mu\nu}}{(p-k)^2 + i\epsilon} \\ &= -C_F \delta^{ab} g_s^2 \int \frac{d^4k}{(2\pi)^4} \gamma^\mu \frac{(\not{k} + m)}{(k^2 - m^2 + i\epsilon)((p-k)^2 + i\epsilon)} \gamma^\mu. \end{aligned}$$

The prefactor  $C_F \delta^{ab}$  is a color-factor coming from the summation over all possible color states

$$(2.57) \quad \sum_{A,B,c,d} t_{ca}^A t_{bd}^B \delta^{AB} \delta^{cd} = \sum_A (t^A t^A)_{ab} = C_F \delta_{ab}.$$

Using the formula for Feynman parametrization

$$(2.58) \quad \frac{1}{AB} = \int_0^1 dx \frac{1}{[A + (B-A)x]^2},$$

we can write (2.56) as

$$(2.59) \quad i\Sigma_2^{ab}(\not{p}) = -C_F \delta^{ab} g_s^2 \int \frac{d^4 k}{(2\pi)^4} \\ \times \int_0^1 dx \gamma^\mu \frac{(\not{k} + m)}{[k^2 - m^2 + i\varepsilon + ((p-k)^2 - k^2 + m^2)x]^2} \gamma^\mu.$$

Completing the square in the denominator with  $x^2 p^2$  yields

$$(2.60) \quad i\Sigma_2^{ab}(\not{p}) = -C_F \delta^{ab} g_s^2 \int \frac{d^4 k}{(2\pi)^4} \int_0^1 dx \gamma^\mu \frac{(\not{k} + m)}{[(k - px)^2 - \Delta + i\varepsilon]^2} \gamma^\mu,$$

where we have defined

$$(2.61) \quad \Delta := (m^2 - p^2 x)(1 - x).$$

Using the relations of the gamma matrices in  $D$  dimensions

$$(2.62) \quad \gamma^\mu \gamma_\mu = DI_4, \\ \gamma^\mu \gamma^\nu \gamma_\mu = (2 - D)\gamma^\nu,$$

we find

$$(2.63) \quad \gamma^\mu (\gamma^\nu k_\nu + m) \gamma_\mu = -2\not{k} + 4m,$$

for the numerator in  $D = 4$ . Shifting  $k \rightarrow k + px$ , we obtain:

$$(2.64) \quad i\Sigma_2^{ab}(\not{p}) = 2C_F \delta^{ab} g_s^2 \int \frac{d^4 k}{(2\pi)^4} \int_0^1 dx \frac{(\not{k} + \not{p}x - 2m)}{[(k^2 - \Delta + i\varepsilon]^2}.$$

The first term in the integral, which is proportional to  $k$ , vanishes when integrated since it is odd in  $k \leftrightarrow -k$ . Hence, our integral for the self-energy loop graph reads

$$(2.65) \quad i\Sigma_2^{ab}(\not{p}) = 2C_F \delta^{ab} g_s^2 \int \frac{d^4 k}{(2\pi)^4} \int_0^1 dx \frac{(\not{p}x - 2m)}{[(k^2 - \Delta + i\varepsilon]^2}.$$

The integral scales as  $d^4 k/k^4$  and is, therefore, logarithmically divergent in the ultraviolet (UV) region.

In order to get rid of this divergency, we use dimensional regularization and consider the integral in  $D = 4 - \epsilon$  dimensions. The self-energy contribution in



$D$  dimensions reads

$$(2.66) \quad \Sigma_2^{ab}(\not{p}) = -i C_F \delta^{ab} g_s^2 \times \int_0^1 dx \underbrace{[(D-2)\not{p}x - Dm]}_{=:\mathcal{K}} \int \underbrace{\frac{d^D k}{(2\pi)^D} \frac{\mu^{4-D}}{[k^2 - \Delta + i\varepsilon]^2}}_{=:\mathcal{I}}.$$

### Calculating the Integral $\mathcal{I}$

Let us first compute the integral  $\mathcal{I}$  in (2.66). We use the general formula for the loop integral over a propagator to the power  $n$  in  $D$  dimensions

$$(2.67) \quad \int \frac{d^D k}{(2\pi)^D} \frac{1}{(p^2 - \Delta)^n} = i \frac{(-1)^n}{(4\pi)^{\frac{D}{2}}} \frac{\Gamma(n - \frac{D}{2})}{\Gamma(n)} \left(\frac{1}{\Delta}\right)^{2 - \frac{D}{2}}.$$

Applying (2.67) to our integral  $\mathcal{I}$  yields

$$(2.68) \quad \mathcal{I} = \int \frac{d^D k}{(2\pi)^D} \frac{\mu^{4-D}}{[k^2 - \Delta + i\varepsilon]^2} = i \frac{1}{(4\pi)^{\frac{D}{2}}} \Gamma\left(\frac{4-D}{2}\right) \left(\frac{\mu^2}{\Delta}\right)^{2 - \frac{D}{2}}.$$

Inserting  $D = 4 - \epsilon$  gives us

$$(2.69) \quad \mathcal{I} = i \frac{1}{(4\pi)^{2 - \frac{\epsilon}{2}}} \Gamma\left(\frac{\epsilon}{2}\right) \left(\frac{\mu^2}{\Delta}\right)^{\frac{\epsilon}{2}}.$$

Next, we expand around  $\epsilon = 0$ . The Laurent expansion of the gamma function around  $x = 0$  is given by

$$(2.70) \quad \Gamma(x) = \frac{1}{x} - \gamma_E + \mathcal{O}(x),$$

where  $\gamma_E \approx 0,577\dots$  is the Euler–Mascheroni constant. Hence, we find

$$(2.71) \quad \Gamma\left(\frac{\epsilon}{2}\right) = \frac{2}{\epsilon} - \gamma_E + \mathcal{O}(\epsilon).$$

The expansion of the remaining factors yields

$$(2.72) \quad \left(\frac{4\pi\mu^2}{\Delta}\right)^{\frac{\epsilon}{2}} = \exp\left[\frac{\epsilon}{2} \log\left(\frac{4\pi\mu^2}{\Delta}\right)\right] = 1 + \frac{\epsilon}{2} \log\left(\frac{4\pi\mu^2}{\Delta}\right),$$

and, therefore, we have

$$\begin{aligned}
 \mathcal{I} &= \frac{i}{16\pi^2} \left( \frac{2}{\epsilon} - \gamma_E \right) \left( 1 + \frac{\epsilon}{2} \log \left( \frac{4\pi\mu^2}{\Delta} \right) \right) \\
 (2.73) \quad &= \frac{i}{16\pi^2} \left[ \frac{2}{\epsilon} - \gamma_E + \log \left( \frac{4\pi\mu^2}{\Delta} \right) - \underbrace{\frac{\epsilon}{2} \gamma_E \log \left( \frac{4\pi\mu^2}{\Delta} \right)}_{\mathcal{O}(\epsilon^1)} \right],
 \end{aligned}$$

where we can neglect terms of order higher than  $\epsilon^0$  since we consider  $\epsilon \rightarrow 0$ .

### *The Final Formula*

Before we can write the final formula for  $\Sigma_2(\not{p})$ , we insert  $D = 4 - \epsilon$  in  $\mathcal{K}$  of (2.66) and find

$$(2.74) \quad \mathcal{K} = 2\not{p}x - 4m - \epsilon(\not{p}x - m).$$

Now, we are able to insert  $\mathcal{I}$  and  $\mathcal{K}$  into (2.66):

$$\begin{aligned}
 \Sigma_2^{ab}(\not{p}) &= \frac{C_F \delta^{ab} g_s^2}{16\pi^2} \int_0^1 dx [2\not{p}x - 4m - \epsilon(\not{p}x - m)] \\
 &\quad \times \left[ \frac{2}{\epsilon} - \gamma_E + \log \left( \frac{4\pi\mu^2}{\Delta} \right) + \mathcal{O}(\epsilon^1) \right] \\
 (2.75) \quad &= \frac{C_F \delta^{ab} g_s^2}{16\pi^2} \left[ \int_0^1 dx \left[ \frac{2}{\epsilon} - \gamma_E + \log(4\pi) \right] [2\not{p}x - 4m] \right. \\
 &\quad \left. - 2 \int_0^1 dx (\not{p}x - m) + 2 \int_0^1 dx \log \left( \frac{\mu^2}{\Delta} \right) (\not{p}x - 2m) \right] + \mathcal{O}(\epsilon^1).
 \end{aligned}$$

Integrating the terms proportional to  $x$  and writing the loop integral in a form where all divergences are separated from the finite part, gives us a useful expression for the quark self-energy

$$\begin{aligned}
 \Sigma_2^{ab}(\not{p}) &= \frac{C_F \delta^{ab} g_s^2}{16\pi^2} \left[ \left( \frac{2}{\epsilon} - \gamma_E + \log(4\pi) \right) (\not{p} - 4m) - (\not{p} - 2m) \right. \\
 (2.76) \quad &\quad \left. + 2 \int_0^1 dx \log \left( \frac{\mu^2}{\Delta} \right) (\not{p}x - 2m) \right],
 \end{aligned}$$

or

$$(2.77) \quad \Sigma_2^{ab}(\not{p}) = \frac{C_F \delta^{ab} g_s^2}{16\pi^2} \left[ \frac{2\not{p} - 8m}{\epsilon} + \text{finite} \right].$$

Note that we have divergences proportional to both  $\not{p}$  and  $m$ . Hence, we need to renormalize two quantities. This is the topic we address next.

### 2.5.2. Renormalization

As we can see from equation (2.77), there are two different kinds of infinities in  $\Sigma_2^{ab}$ . One that is proportional to  $\not{p}$  and one that is independent from  $\not{p}$ , but proportional to  $m$ .

In order to find the right counterterms, we have to renormalize the (bare) quark field  $q(x)$  and the corresponding (bare) quark mass  $m$ . For the renormalized quark field at one-loop order, we can write

$$(2.78) \quad q_{\text{R}}(x) = \frac{1}{\sqrt{Z_2}} q(x), \quad \text{with } Z_2 = 1 + \delta_2,$$

where  $\delta_2$  is the counterterm for the quark field. The corresponding relation for the quark mass reads

$$(2.79) \quad m_{\text{R}} = \frac{1}{Z_m} m, \quad \text{with } Z_m = 1 + \delta_m.$$

The renormalized Green's function using  $Z_2$  is

$$(2.80) \quad G_{\text{R}}(\not{p}) = \frac{1}{Z_2} G_{\text{bare}}(\not{p}).$$

With this relation, we can write the tree-level propagator in terms of the propagator of the bare fields

$$(2.81) \quad iG_{\text{R}}(\not{p}) = \frac{1}{Z_2} \frac{i}{\not{p} - m} + \text{loops}.$$

Using the relations for the renormalized quark field (2.78) and the renormalized mass (2.79) yields

$$(2.82) \quad \begin{aligned} iG_{\text{R}}(\not{p}) &= \left( \frac{1}{1 + \delta_2} \right) \left( \frac{i}{\not{p} - m_{\text{R}} - \delta_m m_{\text{R}}} \right) + \text{loops} \\ &= \frac{i}{\not{p} - m_{\text{R}} - \delta_m m_{\text{R}} + \delta_2 \not{p} - \delta_2 m_{\text{R}} - \delta_2 \delta_m m_{\text{R}}} + \text{loops}. \end{aligned}$$

Since we are interested in first-order corrections, we only need to consider terms linear in the counterterms  $\delta_a$ . Hence, we can neglect the last term in the denominator.

For arbitrary matrices  $A$  and  $B$ , the following relation holds

$$(2.83) \quad (A - B)^{-1} = A^{-1} + A^{-1}BA^{-1} + \mathcal{O}(B^2).$$

Setting  $A = \not{p} - m_{\text{R}}$  and  $B = \delta_2 - (\delta_2 + \delta_m)m_{\text{R}}$  provides

$$(2.84) \quad \begin{aligned} iG_{\text{R}}(\not{p}) &= \frac{i}{\not{p} - m_{\text{R}}} + \frac{i}{\not{p} - m_{\text{R}}} [i(\delta_2 \not{p} - (\delta_2 + \delta_m)m_{\text{R}})] \frac{i}{\not{p} - m_{\text{R}}} \\ &\quad + \text{loops} + \mathcal{O}(g_{\text{s}}^4). \end{aligned}$$

The term for the one-loop correction reads

$$(2.85) \quad iG_2(\not{p}) = iG_0(\not{p})[i\Sigma_2^{ab}(\not{p})]iG_0(\not{p}).$$

Insertion into (2.84) yields

$$(2.86) \quad \begin{aligned} iG_{\text{R}}(\not{p}) &= \frac{i}{\not{p} - m_{\text{R}}} + \frac{i}{\not{p} - m_{\text{R}}} [i(\delta_2 \not{p} - (\delta_2 + \delta_m)m_{\text{R}} + \Sigma_2^{ab}(\not{p}))] \frac{i}{\not{p} - m_{\text{R}}} \\ &\quad + \mathcal{O}(g_{\text{s}}^4). \end{aligned}$$

### 2.5.3. Renormalization Schemes

Now, we can choose the counterterms  $\delta_2$  and  $\delta_m$  such that they cancel the divergences in  $\Sigma_2^{ab}$ . This type of renormalization is called subtraction scheme. There are many different subtraction schemes that differ in the way the counterterms are chosen. The most commonly used schemes are the minimal subtraction (MS) scheme, or rather the modified minimal subtraction ( $\overline{\text{MS}}$ ) scheme, and the on-shell scheme.

In the MS scheme, the counterterms are chosen such that they exactly cancel the divergences in  $\Sigma_2^{ab}$ , but do not include finite terms. Hence, we obtain

$$(2.87) \quad \begin{aligned} \delta_2 &= \frac{1}{\epsilon} \frac{g_{\text{s}}^2}{16\pi^2} [-2C_{\text{F}}], \\ \delta_m &= \frac{1}{\epsilon} \frac{g_{\text{s}}^2}{16\pi^2} [-6C_{\text{F}}], \end{aligned}$$

for the counterterms in the MS scheme, leaving out the Kronecker delta for the flavor indices.

The full set of counterterms at one-loop order can be calculated from the remaining two- and three-point functions in a similar way. For the sake of completeness,

we give the full set of one-loop counterterms in Feynman gauge ( $\xi = 1$ ) [13]

$$\begin{aligned}
\delta_1 &= \frac{1}{\epsilon} \frac{g_s^2}{16\pi^2} [-2C_F - 2C_A], \\
\delta_2 &= \frac{1}{\epsilon} \frac{g_s^2}{16\pi^2} [-2C_F], \\
\delta_m &= \frac{1}{\epsilon} \frac{g_s^2}{16\pi^2} [-6C_F], \\
\delta_3 &= \frac{1}{\epsilon} \frac{g_s^2}{16\pi^2} \left[ \frac{10}{3} C_A - \frac{8}{3} n_f T_R \right], \\
\delta_{3c} &= \frac{1}{\epsilon} \frac{g_s^2}{16\pi^2} [C_A], \\
\delta_{A^3} &= \frac{1}{\epsilon} \frac{g_s^2}{16\pi^2} \left[ \frac{4}{3} C_A - \frac{8}{3} n_f T_R \right], \\
\delta_{A^4} &= \frac{1}{\epsilon} \frac{g_s^2}{16\pi^2} \left[ -\frac{2}{3} C_A - \frac{8}{3} n_f T_R \right], \\
\delta_{1c} &= \frac{1}{\epsilon} \frac{g_s^2}{16\pi^2} [-C_A].
\end{aligned}$$

In the following, we define the pole mass  $m_{\text{pole}}$ , a physical mass quantity, and show two examples of renormalization schemes. First, the on-shell scheme where the renormalized mass  $m_R$  is set equal to the pole mass. Secondly, the modified minimal subtraction scheme ( $\overline{\text{MS}}$ ) where the counterterms are defined similarly to the MS scheme but with additional finite terms.

### *The Pole Mass*

One particle irreducible (1PI) Feynman graphs are graphs that cannot be cut into two by slicing one single propagator.  $i\Sigma(\not{p})$  can be defined as the sum of all 1PI graphs. Resumming the corresponding Green's function to all orders yields

$$(2.88) \quad iG(\not{p}) = \frac{i}{\not{p} - m + \Sigma(\not{p})}.$$

At order  $g_s^2$ , the renormalized Green's function reads as

$$(2.89) \quad iG_R(\not{p}) = \frac{i}{\not{p} - m_R + \Sigma_R(\not{p})},$$

with

$$(2.90) \quad \Sigma_{\text{R}}(\not{p}) = \Sigma_2(\not{p}) + \delta_2 \not{p} - (\delta_m + \delta_2)m_{\text{R}} + \mathcal{O}(g_s^4).$$

The physical quark mass  $m_{\text{pole}}$ , or the pole mass, is the location of the propagator's pole. The renormalized propagator has a single pole at  $\not{p} = m_{\text{pole}}$  with residue  $i$ . Hence, we find

$$(2.91) \quad \Sigma_{\text{R}}(m_{\text{pole}}) = m_{\text{R}} - m_{\text{pole}},$$

for the 1PI graphs. With the residue  $i$ , we find

$$(2.92) \quad i = \lim_{\not{p} \rightarrow m_{\text{pole}}} (\not{p} - m_{\text{pole}}) \frac{i}{\not{p} - m_{\text{R}} + \Sigma_{\text{R}}(\not{p})} = \lim_{\not{p} \rightarrow m_{\text{pole}}} \frac{i}{1 + \frac{d}{d\not{p}} \Sigma_{\text{R}}(\not{p})},$$

which gives us

$$(2.93) \quad \left. \frac{d}{d\not{p}} \Sigma_{\text{R}}(\not{p}) \right|_{\not{p}=m_{\text{pole}}} = 0.$$

These two equations define the pole mass.

In the on-shell subtraction scheme the finite parts of the counterterms are chosen such that the renormalized mass is equal to the pole mass,  $m_{\text{R}} = m_{\text{pole}}$ . Hence, the counterterms are given by

$$(2.94) \quad \begin{aligned} \delta_2 &= - \left. \frac{d}{d\not{p}} \Sigma_2(\not{p}) \right|_{\not{p}=m_{\text{pole}}}, \\ \delta_m m_{\text{pole}} &= \Sigma_2(m_{\text{pole}}). \end{aligned}$$

When calculating the counterterms, we encounter the problem of arising IR divergences. We address this problem in Chapter 3 where we discuss the subtraction method for the cancellation of IR singularities in NLO calculations.

### $\overline{\text{MS}}$ Scheme

The  $\overline{\text{MS}}$  scheme is closely related to the  $\text{MS}$  scheme. The only difference is that there are some additional finite terms in the counterterms, namely

$$(2.95) \quad \delta_2 = - \frac{g_s^2}{16\pi^2} \left[ \frac{2}{\epsilon} - \gamma_{\text{E}} + \log(4\pi) \right] C_{\text{F}},$$

$$(2.96) \quad \delta_m = - \frac{3g_s^2}{16\pi^2} \left[ \frac{2}{\epsilon} - \gamma_{\text{E}} + \log(4\pi) \right] C_{\text{F}}.$$

With this choice for the counterterms, we find

$$(2.97) \quad \Sigma_{\text{R}}(\not{p}) = \frac{g_{\text{s}}^2}{8\pi^2} C_{\text{F}} \int_0^1 dx \log\left(\frac{\mu^2}{\Delta}\right) (\not{p}x - 2m_{\text{R}}) - \frac{g_{\text{s}}^2}{16\pi^2} (\not{p} - 2m_{\text{R}}).$$

Note that the renormalized propagator has no pole at  $\not{p} = m_{\text{R}}$  but at  $\not{p} = m_{\text{pole}}$ , which gives us the relation

$$(2.98) \quad m_{\text{pole}} - m_{\text{R}} + \Sigma_{\text{R}}(m_{\text{pole}}) = 0.$$

Using  $m_{\text{pole}} = m_{\text{R}}$  at leading order, we obtain the relation

$$(2.99) \quad m_{\text{R}} = m_{\text{pole}} \left[ 1 - \frac{g_{\text{s}}^2}{16\pi^2} \left( 4 + 3 \log\left(\frac{\mu^2}{m_{\text{pole}}^2}\right) \right) + \mathcal{O}(g_{\text{s}}^4) \right].$$

Since the parameter  $\mu$  is unphysical, every physical observable  $O$  has to be independent of  $\mu$ . This leads to the renormalization group equation

$$(2.100) \quad \frac{d}{d\mu} O = 0.$$

#### 2.5.4. Pole Mass Renormalon Ambiguity

As already mentioned in the context of resummation of observables in QCD (cf. Section 2.4.2), we now want to address the problem that arises when trying to resum the series in the conversion from the pole mass to the  $\overline{\text{MS}}$  mass.

The conversion from the pole mass scheme ( $m_{\text{pole}}$ ) to the  $\overline{\text{MS}}$  mass scheme ( $\bar{m}$ ) reads

$$(2.101) \quad m_{\text{pole}} = \bar{m} + \sum_{n=0}^{\infty} r_n \alpha_{\text{s}}^{n+1}.$$

The coefficients  $r_n$  are strongly contributed by infrared momenta in the integration over the gluon line. They diverge as

$$(2.102) \quad r_n \stackrel{n \rightarrow \infty}{\sim} \frac{C_{\text{F}}}{\pi} e^{5/6} \mu (-2\beta_0)^n n!,$$

where  $\beta_0$  is the first coefficient of the QCD  $\beta$ -function of Eq. (2.41).

The function we want to resum is then defined by

$$(2.103) \quad f(\alpha_{\text{s}}) := \sum_{n=0}^{\infty} r_n \alpha_{\text{s}}^{n+1} \sim \sum_{n=0}^{\infty} (-2\beta_0)^n n! \alpha_{\text{s}}^{n+1}.$$

Trying Borel resummation (cf. Section 2.4.2), we find the following Borel transform

$$(2.104) \quad B[f](t) = \sum_{n=0}^{\infty} (-2\beta_0)^n t^n = \frac{1}{1 + 2\beta_0 t}, \quad \text{for } |2\beta_0 t| < 1.$$

In the corresponding Borel integral

$$(2.105) \quad \int_0^{\infty} e^{-t/\alpha_s} \frac{1}{1 + 2\beta_0 t},$$

we encounter a pole at  $t = -1/(2\beta_0)$  which leads to an ambiguity of order  $\Lambda_{\text{QCD}}$  in the pole mass. This ambiguity makes the pole mass impractical for quarks. A short-distance mass (a practical quark mass definition without the  $\mathcal{O}(\Lambda_{\text{QCD}})$  ambiguity) has to depend on an additional IR scale  $R$ . Examples for short-distance masses are the  $\overline{\text{MS}}$  mass and the MSR mass [30, 31].



**Part 2**

**The Top Quark Mass in Parton  
Showers**



## CHAPTER 3

# NLO Computations and Dipole Subtraction

## Contents

---

<b>3.1. The Structure of NLO Computations</b>	<b>34</b>
3.1.1. Born Cross Section	35
3.1.2. Virtual Corrections	35
3.1.3. Real Corrections	36
3.1.4. Hadronic Counterterms	36
<b>3.2. Dipole Subtraction – General Overview</b>	<b>37</b>
<b>3.3. Dipole for Colorless Initial State</b>	<b>41</b>
3.3.1. Massless Case	41
3.3.2. Massive Case	44

---

When dealing with NLO computations, one encounters infrared singularities that may spoil the calculations. There are two different ways to deal with these singularities:

- (1) The phase space slicing method [32–38].
- (2) The subtraction method [39–58].

In the subtraction scheme, one introduces a counterterm that approximates the singularities of the real emission term and the virtual contribution. This makes both contributions integrable separately.

In the phase space slicing approach, a cutoff (or in some examples two cutoffs [35]) is applied to the phase space such that the singular regions are separated from the rest. The latter can then be integrated numerically. In the singular region the real emission matrix element is approximated with its collinear and soft limits and then integrated.

Here, we focus on the subtraction method, in particular the dipole subtraction method [42–44], since its properties will play a crucial role for the definition of the dipole shower in Section 4.2.

Before we start with a description of the dipole subtraction method, we take a look at the general structure of NLO computations in perturbative QCD.

### 3.1. THE STRUCTURE OF NLO COMPUTATIONS

The differential cross section of any scattering process in QCD can generally be written as

$$(3.1) \quad d\sigma^{\text{NLO}} = [B(\phi_n) + V(\phi_n) + C(\phi_n)] d\phi_n + R(\phi_{n+1}) d\phi_{n+1}.$$

Here,  $B(\phi_n)$  denotes the Born contribution, i.e. the LO contribution. The NLO contributions are the renormalized virtual contribution  $V(\phi_n)$  and the real contribution  $R(\phi_{n+1})$ . For hadronic collisions, as for example in the LHC, an additional counterterm  $C(\phi_n)$  has to be added to cancel singularities in the initial state.

Since, in collider experiments, we observe the scattering of two initial-state particles into  $n$  final-state particles, it is sufficient to consider the process  $2 \rightarrow n$ . For two colliding hadrons  $A$  and  $B$ , we denote their four-momenta by  $p_A$  and  $p_B$ , respectively. The momenta of the incoming partons  $a$  and  $b$  are then defined by

$$(3.2) \quad p_a := x_a p_A, \quad p_b := x_b p_B,$$

where  $x_a$  ( $x_b$ ) is the momentum fraction of parton  $a$  ( $b$ ) in hadron  $A$  ( $B$ ). The scattering process then fulfills the momentum conservation

$$(3.3) \quad x_a p_A + x_b p_B = \sum_{i=1}^n p_i,$$

where  $p_i$  is the four-momentum of the final-state particle  $i$ . The set of kinematic variables that specify the resulting  $n$ -particle phase space is denoted by

$$(3.4) \quad \Phi_n = \{p_1, \dots, p_n\},$$

and a point in this phase space by  $\phi_n$ .

It is apparent that for initial-state particles that are not hadrons the corresponding momentum fraction  $x_j$  has to be set to 1.

3.1.1. *Born Cross Section*

The Born contribution represents the LO part of the differential NLO cross section in (3.1). It is given by

$$(3.5) \quad d\sigma^{\text{B}} = \sum_{f_a, f_b} \int dx_a \int dx_b \frac{f_{f_a}(x_a) f_{f_b}(x_b)}{2\hat{s} n_s(a) n_s(b) n_c(a) n_c(b)} \sum_{\text{spins, color}} |\mathcal{M}_n|^2 d\phi_n,$$

where the first sum is over the flavors of the initial-state partons  $a$  and  $b$ . The center-of-mass energy of the hard collision is given by  $\hat{s}$ , whereas  $n_s(j)$  and  $n_c(j)$  denote the degrees of freedom for the spin and color of parton  $j$ . The relevant tree-level matrix element is denoted by  $\mathcal{M}_n$ .

The usual  $n$ -particle phase space element in four dimensions is given by

$$(3.6) \quad d\phi_n(P; p_1, \dots, p_n) = (2\pi)^4 \delta^4 \left( P - \sum_{i=1}^n p_i \right) \prod_{i=1}^n \frac{d^3 p_i}{(2\pi)^3 2p_i^0},$$

with  $P = p_a + p_b$ . For convenience we abbreviate (3.5) by

$$(3.7) \quad d\sigma^{\text{B}} = B(\phi_n) d\phi_n.$$

3.1.2. *Virtual Corrections*

The virtual corrections assemble the contribution from the one-loop diagrams to a corresponding process. The matrix element squared contributing to the differential cross section of the virtual corrections (cf. (3.5)) is calculated as an interference of the one-loop contribution with the Born amplitude

$$(3.8) \quad 2 \operatorname{Re} \left( \mathcal{M}_{(1\text{-loop})} \mathcal{M}_n^* \right).$$

This interference of the Born amplitude with the one-loop amplitude leads to UV divergences. These can be removed by renormalization (cf. Section 2.5). We assume that the virtual contribution  $V(\phi_n)$  in our abbreviated form

$$(3.9) \quad d\sigma^{\text{V}} = V(\phi_n) d\phi_n,$$

is already renormalized and, hence, free of UV divergences.

However, IR divergences remain in  $V(\phi_n)$  arising from collinear or soft partons in the loop. Applying dimensional regularization, these divergences show up as  $1/\epsilon$  and  $1/\epsilon^2$  poles in the virtual contribution. As already mentioned, these divergences can be tackled using the subtraction method.

### 3.1.3. Real Corrections

The structure of the real corrections to the NLO cross section is very similar to the structure of the Born cross section, but with an additional parton coming from a real emission. Thus, it is sufficient to consider the Born amplitude for a  $2 \rightarrow n + 1$  process.

Using the familiar abbreviation, we can write the differential cross section for the real emission part as

$$(3.10) \quad d\sigma^{\text{R}} = R(\phi_{n+1})d\phi_{n+1}.$$

The  $n + 1$ -particle phase space element in  $D$  dimensions reads

$$(3.11) \quad d\phi_{n+1}(P; p_1, \dots, p_{n+1}) = (2\pi)^D \delta^D \left( P - \sum_{i=1}^{n+1} p_i \right) \prod_{i=1}^{n+1} \frac{d^{D-1}p_i}{(2\pi)^{D-1} 2p_i^0}.$$

In phase space regions where the emitted parton becomes soft or collinear to one of the other partons, the real contribution also contains IR singularities. Additionally, the  $n + 1$ -particle phase space can be factorized into a Born like  $n$ -particle phase space times a radiation phase space which depends on three radiation variables.

### 3.1.4. Hadronic Counterterms

Hadronic collisions are collisions where at least one of the colliding particles is a hadron. In these events, initial-state IR divergences occur. To solve this problem, the factorization counterterm

$$(3.12) \quad d\sigma^{\text{C}} = C(\phi_n)d\phi_n,$$

has to be added to the differential NLO cross section (cf. (3.1)). The infrared divergences in this counterterm again appear as  $1/\epsilon$  poles in dimensional regularization. For leptonic collisions the counterterm is set to zero.

## 3.2. DIPOLE SUBTRACTION – GENERAL OVERVIEW

Let us reconsider the formula for the differential NLO cross section (3.1)

$$(3.13) \quad d\sigma^{\text{NLO}} = [B(\phi_n) + V(\phi_n) + C(\phi_n)] d\phi_n + R(\phi_{n+1}) d\phi_{n+1}.$$

As discussed in the last section, each term of the NLO correction, i.e. the virtual contribution  $V(\phi_n)$  and the real emission correction  $R(\phi_n)$ , contains infrared singularities. Two types of infrared singular regions in phase space can be distinguished:

- (1) **Soft region:** A final-state parton with a four-momentum near zero is called a soft parton, i.e. a parton  $j$  with four-momentum

$$(3.14) \quad p_j = \lambda q, \quad \text{with } \lambda \rightarrow 0,$$

for an arbitrary four-momentum  $q$ .

- (2) **Collinear region:** The final-state parton  $i$  is called collinear to another parton  $j$  if

$$(3.15) \quad p_i \rightarrow zp, \quad p_j \rightarrow (1-z)p,$$

holds for the four-momenta of the both partons. Here, we have  $p = p_i + p_j$ , and  $z$  is the momentum fraction of the parton  $i$  of  $p$ . The parton  $j$  can either be a parton in the final state or in the initial state.

Additionally, there are regions where both types of singularities overlap. These are called soft-collinear regions.

The singularities lead to divergences in the integrals which make them not integrable. However, the Kinoshita–Lee–Nauenberg (KLN) theorem [59, 60] states that the computation of infrared safe observables at fixed-order is infrared finite. In our case, at NLO, the infrared singularities of the real emission term cancel the infrared singularities of the virtual contribution after phase space integration.

A convenient tool to make the separate terms of (3.13) suitable for numerical calculations is the subtraction method [39–58]. Here, we only give an overview of the general aspects of the subtraction method which fit our purposes of discussing a special subtraction scheme, i.e. subtraction in the Catani–Seymour dipole formalism [42–44]. A more detailed description of the subtraction method in a general framework can be found in [61].

The subtraction method makes use of a counterterm  $A(\phi_{n+1})$  that approximates the singular behavior of the virtual correction and the real emission part of (3.13). Adding and subtracting this counterterm lets us rewrite the differential NLO cross section as

$$(3.16) \quad d\sigma^{\text{NLO}} = [B(\phi_n) + V(\phi_n) + C(\phi_n) + A(\phi_{n+1})d\phi_{\text{rad}}] d\phi_n + [R(\phi_{n+1}) - A(\phi_{n+1})] d\phi_{n+1}.$$

Note that the counterterm and the real emission term live on the phase space of  $n + 1$  final-state particles. In order to make it also suitable to the virtual contribution, which lives on the  $n$ -particle phase space, we used the factorization property of the  $n + 1$ -particle phase space into a product of an  $n$ -particle configuration and a radiation phase space

$$(3.17) \quad d\phi_{n+1} = d\phi_n d\phi_{\text{rad}}.$$

The involved part when applying the subtraction method is the task of finding a suitable form for the counterterms. One method to find these counterterms, we want to focus on, is the dipole subtraction method. It was first introduced by Catani and Seymour in [42] for massless final-state partons. Hence, it is often referred to as Catani–Seymour subtraction. It has been extended to massive final-state partons in [43, 44].

The dipole subtraction method is based upon the external-leg insertion rule: In the soft or collinear regions, the tree-level amplitude  $\mathcal{M}_{n+1}$  can always be obtained by inserting a parton  $j$  (that is either soft or collinear to another of the  $n$  partons) between two external legs of the tree-level amplitude  $\mathcal{M}_n$  and summing over all possible insertions (see Figure 3.1). From this external leg

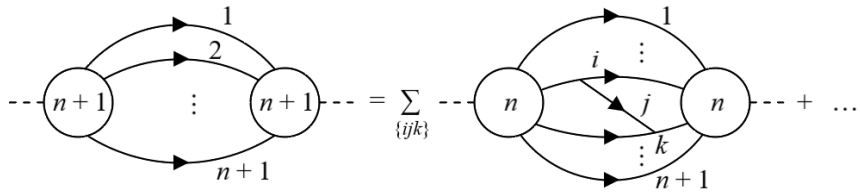


FIGURE 3.1. Schematic representation of the external leg insertion for squared matrix elements.

insertion, one can derive the dipole factorization formulae [42]. Introducing the dipole splitting functions  $V_{ij,k}$ , the  $n + 1$  final-state parton matrix element



squared of the real emission term can symbolically be expressed as

$$(3.18) \quad |\mathcal{M}_{n+1}|^2 \rightarrow |\mathcal{M}_n|^2 \otimes V_{ij,k}.$$

Here,  $\otimes$  denotes a convolution between the squared Born level amplitude and the singular factor  $V_{ij,k}$ . A pictorial representation of this factorization can be found in Figure 3.2. Note that, in the soft and collinear limits, the splitting functions  $V_{ij,k}$  become proportional to the Altarelli–Parisi splitting functions [62–64].

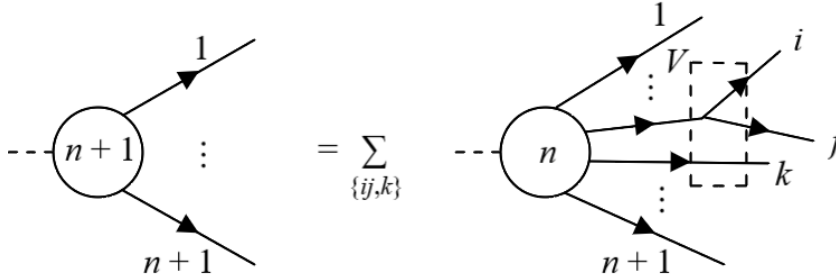


FIGURE 3.2. Dipole factorization of an amplitude with  $n + 1$ -particles in the final state.

Making use of the splitting functions  $V_{ij,k}$ , the singular behavior of the real correction can be expressed as a sum over dipoles

$$(3.19) \quad |\mathcal{M}_{n+1}|^2 = \sum_{i,j} \sum_{k \neq i,j} \mathcal{D}_{ij,k} + \sum_{i,j} \sum_a \mathcal{D}_{ij}^a + \sum_{a,i} \sum_{k \neq i} \mathcal{D}_k^{ai} + \sum_{a,i} \sum_{b \neq a} \mathcal{D}^{ai,b} + \dots,$$

where the dots represent non-divergent terms in the singular regions of the  $n + 1$ -particle phase space. The dipole functions  $\mathcal{D}$  can be obtained from the corresponding splitting functions  $V$ . By  $i$ ,  $j$ , and  $k$ , we denote partons in the final state while  $a$  and  $b$  are initial-state partons.

Each of the dipole contributions depends on three partons. The three partons are distinguished as emitter, emitted parton, and spectator. There exist four different phase space configurations depending on which of these three partons are in the final or in the initial state (see Figure 3.3):

- Final-state emitter with final-state spectator  $\mathcal{D}_{ij,k}$ .
- Final-state emitter with initial-state spectator  $\mathcal{D}_{ij}^a$ .
- Initial-state emitter with final-state spectator  $\mathcal{D}_k^{ai}$ .
- Initial-state emitter with initial-state spectator  $\mathcal{D}^{ai,b}$ .

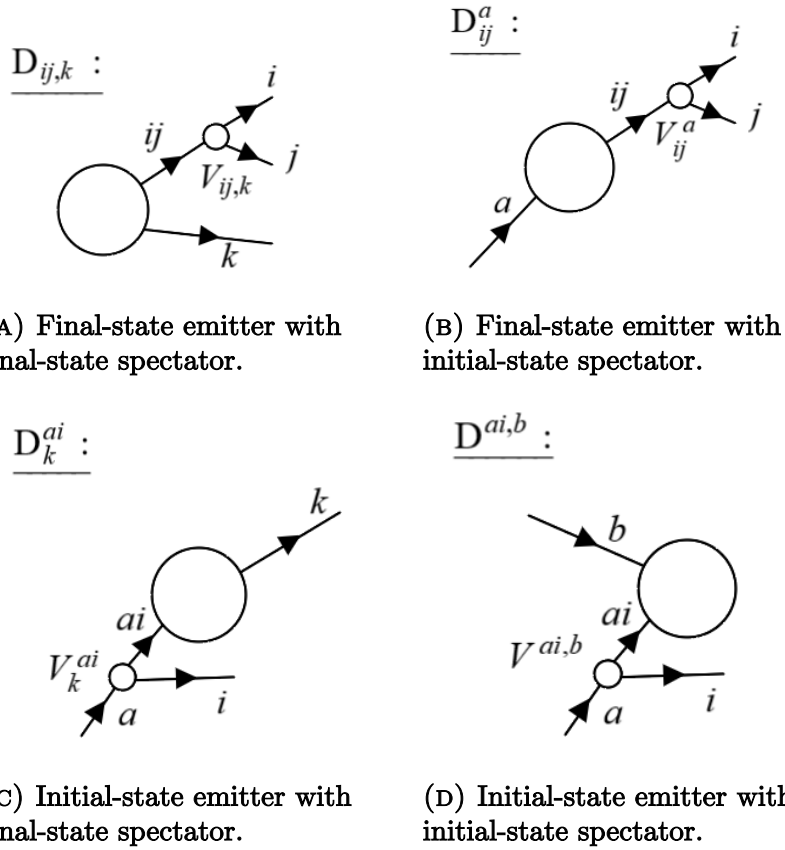


FIGURE 3.3. Pictorial representation of the four possible emitter-spectator pairs.

The dipole functions approximate the  $n + 1$ -particle matrix element pointwise in the singular regions (cf. (3.19)). Hence, they provide a suitable form for the counterterms in the subtraction method.

Since we will focus on dipole parton showers in electron-positron annihilation processes later on, it is sufficient to discuss the properties of the dipole for a final-state emitter with a final-state spectator,  $\mathcal{D}_{ij,k}$ . The properties of the other dipoles and their extension to massive particles can be found in [42–44].

## 3.3. DIPOLE FOR COLORLESS INITIAL STATE

For the case of a final-state emitter and a final-state spectator, the  $n+1$ -parton matrix element squared can be expressed by the sum over the corresponding dipoles plus non-singular terms

$$(3.20) \quad |\mathcal{M}_{n+1}|^2 = \sum_{i,j} \sum_{k \neq i,j} \mathcal{D}_{ij,k} + \dots$$

The dipole contribution reads

$$(3.21) \quad \mathcal{D}_{ij,k} = -\frac{1}{2p_i \cdot p_j} \times \mathcal{M}_n^*(p_1, \dots, \bar{p}_{ij}, \dots, \bar{p}_k, \dots) \frac{\mathbf{T}_k \cdot \mathbf{T}_{ij}}{\mathbf{T}_{ij}^2} V_{ij,k} \mathcal{M}_n(p_1, \dots, \bar{p}_{ij}, \dots, \bar{p}_k, \dots),$$

where  $\mathbf{T}_j$  denotes the color charge operator for the parton  $j$ . In the final state the color operators  $\mathbf{T}_j$  are given by

$$(3.22) \quad \begin{aligned} & \mathcal{M}^*(\dots q_i \dots)(t_{ij}^a) \mathcal{M}(\dots q_j \dots), \\ & \mathcal{M}^*(\dots \bar{q}_i \dots)(-t_{ji}^a) \mathcal{M}(\dots \bar{q}_j \dots), \\ & \mathcal{M}^*(\dots g_i^C \dots)(if^{CAB}) \mathcal{M}(\dots g_j^B \dots), \end{aligned}$$

for a quark, antiquark, and gluon, respectively. It is obvious that the color operators  $\mathbf{T}_j$  lead to color correlations.

The splitting functions  $V_{ij,k}$  are matrices in the helicity space of the emitter  $\bar{i}\bar{j}$ . Hence, they lead to spin correlations as well.

After this discussion of the general properties of the dipole function  $\mathcal{D}_{ij,k}$ , we will now present the features that are necessary for the definition of the dipole shower in Section 4.2, i.e. the kinematics of the splitting, the factorized phase space measure, and the form of the spin averaged splitting functions  $V_{ij,k}$ . We start with the massless case and extend it to the massive case.

## 3.3.1. Massless Case

Considering the splitting  $\bar{i}\bar{j} + \bar{k} \rightarrow i + j + k$ , we require exact momentum conservation

$$(3.23) \quad p_i + p_j + p_k = \bar{p}_{ij} + \bar{p}_k,$$

where  $\bar{p}_{ij}$  and  $\bar{p}_k$  are the four-momenta of the emitter parton  $\bar{i}\bar{j}$  and the spectator parton  $\bar{k}$ . The momenta  $p_i, p_j, p_k$  are the four-momenta of the partons  $i, j, k$  after the splitting.

For the massless case we have

$$(3.24) \quad p_i^2 = p_j^2 = p_k^2 = 0.$$

### *Kinematics*

We start with the definition of the kinematic variables for the splitting, i.e.  $y_{ij,k}$  and the momentum fraction like variables  $\bar{z}_i$  and  $\bar{z}_j$ :

$$(3.25) \quad \begin{aligned} y_{ij,k} &:= \frac{p_i p_j}{p_i p_j + p_j p_k + p_k p_i} = \frac{s_{ij}}{s_{ij} + s_{jk} + s_{ik}}, \\ \bar{z}_i &:= \frac{p_i p_k}{p_j p_k + p_i p_k} = \frac{s_{ik}}{s_{jk} + s_{ik}}, \\ \bar{z}_j &:= \frac{p_j p_k}{p_j p_k + p_i p_k} = \frac{s_{jk}}{s_{jk} + s_{ik}} = 1 - \bar{z}_i, \end{aligned}$$

where we used

$$(3.26) \quad s_{lm} := (p_l + p_m)^2, \quad \text{for } l, m \in \{i, j, k\}, \quad l \neq m.$$

The momenta of the emitter and the spectator are defined as in [42]:

$$(3.27) \quad \begin{aligned} \bar{p}_{ij} &= p_i + p_j - \frac{y_{ij,k}}{1 - y_{ij,k}} p_k, \\ \bar{p}_k &= \frac{1}{1 - y_{ij,k}} p_k, \\ \bar{p}_m &= p_m, \quad \text{for } m \neq i, j, k, \end{aligned}$$

which ensures exact momentum conservation

$$(3.28) \quad \sum_{l=1}^n \bar{p}_l = \sum_{l=1}^{n+1} p_l.$$

### *Factorized Phase Space Measure*

The three-particle phase space element of the partons  $i, j, k$  contributes to the  $n + 1$ -particle phase space element of the final-states. It can be factorized into a two-particle phase space and an unresolved radiation phase space

$$(3.29) \quad d\phi_3(Q; p_i, p_j, p_k) = d\phi_2(Q; \bar{p}_{ij}, \bar{p}_k) d\phi_{\text{rad}}(p_i; \bar{p}_{ij}, \bar{p}_k),$$

with  $Q = p_i + p_j + p_k$ , the total outgoing momentum of the final-state particles that form the dipole.

The measure of the radiation phase space  $d\phi_{\text{rad}}(p_i; \bar{p}_{ij}, \bar{p}_k)$  can be expressed in terms of the kinematic variables  $y_{ij,k}$  and  $\bar{z}_i$ . In  $D$  dimensions, the radiation phase space measure reads

$$(3.30) \quad d\phi_{\text{rad}}(p_i; \bar{p}_{ij}, \bar{p}_k) = \frac{(2\bar{p}_{ij}\bar{p}_k)^{1-\epsilon}}{16\pi^2} \frac{d\Omega^{(D-3)}}{(2\pi)^{1-2\epsilon}} d\bar{z}_i dy_{ij,k} \Theta(\bar{z}_i(1-\bar{z}_i)) \\ \times \Theta(y_{ij,k}(1-y_{ij,k})) (\bar{z}_i(1-\bar{z}_i))^{-\epsilon} (1-y_{ij,k})^{1-2\epsilon} y_{ij,k}^{-\epsilon}.$$

For the parton shower splitting (cf. Chapter 4), it is reasonable to consider the phase space measure in  $D = 4$  dimensions. In this case, the element of solid angle  $d\Omega^{(D-3)}$  simplifies as follows

$$(3.31) \quad \int d\Omega^{(D-3)} = \frac{2\pi}{\pi^\epsilon \Gamma(1-\epsilon)} \xrightarrow{D=4} \int d\Omega = 2\pi.$$

In four dimensions, the differential  $d\Omega$  corresponds to the differential of the azimuthal angle  $\varphi$ . Thus, the following replacement holds

$$(3.32) \quad d\Omega \rightarrow d\varphi \Theta(\varphi(2\pi - \varphi)).$$

It is apparent that the radiation phase space  $\Phi_{\text{rad}}$  is now parametrized in terms of three radiation variables

$$(3.33) \quad \Phi_{\text{rad}} = \{y_{ij,k}, \bar{z}_i, \varphi\}.$$

Hence, we are now able to write the differential of the radiation phase space in  $D = 4$  dimensions in terms of these three radiation variables

$$(3.34) \quad d\phi_{\text{rad}}(p_i; \bar{p}_{ij}, \bar{p}_k) = \frac{(2\bar{p}_{ij}\bar{p}_k)}{4(2\pi)^3} d\varphi d\bar{z}_i dy_{ij,k} (1-y_{ij,k}) \\ \times \Theta(\varphi(2\pi - \varphi)) \Theta(\bar{z}_i(1-\bar{z}_i)) \Theta(y_{ij,k}(1-y_{ij,k})).$$

Defining  $s_{ijk} := (\bar{p}_{ij} + \bar{p}_k)^2 = (p_i + p_j + p_k)^2$  and writing out the integrals, we obtain

$$(3.35) \quad \int d\phi_{\text{rad}} = \frac{s_{ijk}}{32\pi^3} \int_0^1 dy_{ij,k} (1-y_{ij,k}) \int_0^1 d\bar{z}_i \int_0^{2\pi} d\varphi,$$

for the phase space measure in the massless case.

### *Dipole Splitting Functions*

The dipole splitting functions  $V_{ij,k}$  for the different splittings are obtained from [42]. In their spin-averaged form they read:

For  $q \rightarrow qg$ :

$$(3.36) \quad \langle V_{qg,k} \rangle = 8\pi\mu^{2\epsilon}\alpha_s C_F \left[ \frac{2}{1 - \bar{z}_i(1 - y_{ij,k})} - (1 + \bar{z}_i) + \epsilon(1 - \bar{z}_i) \right].$$

For  $g \rightarrow q\bar{q}$ :

$$(3.37) \quad \langle V_{q\bar{q},k} \rangle = 8\pi\mu^{2\epsilon}\alpha_s T_R \left[ 1 - \frac{2\bar{z}_i(1 - \bar{z}_i)}{1 - \epsilon} \right].$$

For  $g \rightarrow gg$ :

$$(3.38) \quad \langle V_{gg,k} \rangle = 8\pi\mu^{2\epsilon}\alpha_s C_A \left[ \frac{2}{1 - \bar{z}_i(1 - y_{ij,k})} + \frac{2}{1 - (1 - \bar{z}_i)(1 - y_{ij,k})} - 4 + 2\bar{z}_i(1 - \bar{z}_i) \right].$$

#### 3.3.2. *Massive Case*

In the massive case, we consider arbitrary masses for the final-state particles:

$$(3.39) \quad p_i^2 = m_i^2, \quad p_j^2 = m_j^2, \quad \bar{p}_k^2 = p_k^2 = m_k^2, \quad \bar{p}_{ij}^2 = m_{ij}^2.$$

Again, we require that the splitting fulfills exact momentum conservation

$$(3.40) \quad Q := p_i + p_j + p_k = \bar{p}_{ij} + \bar{p}_k,$$

where we defined the sum of the outgoing momenta as  $Q$ .

#### *Kinematics*

The kinematic variables  $y_{ij,k}$  and  $\bar{z}_i$  are defined as in the massless case.

Additionally, we define the rescaled parton mass as

$$(3.41) \quad \mu_l := \frac{m_l}{\sqrt{Q^2}}, \quad \text{with } l \in \{i, j, k, ij\}.$$

The relative velocity between two massive momenta  $p, q$  is defined as

$$(3.42) \quad v_{p,q} := \sqrt{1 - \frac{p^2 q^2}{(pq)^2}} = \frac{\sqrt{\lambda((p+q)^2, p^2, q^2)}}{(p+q)^2 - p^2 - q^2},$$

where the Källén function  $\lambda(x, y, z)$  is given by

$$(3.43) \quad \lambda(x, y, z) := x^2 + y^2 + z^2 - 2xy - 2xz - 2yz.$$

For example, the velocity  $\bar{v}_{ij,k}$  between  $\bar{p}_{ij}$  and  $\bar{p}_k$  is given by

$$(3.44) \quad \bar{v}_{ij,k} = \frac{\sqrt{\lambda(1, \mu_{ij}^2, \mu_k^2)}}{1 - \mu_{ij}^2 - \mu_k^2}.$$

The definition of the parton momenta before the splitting is as follows

$$(3.45) \quad \begin{aligned} \bar{p}_k &:= \sqrt{\frac{\lambda(Q^2, m_{ij}^2, m_k^2)}{\lambda(Q^2, (p_i + p_j)^2, m_k^2)}} \left( p_k - \frac{Q \cdot p_k}{Q^2} Q \right) + \frac{Q^2 + m_k^2 - m_{ij}^2}{2Q^2} Q, \\ \bar{p}_{ij} &:= Q - \bar{p}_k, \\ \bar{p}_m &:= p_m, \quad \text{for } m \neq ij, k. \end{aligned}$$

Together with the definition  $s_{ij} := (p_i + p_j)^2$ , the spectator momentum  $\bar{p}_k$  can be written in terms of the rescaled masses  $\mu_i$

$$(3.46) \quad \bar{p}_k = \sqrt{\frac{\lambda(1, \mu_{ij}^2, \mu_k^2)}{\lambda(1, \frac{s_{ij}}{Q^2}, \mu_k^2)}} p_k + \left( 1 + \mu_k^2 - \mu_{ij}^2 - \sqrt{\frac{\lambda(1, \mu_{ij}^2, \mu_k^2)}{\lambda(1, \frac{s_{ij}}{Q^2}, \mu_k^2)}} \frac{2Q \cdot p_k}{Q^2} \right) \frac{Q}{2}.$$

### *Factorized Phase Space Measure*

According to [44], the three-parton phase space of  $p_i, p_j$ , and  $p_k$  is factorizable into a two-particle phase space of the momenta  $\bar{p}_{ij}$  and  $\bar{p}_k$  times a radiation phase space

$$(3.47) \quad d\phi_3(Q; p_i, p_j, p_k) = d\phi_2(Q; \bar{p}_{ij}, \bar{p}_k) d\phi_{\text{rad}}(p_i; \bar{p}_{ij}, \bar{p}_k).$$

The radiation phase space element in  $D$  dimensions is given by

$$\begin{aligned}
(3.48) \quad d\phi_{\text{rad}}(p_i; \bar{p}_{ij}, \bar{p}_k) &= \frac{1}{4} (2\pi)^{-3+2\epsilon} (Q^2)^{1-\epsilon} (1 - \mu_i^2 - \mu_j^2 - \mu_k^2)^{2-2\epsilon} \\
&\times [\lambda(1, \mu_{ij}^2, \mu_k^2)]^{\frac{-1+2\epsilon}{2}} d\Omega^{(D-3)} d\bar{z}_i dy_{ij,k} \\
&\times \Theta((\bar{z}_i - z_-)(z_+ - \bar{z}_i)) \Theta((y_{ij,k} - y_-)(y_+ - y_{ij,k})) \\
&\times [(z_+ - \bar{z}_i)(\bar{z}_i - z_-)]^{-\epsilon} (1 - y_{ij,k})^{1-2\epsilon} \\
&\times [\mu_i^2 + \mu_j^2 + (1 - \mu_i^2 - \mu_j^2 - \mu_k^2)y_{ij,k}]^{-\epsilon}
\end{aligned}$$

Here, the kinematic variables  $y_{ij,k}$  and  $\bar{z}_i$  are the same as in the definitions in (3.25). The element of solid angle  $d\Omega^{(D-3)}$  is perpendicular to  $\bar{p}_{ij}$  and  $\bar{p}_k$ . The integration boundaries of  $y_{ij,k}$  and  $\bar{z}_i$  are given in equation (5.13) of [44]:

$$\begin{aligned}
(3.49) \quad y_- &= \frac{2\mu_i\mu_j}{1 - \mu_i^2 - \mu_j^2 - \mu_k^2}, \\
y_+ &= 1 - \frac{2\mu_k(1 - \mu_k)}{1 - \mu_i^2 - \mu_j^2 - \mu_k^2}, \\
z_{\pm} := z_{\pm}(y_{ij,k}) &= \frac{2\mu_i^2 + (1 - \mu_i^2 - \mu_j^2 - \mu_k^2)y_{ij,k}}{2[\mu_i^2 + \mu_j^2 + (1 - \mu_i^2 - \mu_j^2 - \mu_k^2)y_{ij,k}]} (1 \pm v_{ij,i} v_{ij,k}).
\end{aligned}$$

The labels of the relative velocities stand for the parton momenta  $p_{ij} = p_i + p_j$ ,  $p_i$ , and  $p_k$ . They are obtained by (3.42). Their explicit forms read

$$\begin{aligned}
(3.50) \quad v_{ij,k} &= \frac{\sqrt{[2\mu_k^2 + (1 - \mu_i^2 - \mu_j^2 - \mu_k^2)(1 - y_{ij,k})]^2 - 4\mu_k^2}}{(1 - \mu_i^2 - \mu_j^2 - \mu_k^2)(1 - y_{ij,k})}, \\
v_{ij,i} &= \frac{\sqrt{(1 - \mu_i^2 - \mu_j^2 - \mu_k^2)^2 y_{ij,k}^2 - 4\mu_i^2 \mu_j^2}}{(1 - \mu_i^2 - \mu_j^2 - \mu_k^2)y_{ij,k} + 2\mu_i^2}.
\end{aligned}$$

In four dimensions, the radiation phase space element is obtained by setting  $\epsilon \rightarrow 0$ . The element of solid angle transforms in the same way as in the massless case. The radiation phase space, again, is parameterized by  $\bar{z}_i$ ,  $y_{ij,k}$  and  $\varphi$ . Its measure reads

$$\begin{aligned}
(3.51) \quad d\phi_{\text{rad}}(p_i; \bar{p}_{ij}, \bar{p}_k) &= \frac{Q^2}{4(2\pi)^3} \frac{1 - \mu_i^2 - \mu_j^2 - \mu_k^2}{\sqrt{\lambda(1, \mu_{ij}^2, \mu_k^2)}} \Theta(1 - \mu_i - \mu_j - \mu_k) \\
&\times d\varphi d\bar{z}_i dy_{ij,k} (1 - y_{ij,k}) \Theta(\varphi(2\pi - \varphi)) \\
&\times \Theta((\bar{z}_i - z_-)(z_+ - \bar{z}_i)) \Theta((y_{ij,k} - y_-)(y_+ - y_{ij,k})).
\end{aligned}$$



Defining  $s_{ijk} := Q^2$  and writing out the integrals, it can be written as

$$(3.52) \quad \int d\phi_{\text{rad}} = \frac{s_{ijk}}{32\pi^3} \frac{1 - \mu_i^2 - \mu_j^2 - \mu_k^2}{\sqrt{\lambda(1, \mu_{ij}^2, \mu_k^2)}} \int_{y_-}^{y_+} dy_{ij,k} (1 - y_{ij,k}) \int_{z_-}^{z_+} d\bar{z}_i \int_0^{2\pi} d\varphi.$$

### *Dipole Splitting Functions*

The dipole splitting functions  $V_{ij,k}$  for the different splittings can be found in [44]. In their spin-averaged form they read:

For  $Q \rightarrow g(p_i) + Q(p_j)$ ,  $m_i = 0$ ,  $m_j = m_{ij} = m_Q$ :

$$(3.53) \quad \langle V_{gQ,k} \rangle = 8\pi\mu^{2\epsilon}\alpha_s C_F \left[ \frac{2}{1 - \bar{z}_j(1 - y_{ij,k})} - \frac{\bar{v}_{ij,k}}{v_{ij,k}} \left( 1 + \bar{z}_j + \frac{m_Q^2}{p_i p_j} + \epsilon(1 - \bar{z}_j) \right) \right].$$

For  $g \rightarrow Q(p_i) + \bar{Q}(p_j)$ ,  $m_i = m_j = m_Q$ ,  $m_{ij} = 0$ :

$$(3.54) \quad \langle V_{Q\bar{Q},k} \rangle = 8\pi\mu^{2\epsilon}\alpha_s T_R \frac{1}{v_{ij,k}} \left[ 1 - \frac{2}{1 - \epsilon} \left( \bar{z}_i(1 - \bar{z}_i) - (1 - \xi)z_+z_- - \frac{\xi\mu_Q^2}{2\mu_Q^2 + (1 - 2\mu_Q^2 - \mu_k^2)y_{ij,k}} \right) \right].$$

For  $g \rightarrow g(p_i) + g(p_j)$ ,  $m_i = m_j = m_{ij} = 0$ :

$$(3.55) \quad \langle V_{gg,k} \rangle = 16\pi\mu^{2\epsilon}\alpha_s C_A \left[ \frac{1}{1 - \bar{z}_i(1 - y_{ij,k})} + \frac{2}{1 - (1 - \bar{z}_i)(1 - y_{ij,k})} + \frac{\bar{z}_i(1 - \bar{z}_i) - (1 - \xi)z_+z_- - 2}{v_{ij,k}} \right].$$

Here,  $\xi$  is a free constant parameter that redistributes non-singular contributions between the different terms in the subtraction method. It can simplify the expressions of the subtraction term ( $\xi = 0$ ) or its integral ( $\xi = 3/2$ ). The velocity factors in the definitions of the dipole splitting functions, i.e. the terms containing  $v_{ij,k}$  and  $\bar{v}_{ij,k}$ , are introduced to simplify their integration.



## CHAPTER 4

# Parton Showers

### Contents

---

<b>4.1. From Evolution Equation to Parton Branching</b>	<b>50</b>
4.1.1. The Sudakov Factor	54
4.1.2. Parton Shower and Monte Carlo Event Generation	54
<b>4.2. The Dipole Parton Shower</b>	<b>56</b>
4.2.1. Massless Final-State Partons	56
4.2.2. Massive Final-State Partons	59
4.2.3. Inserting the Particles after Branching	60

---

The parton shower [65–67] is a theoretical tool for modeling soft and collinear radiation off partons starting from the hard collision inside a collider. Thus, it increases the multiplicity of partons coming from the hard event. In this way, the situation inside a collider experiment can be modelled much more adequate than by only using fixed-order calculations.

Starting from the DGLAP equation [62–64], we present the classical approach to parton branching to gain a fundamental understanding of the parton shower. The description of the classical approach largely follows chapter five of [12].

In the second section of this chapter, we review the main aspects of the so-called dipole shower algorithm. The dipole shower makes use of the dipole splitting functions, discussed in Chapter 3. The possibility that such a shower might be practicable was first proposed by Nagy and Soper [68, 69]. The first implementations were provided by two different groups [10, 70]. We orientate us on the algorithm presented in [10].

## 4.1. FROM EVOLUTION EQUATION TO PARTON BRANCHING

In order to describe the branching of partons and end up with the parton shower, we start from the DGLAP equation for parton evolution [62–64]

$$(4.1) \quad t \frac{\partial}{\partial t} f(x, t) = \int_x^1 \frac{dz}{z} \frac{\alpha_s}{2\pi} P(z) f\left(\frac{x}{z}, t\right).$$

It describes the dependence of the parton distribution  $f(x, t)$  on the scale variable  $t$ . With  $P(z) := \hat{P}_+(z)$ , we denote the regularized Altarelli–Parisi splitting functions, using the plus-prescription defined by

$$(4.2) \quad \int_0^1 dx \frac{f(x)}{(1-x)_+} = \int_0^1 dx \frac{f(x) - f(1)}{(1-x)}.$$

Or in general

$$(4.3) \quad \int_0^1 dx f(x) [F(x)]_+ = \int_0^1 dx (f(x) - f(1)) F(x),$$

with

$$(4.4) \quad \int_0^1 dx [F(x)]_+ = 0.$$

By using the plus-prescription, the (soft gluon) singularity at  $z = 1$  is removed. Also, we do not encounter the singularity at  $z = 0$  due to the region of integration  $x < z < 1$ .

Next, we want to use MC simulation to obtain a numerical solution of the DGLAP equation in (4.1). We start with the definition of the Sudakov factor

$$(4.5) \quad \Delta(t) := \exp \left[ - \int_{t_0}^t \frac{dt'}{t'} \int dz \frac{\alpha_s}{2\pi} \hat{P}(z) \right].$$

To combine the Sudakov factor (4.5) with the DGLAP equation, we have to write (4.1) in terms of the unregularized splitting functions  $\hat{P}(z)$ , i.e. to eliminate the plus prescription. With

$$(4.6) \quad \begin{aligned} \int_0^1 dz \frac{f(z)}{z} P(z) &= \int_0^1 dz \left( \frac{f(x/z)}{z} - f(x) \right) \hat{P}(z) \\ &= \int_0^1 dz \frac{f(x/z)}{z} \hat{P}(z) - f(x) \int_0^1 dz \hat{P}(z), \end{aligned}$$

we obtain

$$(4.7) \quad t \frac{\partial}{\partial t} f(x, t) = \int \frac{dz}{z} \frac{\alpha_s}{2\pi} \hat{P}(z) f\left(\frac{x}{z}, t\right) - \frac{\alpha_s}{2\pi} f(x, t) \int dz \hat{P}(z).$$

Using the derivative of the Sudakov factor with respect to  $t$

$$(4.8) \quad \frac{t}{\Delta} \frac{\partial \Delta}{\partial t} = - \int dz \frac{\alpha_s}{2\pi} \hat{P}(z),$$

we find

$$(4.9) \quad t \frac{\partial}{\partial t} f(x, t) = \int \frac{dz}{z} \frac{\alpha_s}{2\pi} \hat{P}(z) f\left(\frac{x}{z}, t\right) - f(x, t) \frac{t}{\Delta} \frac{\partial \Delta}{\partial t}.$$

Multiplying with  $1/\Delta$  and using

$$(4.10) \quad \frac{\partial f}{\partial t \Delta} = \frac{1}{\Delta} \frac{\partial f}{\partial t} - \frac{f}{\Delta^2} \frac{\partial \Delta}{\partial t},$$

we finally arrive at the DGLAP equation using the Sudakov factor

$$(4.11) \quad t \frac{\partial}{\partial t} \frac{f(x, t)}{\Delta} = \int \frac{dz}{z} \frac{1}{\Delta} \frac{\alpha_s}{2\pi} \hat{P}(z) f\left(\frac{x}{z}, t\right).$$

Integrating this equation leads to

$$(4.12) \quad f(x, t) = \Delta(t) f(x, t_0) + \int_{t_0}^t \frac{dt'}{t'} \frac{\Delta(t)}{\Delta(t')} \int \frac{dz}{z} \frac{\alpha_s}{2\pi} \hat{P}(z) f\left(\frac{x}{z}, t'\right).$$

The first term on the right-hand-side stands for no branching from  $t_0$  to  $t$ . The quotient  $\Delta(t)/\Delta(t')$  in the second term gives the probability that no branching occurs between  $t'$  and  $t$ . Additionally, the entire second term gives the probability for the last branching to occur at  $t'$ .

The generalized forms of the Sudakov factor (4.5) and the DGLAP equation with the Sudakov factor (4.11) for the case of more involved partons are given

by

$$(4.13) \quad \begin{aligned} \Delta_i(t) &:= \exp \left[ - \sum_j \int_{t_0}^t \frac{dt'}{t'} \int dz \frac{\alpha_s}{2\pi} \hat{P}_{ji}(z) \right], \\ t \frac{\partial}{\partial t} \frac{f_i(x,t)}{\Delta_i} &= \sum_j \int \frac{dz}{z} \frac{1}{\Delta_i} \frac{\alpha_s}{2\pi} \hat{P}_{ij}(z) f_j \left( \frac{x}{z}, t \right), \end{aligned}$$

where  $\hat{P}_{ji}(z)$  is the unregularized  $i \rightarrow j$  splitting function.

To deal with the IR singularity at  $z = 1$  in the unregularized splitting functions, one introduces an IR cutoff. This ensures that resolvable branching only occurs at  $z < 1 - \epsilon(t)$ .

The equation in (4.12) can be identified as an integral equation of Fredholm type

$$(4.14) \quad \Phi(x) = f(x) + \lambda \int_a^b dy K(x, y) \Phi(y),$$

which can be solved by iteration using a Neumann series:

$$(4.15) \quad \begin{aligned} \Phi_n(x) &= \sum_{i=0}^n \lambda^i u_i(x), \quad \text{with} \\ u_n(x) &= \int_a^b \dots \int_a^b dy_1 \dots dy_n K(x, y_1) K(y_1, y_2) \dots K(y_{n-1}, y_n) f(y_n), \end{aligned}$$

with  $u_0(x) = f(x)$ . The first three iterations of the solution read

$$(4.16) \quad \begin{aligned} \Phi_0(x) &= f(x), \\ \Phi_1(x) &= f(x) + \lambda \int_a^b dy_1 K(x, y_1) f(y_1), \\ \Phi_2(x) &= f(x) + \lambda \int_a^b dy_1 K(x, y_1) f(y_1) \\ &\quad + \lambda^2 \int_a^b dy_1 dy_2 K(x, y_1) K(y_1, y_2) f(y_2). \end{aligned}$$

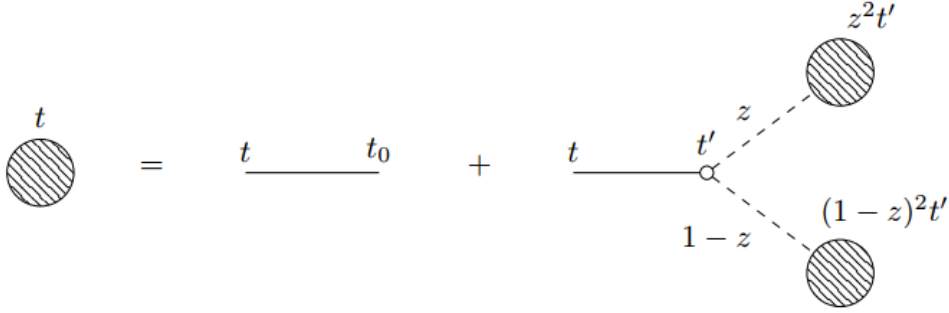


FIGURE 4.1. Graphical illustration of (4.18). The solid lines stand for no branching, the small empty dot is the splitting function and the blobs represent the parton distribution.

With this knowledge about the Fredholm integral equation, we can solve (4.12) iteratively. The first two iterations are given by

$$(4.17) \quad f_0(x, t) = f(x, t_0)\Delta(t),$$

$$(4.18) \quad f_1(x, t) = f(x, t_0)\Delta(t) + \frac{\alpha_s}{2\pi} \int_{t_0}^t \frac{dt'}{t'} \frac{\Delta(t)}{\Delta(t')} \int_x^1 \frac{dz}{z} \hat{P}(z) f\left(\frac{x}{z}, t_0\right) \Delta(t').$$

A graphical illustration of the first iteration (4.18) can be found in Figure 4.1. The term on the right-hand-side, as the first solid line in the figure, stands for no splitting between  $t$  and  $t_0$ . The second solid line represents no branching between  $t$  and  $t'$ , corresponding to  $\Delta(t)/\Delta(t')$  in (4.18). The small empty dot is the splitting into two partons carrying the momentum fractions  $z$  and  $1 - z$ , respectively.

The full solution of (4.12) may be written as

$$(4.19) \quad f_n(x, t) = \sum_n \frac{1}{n!} \log^n \left( \frac{t}{t_0} \right) A^n \otimes \Delta(t) f\left(\frac{x}{z}, t_0\right).$$

Here,

$$(4.20) \quad A = \int \frac{dz}{z} \hat{P}(z),$$

is a symbolic representation of the integral over  $z$  and  $\otimes$  indicates that a convolution has to be performed. We want to stress that this solution of the DGLAP equation (4.11) is a resummation to all orders in  $\alpha_s \log(t)$ .

#### 4.1.1. *The Sudakov Factor*

Let us add some notes on the Sudakov factor. We consider the Poisson distribution with zero mean

$$(4.21) \quad P(0, p) = e^{-p}.$$

If the Poisson distribution  $P(n, p)$  gives the probability to observe  $n$  emissions, then  $P(0, p)$  gives the probability for no emission. The one-branching probability in Poisson statistics reads

$$(4.22) \quad P(1, p) = p \cdot e^{-p},$$

which is exactly the first iteration of the Neumann series for the evolution equation (4.18). This underlines that the Sudakov factor gives the probability of evolving from  $t_0$  to  $t$  without any resolvable branching.

With the Sudakov factor, we sum enhanced virtual (parton loop) and real (parton emission) contributions to all orders. The virtual contributions are included by unitarity: the sum of the branching and the no-branching probabilities must be unity. Hence, the probability for resolvable branchings gives us the sum of virtual and unresolvable real contributions.

#### 4.1.2. *Parton Shower and Monte Carlo Event Generation*

In a parton shower, we use the evolution variable  $t$  to evolve from the scale  $Q$  of a hard event down to a cutoff scale  $Q_0$  by generating subsequent branchings. Typical choices for  $t$  are the opening angle between the two branched partons (angular ordered showers) or the transverse momentum of the daughter partons relative to the mother parton ( $k_T$  ordered showers). The parton shower algorithm yields a numerical implementation of the solution to the DGLAP equation. Using the algorithm, we generate an event with a much higher parton multiplicity than the original hard event.

A typical parton shower algorithm starts at a scale  $t_1$  and proceeds as follows:

- (1) Select scale  $t_2$  at which the next branching occurs:  
Take a uniformly distributed number  $r_1 \in [0, 1]$  and solve

$$\frac{\Delta(t_1)}{\Delta(t_2)} = r_1.$$



(2) If  $t_2 < Q_0 \rightarrow$  shower terminates

(3) Generate value of  $z$ :

Random number  $r_2 \in [0, 1]$ , solve

$$\int_{z_-(t_2)}^z dz' \frac{\alpha_s}{2\pi} \hat{P}(z') = r_2 \int_{z_-(t_2)}^{z_+(t_2)} dz' \frac{\alpha_s}{2\pi} \hat{P}(z').$$

(4) Select the azimuthal angle  $\varphi$ :

Random number  $r_3 \in [0, 1]$ :

$$\varphi = 2\pi r_3.$$

(5) Set  $t_1 = t_2$

$\hookrightarrow$  Go to step 1

Implementing this algorithm into a computer program, it is possible to generate a parton shower simulation from a hard event. Note that it is also possible to implement the algorithm using the spin-dependent form of the splitting functions. This leads to spin-correlations (see [71] and references therein), e.g. without the approximation of spin-averaged splitting functions, the azimuthal angle has to be chosen in a weighted way, i.e. it is not uniformly distributed between zero and  $2\pi$ .

Today, there exist many different general-purpose event generators, such as HERWIG [1–4], PYTHIA [5, 6], and SHERPA [7, 8], just to mention a few. Those MC event generators do not only contain parton showering but also come with tools for the generation of the hard event, hadronization, and particle decay.

Another important topic, when talking about MC event generators, is the matching of the parton shower to NLO calculations. Due to the fact that NLO calculations include a real radiation term (cf. Chapter 3), it may come to a double counting of this emission, when naively applying the parton shower. There exist several methods, used in today's event generators, to overcome this problem [61, 72–74]. For example, in the POWHEG formalism [61, 72, 73] the hardest emission is generated first, using NLO accuracy. Subsequent radiations can, then, be generated using a standard MC parton shower program.

## 4.2. THE DIPOLE PARTON SHOWER

The idea that the splitting functions of the Catani–Seymour dipole subtraction method (cf. Chapter 3) might be sufficient to define a parton shower algorithm first arose in [68, 69]. First implementations were presented by two different groups [10, 70]. Since we use the implementation of the shower algorithm in [10] to perform our analysis presented in Chapter 5, we focus on the shower algorithm presented there. Again, as for the dipole formalism in Chapter 3, we restrict our discussion to the case of final-state dipole showers. This corresponds to the situation found in electron-positron colliders. The extension to initial-state partons can be found in [10].

## 4.2.1. Massless Final-State Partons

A suitable choice for the evolution variable is

$$(4.23) \quad t = \log \left( \frac{-k_{\text{T}}^2}{Q^2} \right),$$

where  $k_{\text{T}}$  is the splitting's transverse momentum and  $Q^2$  is a fixed reference scale.

In the leading color approximation, the emitter and the spectator of the splitting are always adjacent in the cyclic order of the color cluster that is assigned to the final-state partons of the hard event.

For the dipole phase space  $\Phi_{\text{rad}}$  it is convenient to define the variable  $\kappa$  that is proportional to the transverse momentum of the splitting:

$$(4.24) \quad \kappa = 4 \frac{(-k_{\text{T}}^2)}{(\bar{p}_{ij} + \bar{p}_k)^2},$$

and is related to  $y_{ij,k}$  via

$$(4.25) \quad y_{ij,k} = \frac{\kappa}{4\bar{z}_i(1 - \bar{z}_i)}.$$

Hence, we can substitute  $\kappa$  for  $y_{ij,k}$  in the phase space measure (3.35) and obtain

$$(4.26) \quad \int d\phi_{\text{rad}} = \frac{s_{ijk}}{16\pi^2} \int_0^1 d\kappa \int_{z_-(\kappa)}^{z_+(\kappa)} d\bar{z}_i \frac{1}{4\bar{z}_i(1 - \bar{z}_i)} \left( 1 - \frac{\kappa}{4\bar{z}_i(1 - \bar{z}_i)} \right),$$

with

$$(4.27) \quad z_{\pm}(\kappa) = \frac{1}{2} (1 \pm \sqrt{1 - \kappa}).$$

The probability that the pair of an emitter  $\bar{i}\bar{j}$  and a spectator  $\bar{k}$  does not emit an additional parton  $j$  while evolving from  $t_1$  to  $t_2$  is given by the Sudakov factor

$$(4.28) \quad \Delta_{ij,k}(t_1, t_2) = \exp \left( - \int_{t_2}^{t_1} dt \mathcal{C}_{\bar{i}\bar{j},\bar{k}} \int d\phi_{\text{rad}} \delta(t - T_{\bar{i}\bar{j},\bar{k}}) \mathcal{P}_{ij,k} \right).$$

Here,  $\mathcal{C}_{\bar{i}\bar{j},\bar{k}}$  is a color-factor that, in the leading color approximation, is only non-zero if  $\bar{i}\bar{j}$  and  $\bar{k}$  are adjacent in a color cluster. Corresponding to the color-factor in the dipole formula (3.21) it reads

$$(4.29) \quad \mathcal{C}_{\bar{i}\bar{j},\bar{k}} = \frac{\mathbf{T}_{\bar{k}} \cdot \mathbf{T}_{ij}}{\mathbf{T}_{ij}^2} = \begin{cases} 1/2 & \text{for } \bar{i}\bar{j} = g, \\ 1 & \text{for } \bar{i}\bar{j} = q, \bar{q}, \end{cases}$$

$T_{\bar{i}\bar{j},\bar{k}}$  depends on the invariant mass  $s_{ijk}$  of the dipole and the phase space variable  $\kappa$ :

$$(4.30) \quad T_{\bar{i}\bar{j},\bar{k}} = \log \left( \frac{\kappa s_{ijk}}{4 Q^2} \right).$$

Using the delta distribution in (4.28), we can perform the integration over  $\kappa$  and keep the integration over  $t$  and  $\bar{z}_i$ . For  $\kappa$ , we find the  $t$  dependence

$$(4.31) \quad \kappa(t) = \frac{4Q^2 e^t}{s_{ijk}}.$$

The splitting function  $\mathcal{P}_{ij,k}$  in the Sudakov factor (4.28) is given by

$$(4.32) \quad \mathcal{P}_{ij,k} = \frac{\langle V_{ij,k} \rangle}{s_{ij} - m_{ij}^2} \cdot \Theta(\langle V_{ij,k} \rangle),$$

where the theta function ensures that the splitting probability does not become negative. The spin-averaged dipole splitting functions  $\langle V_{ij,k} \rangle$  for the different splittings were given earlier in (3.36)-(3.38).

The total Sudakov factor that gives the probability to evolve from a scale  $t_1$  to a scale  $t_2$  without any resolvable branching is given by the product of the Sudakov factors for each individual splitting type

$$(4.33) \quad \Delta(t_1, t_2) = \prod_{\bar{i}\bar{j},\bar{k}} \Delta_{\bar{i}\bar{j},\bar{k}}(t_1, t_2).$$

If the parton  $\bar{i}j$  can emit different partons  $j$ , and eventually change its flavor, as for  $g \rightarrow q\bar{q}$ , the Sudakov factor on the right hand side factorizes as

$$(4.34) \quad \Delta_{\bar{i}j, \bar{k}}(t_1, t_2) = \prod_j \Delta_{ij, k}(t_1, t_2).$$

Using the Sudakov factor, the probability for a splitting to occur at a scale  $t_2$  is given by

$$(4.35) \quad \sum_{\bar{i}j, \bar{k}} \sum_j C_{\bar{i}j, \bar{k}} \int d\phi_{\text{rad}} \delta(t - T_{\bar{i}j, \bar{k}}) \mathcal{P}_{ij, k} \Delta(t_1, t_2).$$

With these ingredients, we are now able to define a shower algorithm. For convenience, we set  $z := \bar{z}_i$ . In the algorithm, the strong coupling,  $\alpha_s$ , is evaluated at the scale  $\mu^2 = -k_T^2 = \frac{\kappa}{4} s_{ijk}$ .

### *The Shower Algorithm*

Start at a scale  $t_1$  and proceed as follows:

- (1) Select next dipole to branch and scale  $t_2$  at which this occurs:  
Take a uniformly distributed number  $r_{1, ij, k} \in [0, 1]$  for each dipole and solve

$$\Delta_{ij, k}(t_1, t_{2, ij, k}) = r_{1, ij, k}.$$

The dipole with the maximum value of  $t_{2, ij, k}$  is the dipole that emits an additional particle at

$$t_2 = \max(t_{2, ij, k}).$$

- (2) If  $t_2 < Q_0$  (cutoff scale)  $\rightarrow$  shower terminates
- (3) Generate value of  $z$ :

Random number  $r_2 \in [0, 1]$ , solve:

$$\int_{z_-(t_2)}^z dz' \mathcal{J}(t_2, z') \mathcal{P}_{ij, k} = r_2 \int_{z_-(t_2)}^{z_+(t_2)} dz' \mathcal{J}(t_2, z') \mathcal{P}_{ij, k},$$

with Jacobian:

$$\mathcal{J}(t_2, z) = \frac{\kappa(t_2)}{4z(1-z)} \left( 1 - \frac{\kappa(t_2)}{4z(1-z)} \right).$$

- (4) Select azimuthal angle  $\varphi$ :  
Random number  $r_3 \in [0, 1]$ :

$$\varphi = 2\pi r_3.$$

- (5) Use the three kinematical variables  $t_2$ ,  $z$ , and  $\varphi$  to insert the new parton  $j$  and replace the four-momenta  $\bar{p}_{ij}$  and  $\bar{p}_k$  with  $p_i$  and  $p_k$  (see Section 4.2.3)
- (6) Set  $t_1 = t_2$   
↪ Go to step 1

#### 4.2.2. Massive Final-State Partons

Now, we discuss the massive case. For simplification of the notation and readability, we set  $\bar{z}_i = z$  and  $y_{ij,k} = y$  in the following.

The evolution variable in the massive case may be chosen as

$$(4.36) \quad t = \log \left( \frac{-k_{\text{T}}^2 + (1-z)^2 m_i^2 + z^2 m_j^2}{Q^2} \right).$$

The Sudakov factor is defined as for the massless case in (4.28), i.e.

$$(4.37) \quad \Delta_{ij,k}(t_1, t_2) = \exp \left( - \int_{t_2}^{t_1} dt \mathcal{C}_{\bar{i}\bar{j},\bar{k}} \int d\phi_{\text{rad}} \delta(t - T_{\bar{i}\bar{j},\bar{k}}) \mathcal{P}_{ij,k} \right).$$

The radiation phase space is given by (3.52)

$$(4.38) \quad \int d\phi_{\text{rad}} = \frac{s_{ijk}}{16\pi^2} \frac{(1 - \mu_i^2 - \mu_j^2 - \mu_k^2)^2}{\sqrt{\lambda(1, \mu_{ij}^2, \mu_k^2)}} \int_{y_-}^{y_+} dy (1-y) \int_{z_-(y)}^{z_+(y)} dz,$$

with the integration boundaries in (3.49) and the definition of the rescaled parton mass (3.41). In the massive case,  $T_{\bar{i}\bar{j},\bar{k}}$  is given by

$$(4.39) \quad T_{\bar{i}\bar{j},\bar{k}} = \log \left( \frac{(s_{ijk} - m_i^2 - m_j^2 - m_k^2)yz(1-z)}{Q^2} \right).$$

Again, we can perform the integration over  $y$  by substituting in  $\kappa$ , using the delta distribution and keeping the integration over  $t$  and  $z$ . Hence, we obtain

$$(4.40) \quad \int_{y_-}^{y_+} dy (1-y) \int_{z_-(y)}^{z_+(y)} dz \delta(t - T_{i\bar{j},\bar{k}}) = \int_{z_{\min}}^{z_{\max}} dz y(1-y),$$

with the  $\kappa$  dependence of  $y$  in (4.25). The delta distribution yields the  $t$  dependence of  $\kappa$  as

$$(4.41) \quad \kappa(t) = \frac{4Q^2 e^t}{s_{ijk} - m_i^2 - m_j^2 - m_k^2}.$$

The integration boundaries for  $z$ , i.e.  $z_{\min}$  and  $z_{\max}$  are constrained by the physical region

$$(4.42) \quad (1-y)^2 \left[ \frac{\kappa}{4} - (1-z)^2 \bar{m}_i^2 - z^2 \bar{m}_j^2 \right] - y^2 \bar{m}_k^2 + 4\bar{m}_i^2 \bar{m}_j^2 \bar{m}_k^2 \geq 0,$$

where the barred masses are defined by

$$(4.43) \quad \bar{m}_l^2 := \frac{m_l^2}{s_{ijk} - m_i^2 - m_j^2 - m_k^2} \text{ for } l \in \{i, j, k\}.$$

Equation (4.42) can be solved numerically for  $z_{\min}$  and  $z_{\max}$ .

With this knowledge, the parton shower algorithm for the massless case can also be applied for the massive case. In this case, the Jacobian reads

$$\mathcal{J}(t_2, z) = \frac{(1 - \mu_i^2 - \mu_j^2 - \mu_k^2)^2}{\sqrt{\lambda(1, \mu_{ij}^2, \mu_k^2)}} \frac{\kappa(t_2)}{4z(1-z)} \left( 1 - \frac{\kappa(t_2)}{4z(1-z)} \right).$$

### 4.2.3. Inserting the Particles after Branching

To insert the particles after the branching, i.e. assign the momenta  $p_i$ ,  $p_j$ , and  $p_k$ , we have to invert the mapping of the dipole subtraction method

$$(4.44) \quad \{p_1, \dots, p_{n+1}\} \rightarrow \{\bar{p}_1, \dots, \bar{p}_n, \Phi_{\text{rad}}\}.$$

This means, it is necessary to express the momenta of the particles  $i$ ,  $j$ , and  $k$  after the splitting in terms of the momenta of the particles  $i\bar{j}$  and  $\bar{k}$  before the splitting and the radiation variables  $\Phi_{\text{rad}}$ .

*Massless Case*

To obtain the momenta of the partons  $i$ ,  $j$ , and  $k$  after branching, we consider the system in the rest frame of  $P := \bar{p}_i + \bar{p}_k$ . This is achieved by the boost that can be found in Appendix B.1. Additionally, we rotate the system around the  $z$ -axis and the  $y$ -axis such that the momentum  $\bar{p}_k$  points along the  $z$ -axis. The transformed four-momentum can be written as

$$(4.45) \quad p'_m = \Lambda_y^r(-\theta_y) \Lambda_z^r(-\phi_z) \Lambda^b(\hat{P}) p_m, \quad m \in \{i, j, k\}.$$

The explicit form of the transformations can be found in Appendix B.1. Working in this frame, the four-momenta of the particles after branching take the form

$$(4.46) \quad \begin{aligned} p'_i &= E_i (1, \sin(\theta_i) \cos(\phi + \pi), \sin(\theta_i) \sin(\phi + \pi), \cos(\theta_i)), \\ p'_j &= E_j (1, \sin(\theta_j) \cos(\phi), \sin(\theta_j) \sin(\phi), \cos(\theta_j)), \\ p'_k &= E_k (1, 0, 0, 1). \end{aligned}$$

The energies are defined through the kinematical invariants

$$(4.47) \quad \begin{aligned} E_i &= \frac{s_{ij} + s_{ik}}{2\sqrt{s_{ijk}}}, \\ E_j &= \frac{s_{ij} + s_{jk}}{2\sqrt{s_{ijk}}}, \\ E_k &= \frac{s_{ik} + s_{jk}}{2\sqrt{s_{ijk}}}, \end{aligned}$$

and we have

$$(4.48) \quad \theta_i = \arccos\left(1 - \frac{s_{ik}}{2E_i E_k}\right), \quad \theta_j = \arccos\left(1 - \frac{s_{jk}}{2E_j E_k}\right).$$

To obtain the momenta  $p_i$ ,  $p_j$ , and  $p_k$ , we have to transform (4.46) back to the original frame by applying

$$(4.49) \quad p_m = \Lambda^b(P) \Lambda_z^r(\phi_z) \Lambda_y^r(\theta_y) p'_m, \quad m \in \{i, j, k\},$$

with the rotational angles

$$(4.50) \quad \theta_y = \arccos\left(\frac{2\tilde{E}_k E'_k - 2\tilde{\vec{p}}_k \cdot \vec{p}'_k}{2|\tilde{\vec{p}}_k| |\vec{p}'_k|}\right), \quad \phi_z = \arctan\left(\frac{\tilde{p}_k^y}{\tilde{p}_k^x}\right).$$

By  $\tilde{\vec{p}}_k$  and  $\tilde{E}_k$ , we denote the four-momentum and the energy of the momentum  $\bar{p}_k$  that has already been boosted into the rest frame of  $P$ .

*Massive Case*

For the massive case, the momenta  $p_i$ ,  $p_j$  and  $p_k$  are obtained in a way similar to the massless case. Again, the subsequent transformations of (4.45) are applied to work in the rest frame of  $P$ , such that the spatial components of  $\vec{p}_k$  point along the  $z$ -axis.

In this particular coordinate system the transformed momenta of  $i$ ,  $j$  and  $k$  read

$$(4.51) \quad \begin{aligned} p'_i &= |\vec{p}_i| \left( \frac{E_i}{|\vec{p}_i|}, \sin(\theta_i) \cos(\phi + \pi), \sin(\theta_i) \sin(\phi + \pi), \cos(\theta_i) \right), \\ p'_j &= |\vec{p}_j| \left( \frac{E_j}{|\vec{p}_j|}, \sin(\theta_j) \cos(\phi), \sin(\theta_j) \sin(\phi), \cos(\theta_j) \right), \\ p'_k &= |\vec{p}_k| \left( \frac{E_k}{|\vec{p}_k|}, 0, 0, 1 \right), \end{aligned}$$

with the energies

$$(4.52) \quad \begin{aligned} E_i &= \frac{s_{ij} - 2p_j p_k + m_i^2 - m_j^2 - m_k^2}{2\sqrt{s_{ijk}}}, \\ E_j &= \frac{s_{ij} - 2p_i p_k - m_i^2 + m_j^2 - m_k^2}{2\sqrt{s_{ijk}}}, \\ E_k &= \frac{s_{ik} - 2p_i p_j - m_i^2 - m_j^2 + m_k^2}{2\sqrt{s_{ijk}}}. \end{aligned}$$

In the massive case, the angles of (4.48) are given by

$$(4.53) \quad \theta_i = \arccos \left( \frac{2E_i E_k - 2p_i p_k}{2|\vec{p}_i| |\vec{p}_k|} \right), \quad \theta_j = \arccos \left( 1 - \frac{2E_j E_k - 2p_j p_k}{2|\vec{p}_j| |\vec{p}_k|} \right).$$

Transforming  $p'_i$ ,  $p'_j$ , and  $p'_k$  back to the original frame yields the final form of the momenta after branching.



## CHAPTER 5

# The Top Quark Mass in the Dipole Shower

### Contents

---

<b>5.1. General Considerations</b>	<b>64</b>
5.1.1. Status Quo	65
5.1.2. Cutoff Dependence	67
<b>5.2. Analytic Computations</b>	<b>68</b>
5.2.1. Thrust	68
5.2.2. Thrust in soft-collinear effective theory (SCET)	69
5.2.3. Coherent Branching	72
5.2.4. Cutoff Dependence of $\tau_{\text{peak}}$	76
<b>5.3. Analyses and Results</b>	<b>78</b>

---

In this chapter, we discuss some of the general properties of the top quark and the issues that arise within measurements and the theoretical description of its mass. In Section 2.5, we learned that the mass, that is measured in an experiment, is subject to renormalization. Thus, its actual value depends on the chosen renormalization scheme. In this context, we focus on the difficulty of identifying the top quark mass in a parton shower with the mass in a quantum field theoretical renormalization scheme.

Additionally, we pick up the idea of [9] to analyze the peak position of an event shape, namely the thrust distribution, in order to deduce general statements on the dependence of the top quark mass on parameters of the parton shower. For this, we use the implementation of the dipole shower of Section 4.2 to analyze the thrust distribution for different scenarios. Our analyses and results can be found in Section 5.3.

## 5.1. GENERAL CONSIDERATIONS

The mass of the top quark  $m_t$  is one of the fundamental parameters in the SM. From Table 2.1, we can see that, with a mass around 173 GeV, it is by far the heaviest elementary particle. However, the lifetime of the top quark is extremely short. The fact that it is even shorter than the time scale for hadronization yields that the top quark cannot form bound states before it decays. These properties give a strong reason for the top quark to be treated perturbatively.

Despite the importance of the precise knowledge of the value of the top quark mass, the uncertainties on the measured values are still high. These uncertainties arise from the fact that  $m_t$  cannot be measured directly. The measurements rather rely on theoretical input that is used to reconstruct the kinematic properties of a top particle from experimental data. Two commonly used methods of direct reconstruction are the matrix element method and the template method. At present, the most precise measurements from reconstruction come from CMS [75] and ATLAS [76], both using LHC data, and from the Tevatron [77]. The measurements yield

$$\begin{aligned}
 m_t &= 172.44 \pm 0.13 \text{ (stat)} \pm 0.47 \text{ (syst)} \text{ GeV}, \\
 (5.1) \quad m_t &= 172.84 \pm 0.34 \text{ (stat)} \pm 0.61 \text{ (syst)} \text{ GeV}, \\
 m_t &= 173.34 \pm 0.64 \text{ GeV},
 \end{aligned}$$

for CMS, ATLAS, and Tevatron, respectively.

As mentioned above, one issue with these reconstruction methods is that they require theoretical input. Since the theoretical computations, entering the analyses, are based on MC event generators, the measured top quark mass depends on the properties of the MC generator in use. Therefore, the mass of the top quark, that is obtained by analysing experimental data through MC event generators, is often referred to as Monte Carlo mass  $m_t^{\text{MC}}$ .

A typical MC generator starts with the basic hard process that can be calculated analytically (cf. Chapter 3). From there, we apply a parton shower that models collinear and soft radiation. Note that the parton shower starts at the scale of the hard event  $Q$  and evolves down to a user-defined cutoff  $Q_0$ .

The shower cutoff is, typically, chosen to be around 1 GeV, where the perturbative region ends and the event has to be treated non-perturbatively. In this

non-perturbative region, one has to deal with the problems of hadronization and decay.

The different phases of an MC event generator apply to different scales. This makes it possible to, more or less accurately, assign one effective theory to each component. The theory corresponding to the hard process scales from  $Q$  down to the top mass  $m_t$  is QCD. For the phase of the parton shower, the effective theory at hand is SCET. The corresponding scales start at the top mass and go down to the top width  $\Gamma_t$ . In the region between the top width and  $\Lambda_{\text{QCD}}$  the preferred theory is heavy quark effective theory (HQET) [78, 79] adapted for top quarks (top-HQET) [80, 81].

### 5.1.1. *Status Quo*

Until today, it is unclear how the top mass obtained from direct reconstruction, using a certain MC event generator, can be related to a well-defined (renormalized) mass in a quantum field theoretical context. To solve this problem, many aspects have to be taken into account. The mass  $m_t^{\text{MC}}$  depends on the specific implementation of the event generator at hand. Hence, it is natural to ask, on the one hand, how the usage of different event generators, e.g. PYTHIA, HERWIG, etc. (cf. Chapter 4), or hadronization schemes affects the outcome, and on the other hand, how  $m_t^{\text{MC}}$  depends on certain parameters inside the MC event generator (e.g.  $Q_0, \Gamma_t$ ).

So far, there have been different studies making various efforts to quantify the relation between the MC mass and its field theoretical counterpart [82–87]. In most of these studies, the attempt was made to find a relation between  $m_t^{\text{MC}}$  and the pole mass or the MSR mass (cf. Section 2.5).

Similarly to (2.101), the conversion from the pole mass scheme to any short-distance mass scheme, that depends on an additional IR scale  $R$ , reads

$$(5.2) \quad m_t^{\text{pole}} = m_t(R, \mu) + \delta m_t(R, \mu),$$

where the series expansion of the second term on the right-hand-side is given by

$$(5.3) \quad \delta m_t(R, \mu) = R \sum_{n=1}^{\infty} \sum_{k=0}^{\infty} a_{nk} \left( \frac{\alpha_s(\mu)}{4\pi} \right)^n \log^k \left( \frac{\mu}{R} \right).$$

Here, the coefficients  $a_{nk}$  are finite real numbers.

Assuming that the mass in the MC generator plays the role of a short-distance mass implies that the relation in (5.2) also holds for  $m_t^{\text{MC}}$ .

In [82] it was argued that the conversion from the MC mass to  $m_t^{\text{pole}}$  comes with the series expansion of  $\delta m_t^{\text{MC}}(R, \mu)$  of the form

$$(5.4) \quad \delta m_t^{\text{MC}}(R_{\text{sc}}) = R_{\text{sc}} \left( \frac{\alpha_s(\mu)}{\pi} \right) + \dots,$$

where  $R_{\text{sc}}$  is closely related to the cutoff  $Q_0$  implemented in the parton shower program and is around 1 GeV. This conjecture is based on the analogy of the components of an MC event generator to the QCD factorization for jet masses in the peak region initiated by boosted top quarks [80, 81]. The corresponding analyses have been carried out in SCET and boosted heavy quark effective theory (bHQET).

Additionally, it is stated in [82] that the MC mass can be identified with the MSR mass at a low scale  $R$  between 1 and 9 GeV

$$(5.5) \quad m_t^{\text{MC}}(R_{\text{sc}}) = m_t^{\text{MSR}}(R = 1, \dots, 9 \text{ GeV}).$$

The author of [83] argued that the effects of hadronization models lead to properties of  $m_t^{\text{MC}}$  that seem analogous to the mass of a top quark meson. The considerations are based on the concept of heavy quark symmetry [88, 89]. It is conjectured that the conversion term  $\delta m_t^{\text{MC}}(R)$  in

$$(5.6) \quad m_t^{\text{MC}} = m_t^{\text{MSR}}(R = 1 \text{ GeV}) + \delta m_t^{\text{MC}}(R = 1 \text{ GeV}),$$

is subject to perturbative as well as non-perturbative effects. From a comparison of  $B$  meson and bottom quark masses, the author comes to the conclusion that the value of  $\delta m_t^{\text{MC}}(R)$  is around 1 GeV. It is stressed that this uncertainty of  $\mathcal{O}(1 \text{ GeV})$  is not subject of the theoretical uncertainty in the MC parameter  $m_t^{\text{MC}}$  but in the conversion from  $m_t^{\text{MC}}$  to a well-defined mass scheme, as for example the MSR scheme.

First steps towards the numerical evaluation of the conversion parameter  $\delta m_t^{\text{MC}}$  have been made in [90–92].

In [91] a calibration procedure for the MC mass in the process  $e^+e^- \rightarrow$  boosted  $t\bar{t}$  was used to find the numerical relation

$$(5.7) \quad m_t^{\text{MC}} = m_t^{\text{MSR}}(R = 1 \text{ GeV}) + (0.18 \pm 0.22) \text{ GeV}.$$

In this analysis, the factorized hadron level predictions for the 2-jettiness [93] distribution in the peak region [80, 81] are calculated at next-to-next-to-leading logarithmic (NNLL) and  $\mathcal{O}(\alpha_s)$  accuracy. The results are used to fit the predictions obtained from the MC event generator PYTHIA 8.2 to them as a calibration procedure.

Expanding this procedure to hadron collisions, as found at the LHC, is a highly non-trivial task. A first step in this direction has been made in [92]. There, an observable is constructed that is highly kinematically sensitive to the top mass, the soft-drop groomed hadron level jet mass distribution in boosted top production [94, 95]. Additionally, they provide a factorization formula at next-to-leading logarithmic (NLL) accuracy that makes it possible to fit MC predictions to it. The corresponding analyses are less precise than for the case of electron-positron annihilation [91] but show compatible results.

Additional studies investigating the sources of uncertainties in the determination of the top quark mass from reconstruction or using alternative methods can be found in [96–98] and references therein.

### 5.1.2. *Cutoff Dependence*

Regarding the considerations above, it becomes clear that the investigation of the precise field theoretical meaning of  $m_t^{\text{MC}}$  is far from being completed. Besides the question how the MC mass is related to a field theoretical mass scheme, another important task is to quantify the dependence of  $m_t^{\text{MC}}$  on the various parameters of the parton shower, as well as on its specific implementation.

In the following, we focus on the question how a change of the cutoff parameter  $Q_0$  affects the outcome of a parton shower based on the Catani-Seymour subtraction method (cf. Section 4.2). In [9] the dependency of the peak position of the hemisphere jet mass distribution  $\tau$  on the value of the shower cutoff in HERWIG is analyzed. We stress that the use of HERWIG implies the use of an angular ordered shower algorithm.

For this, analytic solutions of the dependency of the peak position of  $\tau$  on  $Q_0$  are derived in two different approaches. Firstly, utilizing the factorized analytic calculations of SCET. Secondly, using the analytic solution of the parton shower evolution based on the coherent branching formalism which is equivalent to the angular ordered shower algorithm.

The main result of this analysis in [9] is that the resulting  $Q_0$  dependence of the peak position of  $\tau$  coincides for both analytic approaches. Additionally, the simulations in HERWIG agree with the results of the analytic examination.

## 5.2. ANALYTIC COMPUTATIONS

Before we come to our analysis of the cutoff dependence of the thrust variable in the dipole shower formalism, we sketch the analytic computations in [9] and present their results. We stress that we only present the basic characteristics of SCET and the coherent branching formalism that are required to understand the results of the corresponding analyses. A full description of SCET or the coherent branching formalism goes beyond the scope of this thesis. An introduction to SCET can be found in [99] or in some textbooks on QFT (e.g. [13]). Chapter five of [12] provides a description of the coherent branching formalism. Note that we restrict our considerations on the case of massless partons in  $e^+e^-$  annihilation.

### 5.2.1. Thrust

The observable analyzed in [9] is what they call the “squared hemisphere mass sum”. It is defined by

$$(5.8) \quad \tau := \frac{M_1^2 + M_2^2}{Q^2},$$

where  $Q$  denotes the center-of-mass energy and  $M_1$  and  $M_2$  are the masses of the hemispheres that are defined with respect to the thrust axis. Relevant for the analyses is the location of the distribution’s peak  $\tau_{\text{peak}}$ . It is strongly affected by configurations containing two jets that are back-to-back. These contributions arise from the LO production of a quark-antiquark pair.

We stress that, in the case of massless quark production, the squared hemisphere mass sum in the peak region is equivalent to the typical thrust variable [100]

$$(5.9) \quad \tau^{\text{thrust}} := 1 - T := 1 - \max_{\vec{n}} \frac{\sum_j |\vec{p}_j \cdot \vec{n}|}{\sum_j |\vec{p}_j|},$$

where the maximum defines the thrust axis  $\vec{n}$ .

This equivalence is at least valid concerning the factors that effect the position and shape of the peak for large  $Q$ , i.e. the structure of the singularities in the limit  $\tau \rightarrow \tau_{\min}$  and the large logarithmic behavior. Hence, the squared hemisphere mass sum as well as the classic thrust variable are both simply denoted as “thrust” in the following.

For massless quark production, the region of the resonance peak is close to  $\tau = 0$ . This location is shifted to positive values due to non-perturbative effects. The size of this shift is of order  $\mathcal{O}(\Lambda/Q)$ , where  $\Lambda \approx 1$  GeV [101].

Let us shortly note on the procedure for massive quarks. In this case the studied variable  $\tau$  is closely related to the 2-jettiness observable [93]. The peak is located around  $\tau = 2m_Q^2/Q^2$ . For top quark examinations the rescaled thrust variable

$$(5.10) \quad M_\tau := \frac{Q^2\tau}{2m_Q},$$

is also a convenient choice as an observable. Its peak is close to  $M_\tau = m_Q$ .

The thrust distribution makes a reasonable choice for the study of the cutoff dependence of the top mass in a parton shower because the effects of the decay of the top quark are power suppressed in the thrust distribution. Additionally, there exist analytical calculations for the thrust distribution based on factorization, that the parton shower outcome can be compared to.

### 5.2.2. Thrust in SCET

Here, we review the computations for the resummation of the thrust distribution in the peak region in SCET. This calculation requires the summation of terms that have singularities at  $\tau \rightarrow \tau_{\min}$  and contain large logarithms. In [102] first calculations regarding perturbative QCD have been studied at NLL. For soft-collinear factorization, the results at NLL+ $\mathcal{O}(\alpha_s)$  can be found in [103]. The extension to the order N<sup>3</sup>LL+ $\mathcal{O}(\alpha_s^3)$  was performed in [101, 104]. In [9] the notation of [101] was adopted, which we will also stick to.

In this notation, and in the context of soft-collinear factorization, the hadron level thrust distribution in the peak region takes the form

$$(5.11) \quad \frac{d\sigma}{d\tau}(\tau, Q) = \int_0^{Q\tau} d\ell \frac{d\hat{\sigma}_s}{d\tau} \left( \tau - \frac{\ell}{Q}, Q \right) S_{\text{mod}}(\ell).$$

In this context,  $d\hat{\sigma}/d\tau$  denotes the resummed factorized singular partonic QCD cross section. In addition,  $S_{\text{mod}}(\ell)$  is the soft model shape function. It describes non-perturbative effects and must satisfy the following conditions:

It must have support for positive  $\ell$ , be peaked around  $\ell = 1$  GeV and fall strongly for  $\ell \rightarrow \infty$ . Additionally,  $S_{\text{mod}}$  should vanish at  $\ell = 0$ .

The soft model shape function causes a smearing of the partonic thrust distribution that shifts the position of the peak to the positive direction. Thus, it is essential for the analysis of thrust distribution in the resonance region. Since we only study the relative dependence of  $\tau_{\text{peak}}$  on the cutoff, the exact form of the soft model shape function is not relevant.

The form of the soft model shape function that is used in [9] as well as in our analysis is given by

$$(5.12) \quad S_{\text{mod}}(\ell) = \frac{128}{3} \frac{\ell^3}{\Lambda_m} \exp\left(-\frac{4\ell}{\Lambda_m}\right),$$

where  $\Lambda_m$  is a smearing parameter, that is varied between 1 and 5 GeV.

For the total partonic cross section at tree level we write  $\sigma_0$ . The singular partonic cross section normalized to  $\sigma_0$  in a resummed factorized form reads

$$(5.13) \quad \frac{1}{\sigma_0} \frac{d\hat{\sigma}_s}{d\tau}(\tau, Q) = Q H_Q(Q, \mu_H) \int_0^{Q^2\tau} ds \int_0^s ds' U_J(s', \mu_H, \mu_J) J^{(\tau)}(s - s', \mu_J) \\ \times \int_0^{Q\tau - \frac{s}{Q}} dk U_S(k, \mu_H, \mu_S) S^{(\tau)}(Q\tau - \frac{s}{Q} - k, \mu_S).$$

All large logarithms are summed in the functions  $U_J$  and  $U_S$ . Hence, the hard, jet, and soft function contain no singularities. The hard function  $H_Q$  describes the effects at the hard production scale  $Q$ . The jet function  $J^{(\tau)}$  models the distribution of the squared invariant mass  $s$  coming from collinear radiation of both jets. The soft radiation with a large angle is accounted for by the soft function  $S^{(\tau)}$ .



The involved renormalization scales  $\mu_H$ ,  $\mu_J$ , and  $\mu_S$  are chosen in such a way that all large logarithms are contained in the  $U$  factors. A suitable choice is

$$(5.14) \quad \begin{aligned} \mu_H &\sim Q, \\ \mu_J &\sim Q\sqrt{\tau}, \\ \mu_S &\sim Q\tau. \end{aligned}$$

The  $U$  factors, then, sum the large logarithms from one scale to the scale  $\mu_H$ . Thus,  $U_J$  sums the large logarithms from  $\mu_J$  to  $\mu_H$  and  $U_S$  does the same from  $\mu_S$  to  $\mu_H$ .

The renormalization group equations for the  $U$  functions and the expressions for the hard, jet, and soft function at  $\mathcal{O}(\alpha_s)$  are given in Appendix A.1 of [9]. The expansion of (5.13) to first order in  $\alpha_s$  yields the commonly known first order thrust distribution

$$(5.15) \quad \frac{1}{\sigma_0} \frac{d\hat{\sigma}_s}{d\tau}(\tau, Q) = \delta(\tau) + \frac{\alpha_s C_F}{4\pi} \left\{ -8 \left[ \frac{\theta(\tau) \log(\tau)}{\tau} \right]_+ - 6 \left[ \frac{\theta(\tau)}{\tau} \right]_+ + \left( \frac{2\pi^2}{3} - 2 \right) \delta(\tau) \right\} + \mathcal{O}(\alpha_s^2),$$

where all scales have been set to  $\mu = \mu_H = \mu_J = \mu_S$ .

The thrust distribution in (5.13) can be transformed to the Laplace space using the convention

$$(5.16) \quad \tilde{\sigma}(\nu, Q) = \int_0^\infty d\tau e^{-\nu\tau} \frac{1}{\sigma_0} \frac{d\hat{\sigma}_s}{d\tau}(\tau, Q).$$

In a condensed form, it can be written as

$$(5.17) \quad \tilde{\sigma}(\nu, Q) = \exp \left[ K(\Gamma_J, \mu_{H,\nu}, \mu_{J,\nu}) + K(\Gamma_S, \mu_{H,\nu}, \mu_{S,\nu}) + \frac{1}{2} \left( \omega(\gamma_J, \mu_{H,\nu}, \mu_{J,\nu}) + \omega(\gamma_S, \mu_{H,\nu}, \mu_{S,\nu}) \right) \right],$$

with the evolution functions  $K$  and  $\omega$

$$(5.18) \quad K(\Gamma, \mu, \mu_0) = 2 \int_{\alpha_s(\mu_0)}^{\alpha_s(\mu)} \frac{d\alpha_s}{\beta[\alpha_s]} \Gamma[\alpha_s] \int_{\alpha_s(\mu_0)}^{\alpha_s} \frac{d\alpha'_s}{\beta[\alpha'_s]},$$

$$\omega(\Gamma, \mu, \mu_0) = 2 \int_{\alpha_s(\mu_0)}^{\alpha_s(\mu)} \frac{d\alpha_s}{\beta[\alpha_s]} \Gamma[\alpha_s].$$

The cusp and non-cusp anomalous dimensions have the form

$$(5.19) \quad \begin{aligned} \Gamma_J[\alpha_s] &= -2\Gamma_S[\alpha_s] = 4\Gamma^{\text{cusp}}[\alpha_s], \\ \gamma_J[\alpha_s] &= 12 C_F \frac{\alpha_s}{4\pi}, \\ \gamma_S[\alpha_s] &= 0, \end{aligned}$$

with

$$(5.20) \quad \begin{aligned} \Gamma^{\text{cusp}}[\alpha_s] &= \Gamma_0^{\text{cusp}}[\alpha_s] \frac{\alpha_s}{4\pi} + \Gamma_1^{\text{cusp}}[\alpha_s] \left( \frac{\alpha_s}{4\pi} \right)^2, \\ \Gamma_0^{\text{cusp}}[\alpha_s] &= 4 C_F, \\ \Gamma_1^{\text{cusp}}[\alpha_s] &= C_F \left[ C_A \left( \frac{268}{9} - \frac{4\pi^2}{3} \right) - \frac{80}{9} T_R n_f \right]. \end{aligned}$$

The corresponding scales can be obtained by combining the  $U$  evolution factors at NLL with the corrections in the Laplace transformed hard, jet, and soft function of Appendix A.1 in [9] containing logarithms or plus-distributions. They read

$$(5.21) \quad \begin{aligned} \mu_{H,\nu} &= Q, \\ \mu_{J,\nu} &= Q (\nu e^{\gamma_E})^{-\frac{1}{2}}, \\ \mu_{S,\nu} &= Q (\nu e^{\gamma_E})^{-1}. \end{aligned}$$

### 5.2.3. Coherent Branching

Another way to resum large logarithms to NLL accuracy, besides the SCET approach, is provided by the coherent branching formalism. It was firstly formulated in [105]. In [106] it was applied for the resummation of the thrust distribution. Additionally, the coherent branching provides an algorithm that forms the basis of angular ordered parton showers such as in HERWIG.

In the coherent branching formalism, the parton level thrust distribution for massless quarks (cf. (5.13)) reads

$$(5.22) \quad \frac{1}{\sigma_0} \frac{d\hat{\sigma}^{\text{cb}}}{d\tau}(\tau, Q) = \int ds_1 ds_2 \delta\left(\tau - \frac{s_1 + s_2}{Q^2}\right) J(s_1, Q^2) J(s_2, Q^2).$$

Here,  $J(s, Q^2)$  denotes the parton level jet mass distributions with the squared jet invariant mass  $s = M_{\text{jet}}^2$ .

In the following, we sketch the main ideas of the coherent branching formalism. For a more detailed description we refer to the original paper [105] and [9, 12]. Furthermore, we quote the results of the NLL resummation of  $J(s, Q^2)$  performed in [9] that coincide with the result for the thrust distribution of the SCET approach in 5.2.2.

Let us consider the production of a quark-antiquark pair with the momenta  $p$  and  $\bar{p}$ , respectively. In the coherent branching formalism we parametrize the momentum of the quark after the  $i$ -th emission using the light-cone decomposition by

$$(5.23) \quad k_i^\mu = \alpha_i p^\mu + \beta_i \bar{n}^\mu + k_{i,\text{T}}^\mu.$$

The reference direction  $\bar{n}$  is, in the massless case, given by  $\bar{n} = \bar{p}$ . For the transverse momentum  $k_{i,\text{T}}^\mu$  we have

$$(5.24) \quad p \cdot k_{i,\text{T}} = n \cdot k_{i,\text{T}} = 0, \quad k_{i,\text{T}}^2 < 0,$$

and the coefficient  $\beta_i$  is given by

$$(5.25) \quad \beta_i = \frac{-k_{i,\text{T}}^2 + k_i^2}{2\alpha_i(p \cdot \bar{n})}.$$

The momentum after the  $i$ -th splitting can be expressed recursively by

$$(5.26) \quad k_i^\mu = z_i k_{i-1}^\mu + \frac{p_{i,\text{T}}^2 + k_i^2 - z_i^2 k_{i-1}^2}{2z_i(k_{i-1} \cdot \bar{n})} \bar{n}^\mu + q_{i,\text{T}}^\mu,$$

with the splitting variables

$$(5.27) \quad z_i = \frac{\alpha_i}{\alpha_{i-1}},$$

$$q_{i,\text{T}}^\mu = k_{i-1,\text{T}}^\mu - z_i k_{i,\text{T}}^\mu,$$

where  $\alpha_0 = 1$  and  $p_{0,\text{T}}^\mu = 0$ .

When implementing a shower, a suitable choice for the evolution variable that encodes angular ordering is given by [105]

$$(5.28) \quad \tilde{q}_i^2 = \frac{p_{i,\text{T}}^2}{z_i^2(1-z_i)^2},$$

with  $p_{i,\text{T}}^2 = -q_{i,\text{T}}^2$ . The conditions

$$(5.29) \quad \tilde{q}_{i+1}^2 < z_i^2 \tilde{q}_i^2 \quad \text{and} \quad \tilde{k}_i^2 < (1-z_i)^2 \tilde{q}_i^2,$$

restrict the opening angle of the  $i+1$ -th radiation to be smaller than the previous one. From the requirement of momentum conservation at each splitting it follows that

$$(5.30) \quad k_{i-1}^2 = \frac{k_i^2}{z_i} + \frac{q_i^2}{1-z_i} + z_i(1-z_i)\tilde{q}_i^2.$$

Following [9] and [106], the evolution equation of the jet mass distribution can be written as

$$(5.31) \quad \begin{aligned} J(s, Q^2) = & \delta(s) + \int_0^{Q^2} \frac{d\tilde{q}^2}{\tilde{q}^2} \int_0^1 dz P_{qq}[\alpha_s(z(1-z)\tilde{q}), z] \\ & \times \left[ \int_0^\infty dk'^2 \int_0^\infty dq^2 \delta\left(s - \frac{k'^2}{z} - \frac{q^2}{1-z} - z(1-z)\tilde{q}^2\right) \right. \\ & \left. \times J(k'^2, z^2\tilde{q}^2) J_g(q^2, (1-z)^2\tilde{q}^2) - J(s, \tilde{q}^2) \right], \end{aligned}$$

with the gluon virtuality  $q^2$ . The gluon jet mass distribution  $J_g(s, Q^2)$  is defined analogously to  $J(s, Q^2)$ . The splitting function yields

$$(5.32) \quad P_{qq}[\alpha_s, z] = \frac{\alpha_s C_F}{2\pi} \frac{1+z^2}{1-z} = \frac{\alpha_s C_F}{2\pi} \left[ \frac{2}{1-z} - (1+z) \right].$$

The evolution equation of the jet mass distribution (5.31) encodes the coherent branching formalism for parton showers (cf. (4.12)). The first term, i.e. the delta distribution, stands for an event without branching. This corresponds to the tree level contribution with a vanishing jet mass. The shower equation is initialized with the starting scale  $\tilde{q}^2 = Q^2$ .

The subsequent resolvable radiation is modelled by the evolution of the quark and gluon jet mass distributions, i.e. the second term in (5.31). Finally, the last term represents the case of evolution with unresolved branchings.

Note that the resolved branchings are subject to the angular ordering constraints (5.29) and momentum conservation while the unresolved branching is unconstrained.

For the analytic resummation to NLL accuracy, it is reasonable to make two approximations:

- (1) At NLL the gluon jet mass contribution is suppressed due to the conditions in (5.29) (cf. [106]). Thus,  $J_g(s, Q^2)$  can be replaced by a delta distribution  $\delta(s)$ .
- (2) Some terms do not get enhanced in the soft limit. For these terms, the limit  $z \rightarrow 1$  can be applied.

Similar to the case in the SCET approach (5.16) the jet mass distribution is transformed to Laplace space by

$$(5.33) \quad \tilde{J}(\bar{\nu}, Q) = \int_0^\infty ds e^{-\bar{\nu}s} J(s, Q).$$

Thus, the thrust distribution in Laplace space reads

$$(5.34) \quad \tilde{\sigma}^{\text{cb}}(\nu, Q) = \left[ \tilde{J} \left( \frac{\nu}{Q^2}, Q \right) \right]^2.$$

Applying the approximations (1) and (2) we arrive at the formula for the jet mass distribution in Laplace space

$$(5.35) \quad \tilde{J}(\bar{\nu}, Q) = 1 + \int_0^{Q^2} \frac{d\tilde{q}^2}{\tilde{q}^2} \int_0^1 P_{qq}[\alpha_s(z(1-z)\tilde{q}), z] (e^{-\bar{\nu}(1-z)\tilde{q}^2} - 1) \tilde{J}(\nu, \tilde{q}).$$

From this integral equation, a differential equation can be derived. After solving this differential equation and carrying out some manipulations we arrive at

$$(5.36) \quad \tilde{\sigma}^{\text{cb}}(\nu, Q) = \exp \left[ K(\Gamma_J, \mu_{H,\nu}, \mu_{J,\nu}) + K(\Gamma_S, \mu_{H,\nu}, \mu_{S,\nu}) + \frac{1}{2} \omega(\gamma_J, \mu_{H,\nu}, \mu_{J,\nu}) \right],$$

with the evolution functions  $K$  and  $\omega$  of (5.18) and the anomalous dimensions in (5.19). A comparison with (5.17) shows that the SCET approach and the coherent branching formalism lead to the same result for the thrust distribution. Note that we left out several steps in the calculation that can be found in Chapter 4 of [9] and are not essential for the general understanding.

#### 5.2.4. Cutoff Dependence of $\tau_{\text{peak}}$

The resummation of the thrust distribution in the SCET approach and in the coherent branching formalism leads to the same result (cf. (5.17) and (5.36)). Note that both calculations go without a shower cut  $Q_0$ . From this, they proved in [9] that, in the coherent branching formalism without a shower cut, i.e. with  $Q_0 = 0$ , the coherent branching mass in the peak region coincides with the pole mass up to order  $\mathcal{O}(\alpha_s)$

$$(5.37) \quad m^{\text{cb}}(Q_0 = 0) \stackrel{\text{peak}}{=} m^{\text{pole}} + \mathcal{O}(\alpha_s).$$

However, in practice a parton shower cannot be used without a cutoff. The reasons for that are twofold:

- (1) The shower cutoff separates the perturbative region of the parton shower from the non-perturbative region, where hadronization has to be applied. Without this cut, the evolution would run into the Landau pole of QCD when approaching scales of order  $\mathcal{O}(\Lambda_{\text{QCD}})$ .
- (2) The shower cutoff is needed to restrict the parton multiplicities. Otherwise, it would generate an infinite number of partons.

Thus, (5.37) does not hold for the top quark mass in parton showers.

In the coherent branching formalism, the cutoff  $Q_0$  can be applied by restricting the integrals over  $\tilde{q}^2$  and  $z$  in (5.31) to the region

$$(5.38) \quad p_{\text{T}}^2 = \tilde{q}^2 z^2 (1 - z)^2 > Q_0^2.$$

This cut in the transverse momentum  $p_{\text{T}}$  can be applied to the jet mass distribution in Laplace space (5.36). After some manipulations we arrive at the relation between the thrust distribution with cut (left-hand-side) and the distribution without cut (right-hand-side)

$$(5.39) \quad \frac{d\hat{\sigma}^{\text{cb}}}{d\tau}(\tau, Q, Q_0) = \frac{d\hat{\sigma}^{\text{cb}}}{d\tau} \left( \tau + 16 \frac{Q_0}{Q} \frac{C_{\text{F}} \alpha_s(Q_0)}{4\pi}, Q \right).$$

The corresponding calculations can be found in Section 5.2 of [9].

For the factorization approach, the shower cut can be interpreted as a cut on the transverse momentum of gluons with respect to the thrust axis. This cut can be implemented separately in each of the hard, jet, and soft functions. This treatment leads to the same results as the coherent branching formalism. The corresponding computations can be found in Section 5.3 of [9].

For the case of massless quarks, the effect of the shower cutoff  $Q_0$  represents a factorization scale between the perturbative region of the parton shower and the non-perturbative region of soft radiation with a large angle. In the peak region, the modification of  $Q_0$  can be interpreted as a change of the non-perturbative contributions, namely a modification of the soft model shape function  $S_{\text{mod}}$ . In [107] this shift in  $S_{\text{mod}}$  is referred to as “gap”.

This gap can be calculated perturbatively (cf. (5.39)). The general expression of the hadron level thrust distribution (cf. (5.11)) incorporating the gap, denoted as  $\Delta_{\text{soft}}(Q_0)$ , reads

$$\begin{aligned}
 (5.40) \quad \frac{d\sigma}{d\tau}(\tau, Q, Q_0) &= \int_0^{Q\tau} d\ell \frac{d\hat{\sigma}_s}{d\tau} \left( \tau - \frac{\ell}{Q}, Q, Q_0 \right) S_{\text{mod}}(\ell) \\
 &= \int_0^{Q\tau} d\ell \frac{d\hat{\sigma}_s}{d\tau} \left( \tau - \frac{\ell}{Q}, Q \right) S_{\text{mod}}(\ell + \Delta_{\text{soft}}(Q_0)) + \mathcal{O}(\alpha_s^2, Q_0^2).
 \end{aligned}$$

The gap function  $\Delta_{\text{soft}}(Q_0)$  depends on the cutoff and is given by

$$(5.41) \quad \Delta_{\text{soft}}(Q_0) = 16 Q_0 \frac{\alpha_s(Q_0) C_F}{4\pi} + \mathcal{O}(\alpha_s^2 Q_0).$$

Similar to the MSR mass, the RGE of the gap function is linear in the renormalization scale

$$(5.42) \quad \frac{d}{d \log(R)} \Delta_{\text{soft}}(R) = 16 R \frac{\alpha_s(R) C_F}{4\pi} + \mathcal{O}(\alpha_s^2 R),$$

which is named  $R$ -evolution [30, 31].

This relation implies that in a parton shower, a change in the cutoff parameter  $Q_0$  has to be accompanied by a change in the parameters of the hadronization model. Considering the factorized formula for the hadron level thrust distribution (5.40) this results in

$$\begin{aligned}
 (5.43) \quad \frac{d\sigma}{d\tau}(\tau, Q, Q_0) &= \int_0^{Q\tau} d\ell \frac{d\hat{\sigma}_s}{d\tau} \left( \tau - \frac{\ell}{Q}, Q, Q'_0 \right) \\
 &\quad \times S_{\text{mod}}(\ell + \Delta_{\text{soft}}(Q_0) - \Delta_{\text{soft}}(Q'_0)),
 \end{aligned}$$

for the relation between two different cutoff scales  $Q_0$  and  $Q'_0$ . The IR insensitive difference between the gap function at the two scales yields

$$(5.44) \quad \Delta_{\text{soft}}(Q_0) - \Delta_{\text{soft}}(Q'_0) = 16 \int_{Q'_0}^{Q_0} dR \left[ \frac{\alpha_s(R) C_F}{4\pi} + \mathcal{O}(\alpha_s^2) \right].$$

The relation above can be verified numerically by varying the cutoff parameter of an MC event generator while keeping the hadronization model unchanged. This leads to a linear dependence of  $\tau_{\text{peak}}$  on  $Q_0$ , since the effect is not compensated by the hadronization model. In [9] this is validated by using the HERWIG event generator. Therefore, the dependence of the peak position of the hadronic thrust variable is studied for different values of the cutoff  $Q_0$ .

Taking (5.40) and (5.41) into account, the dependence of  $\tau_{\text{peak}}(Q_0)$  on the cutoff, in the massless case, is given by

$$(5.45) \quad \tau_{\text{peak}}(Q_0) = \tau_{\text{peak}}(Q'_0) - \frac{16}{Q} \int_{Q'_0}^{Q_0} dR \frac{\alpha_s(R) C_F}{4\pi}.$$

Here,  $\tau_{\text{peak}}(Q'_0)$  is the value of the peak position at some reference scale  $Q'_0$ . The numerical validation of relation (5.45) is carried out by using parton shower simulations from HERWIG in Section 7 of [9]. However, the angular ordered parton shower algorithm implemented in HERWIG is based on the coherent branching formalism, that was used to derive the relation in (5.45). Thus, it is natural to ask, if this relation also holds for a different family of shower algorithms, i.e. the dipole parton shower algorithm discussed in Section 4.2. The search for an answer to this question is subject of the next section.

### 5.3. ANALYSES AND RESULTS

To answer the question that arose in the last section, we start from the generation of the thrust distribution using an implementation of the dipole shower algorithm outlined in Section 4.2. For that, we show that the cutoff dependence of the peak position of the thrust distribution obtained from the dipole shower matches the expected form of the analytical computations that is given in (5.45).



Before we discuss the event generation using the dipole shower and show our results, we stress that the observable we study is the classical thrust variable given in (5.9). For simplification we set

$$(5.46) \quad \tau := \tau^{\text{thrust}},$$

for the rest of this chapter.

We emphasize that the use of the classical thrust variable instead of the squared hemisphere mass sum of (5.8) does not spoil the comparability of our results with the outcomes of [9]. This is explained by the fact that we are only interested in the relative location of the maximum of the distribution in the peak region. However, in the peak region, the classical thrust variable (5.9) and the squared hemisphere mass sum of (5.8) show very similar behavior.

For our analysis we start from the hard event  $e^+e^- \rightarrow q\bar{q}$ , by computing the corresponding tree level matrix element squared. To obtain the full weight of the hard event, we generate a phase space weight from the two initial beam four-momenta using the RAMBO algorithm [108, 109] and multiply it with the squared matrix element. From this event, we can start the parton shower.

For the parton shower we use the implementation of the algorithm depicted in Section 4.2. We evolve the shower from the initial scale of the hard event, in our case from  $Q = 91$  GeV and  $Q = 300$  GeV, down to the cutoff scale  $Q_0$ . Finally, we calculate the thrust  $\tau$ .

In this way, we generate  $10^7$  events for each cutoff scale  $Q_0$  with

$$(5.47) \quad Q_0/\text{GeV} \in \{0.4, 0.6, 0.8, 1.0, 1.2, 1.4, 1.6, 1.8, 2.0\}.$$

For the creation of a histogram for the thrust distribution, the resulting weights of this process are cumulatively ordered into bins of size  $\Delta\tau = 10^{-3}$ . Note that this procedure gives us the partonic thrust distribution (cf. (5.13)) generated by the dipole parton shower algorithm. To make it comparable to the analytic results from Section 5.2 we have to convolve the partonic thrust distribution with the soft model shape function as in (5.11).

For that purpose we convolve the partonic thrust distribution  $d\hat{\sigma}/d\tau$  with the  $S_{\text{mod}}$  of (5.12) using the discretized representation of the convolution integral (5.11), namely

$$(5.48) \quad \frac{d\sigma}{d\tau}(\tau, Q) = \sum_{\ell=0}^{Q\tau} \Delta\ell \frac{d\sigma}{d\tau}\left(\tau - \frac{\ell}{Q}, Q\right) S_{\text{mod}}\left(\ell + \frac{\Delta\ell}{2}\right).$$

Here, the sum over  $\ell$  has to be taken in steps of the size

$$(5.49) \quad \Delta\ell = \frac{Q\tau}{\text{bins}},$$

where “bins” is the number of bins we use to discretize the function  $S_{\text{mod}}$ . In (5.48) the soft model shape function, for each step, is evaluated at the center of the corresponding bin. The value for the partonic thrust distribution at the certain value  $\tau - \ell/Q$  is obtained from its histogram. We vary the smearing parameter  $\Lambda_m$  between 1 and 3 GeV.

As an example, we show the convolved partonic thrust distribution with the cutoff  $Q_0 = 1.2$  GeV and the smearing parameter  $\Lambda_m = 1$  GeV for  $Q = 91$  GeV in Figure 5.1.

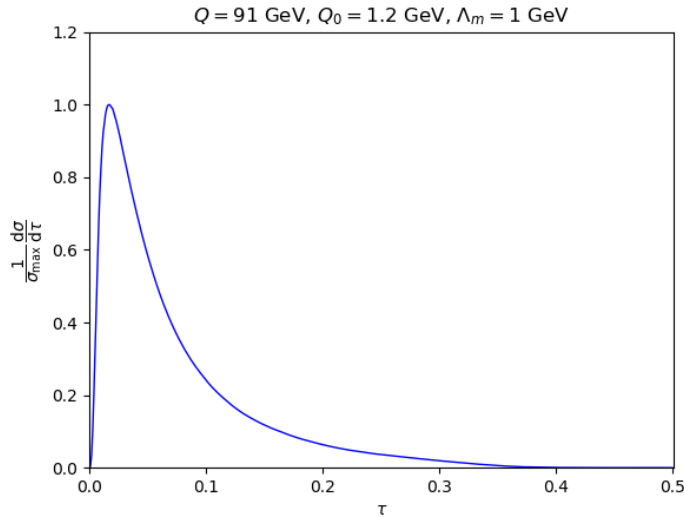


FIGURE 5.1. Thrust distribution for the center-of-mass energy  $Q = 91$  GeV, with the cutoff value  $Q_0 = 1.2$  GeV and the smearing parameter of the soft model shape function  $\Lambda_m = 1$  GeV. The distribution is normalized such that its peak value is one.

In Figure 5.1 we can see that, as expected, the peak position of the thrust distribution is near  $\tau = 0$ . However, it is slightly shifted to positive values of  $\tau$ . As in all plots of the thrust distribution throughout this thesis, we normalize the distribution such that the peak value is one.

The important question we address is, if for fixed parameters  $Q$  and  $\Lambda_m$  and for varying cutoff values  $Q_0$  of the set (5.47), the dependence of the peak position

agrees with the result of the analytic computation (5.45), i.e.

$$(5.50) \quad \tau_{\text{peak}}(Q_0) = \tau_{\text{peak}}(Q'_0) - \frac{16}{Q} \int_{Q'_0}^{Q_0} dR \frac{\alpha_s(R) C_F}{4\pi}.$$

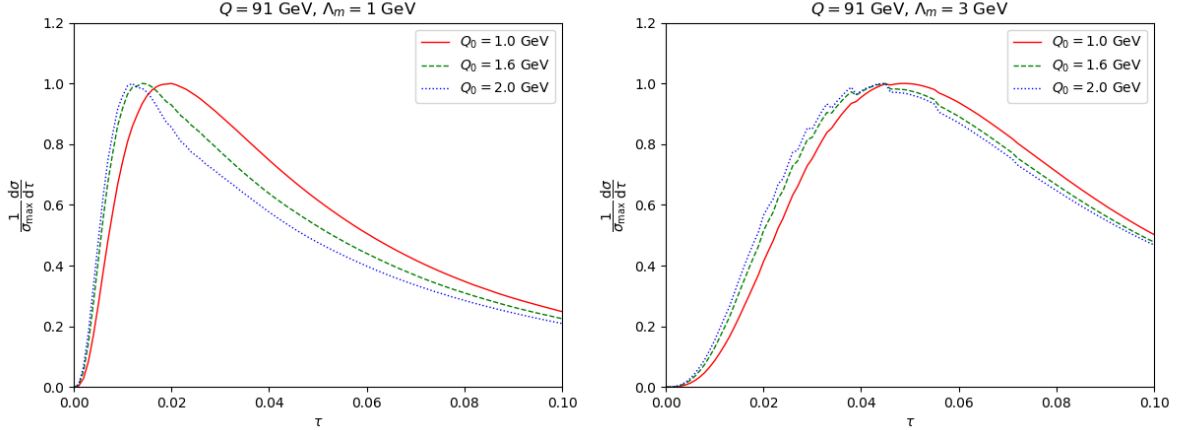


FIGURE 5.2. Plots of the thrust distribution from the dipole shower for the smearing parameters  $\Lambda_m = 1$  (left) and  $\Lambda_m = 3$  GeV with a center-of-mass energy of  $Q = 91$  GeV. Each figure shows the distribution for cutoff values of  $Q = 1$  GeV (red solid line),  $Q = 1.6$  GeV (green dashed line), and  $Q = 2$  GeV (blue dotted line), respectively.

Figure 5.2 shows the thrust distribution for the smearing parameters  $\Lambda_m = 1$  GeV (left figure) and  $\Lambda_m = 3$  GeV with  $Q = 91$  GeV each with three different values for the shower cut. The red solid line represents a cut of  $Q_0 = 1$  GeV. The green dashed line and the blue dotted line stand for the cutoff values  $Q_0 = 1.6$  GeV and  $Q_0 = 2$  GeV, respectively. Already from the plots for the three different cutoff values we can recognize the tendency that is implied by the analytic prediction (5.50): The value of the peak position decreases for bigger cutoff values.

However, we see that increasing the smearing parameter decreases the difference between the peak position for the different values of  $Q_0$ . The same plots of the thrust distribution, but for a center-of-mass energy  $Q = 300$  GeV, are shown in Figure 5.3. Here, the described tendency is also visible.

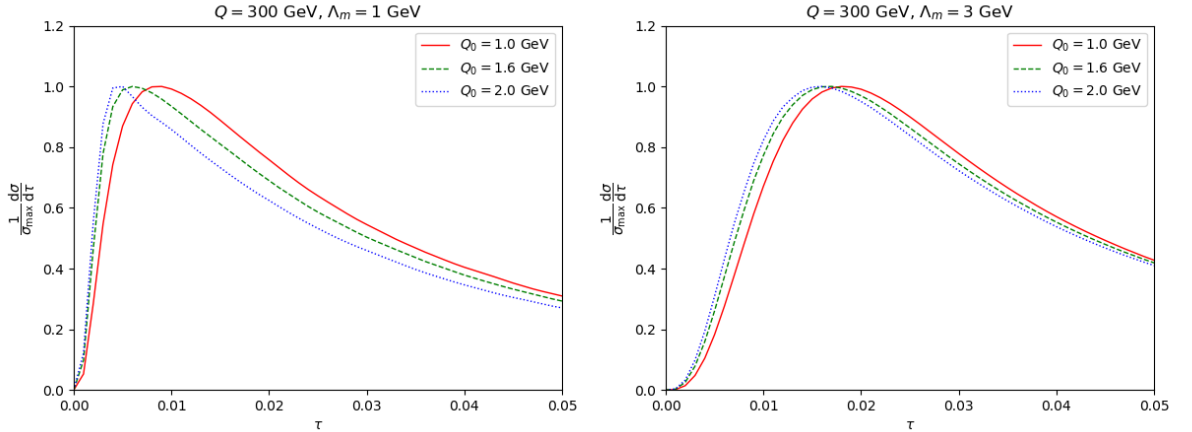


FIGURE 5.3. Plots of the thrust distribution from the dipole shower for the smearing parameters  $\Lambda_m = 1$  (left) and  $\Lambda_m = 3$  GeV with a center-of-mass energy of  $Q = 300$  GeV. Each figure shows the distribution for cutoff values of  $Q = 1$  GeV (red solid line),  $Q = 1.6$  GeV (green dashed line), and  $Q = 2$  GeV (blue dotted line), respectively.

To obtain a more quantitative analysis of the peak position's dependence on the cutoff, we fit a quadratic function to the thrust distribution in the peak region and extract the maximum. This procedure ensures that the statistical uncertainties in the determination of the peak position are so small that we desist from specifying any systematic or statistical errors in our results. Additionally, the visualization only demonstrates the general tendency of the cutoff dependence to test the agreement between the theoretical prediction and the parton shower simulation. It shall not indicate exact numerical statements.

The results from this analysis are shown in Figure 5.4. The plot of the peak position against the cutoff  $Q_0$  from the analytical computations is obtained by solving the integral in (5.50) numerically, using standard MC integration [109]. As the reference value we take the peak position from the parton shower simulation at  $Q'_0 = 1.2$  GeV.

Figure 5.4 illustrates the position of the peak  $\tau_{\text{peak}}$  as a function of the cutoff  $Q_0$  for four different combinations of  $Q$  and  $\Lambda_m$ . The two upper figures correspond to  $Q = 91$  GeV with  $\Lambda_m = 1$  GeV (left) and  $\Lambda_m = 3$  GeV (right), while the two lower figures depict the  $Q_0$  dependence for  $Q = 300$  GeV with  $\Lambda_m = 1$  GeV (left) and  $\Lambda_m = 3$  GeV (right). The blue solid line gives a pictorial representation of

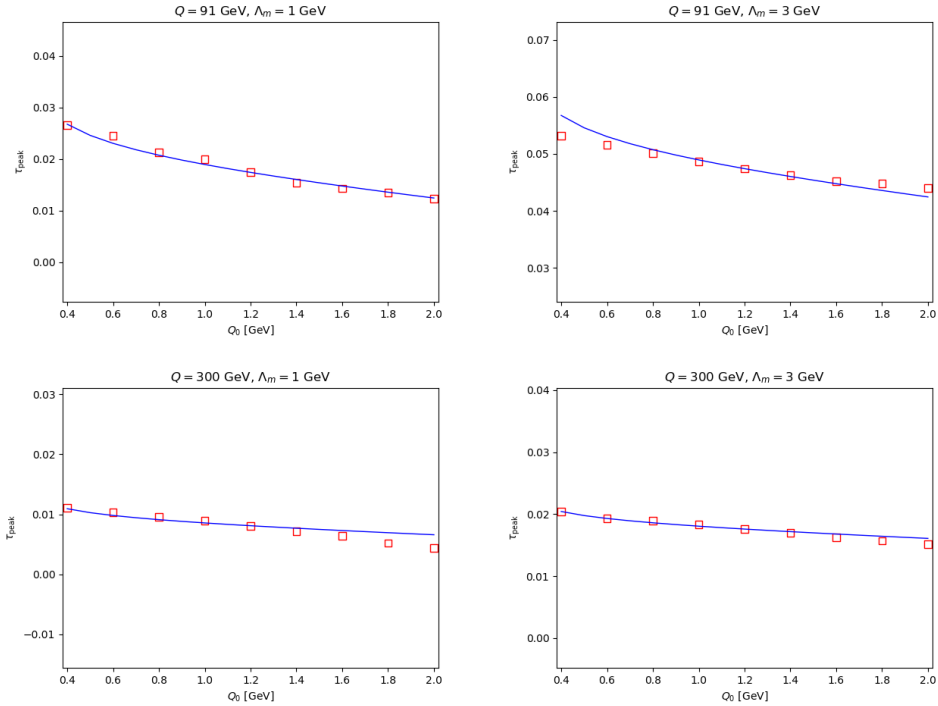


FIGURE 5.4. Position of the peak of the thrust distribution as a function of the shower cut  $Q_0$ . Displayed are the plots for  $Q = 91$  GeV with  $\Lambda_m = 1$  GeV (upper left) and  $\Lambda_m = 3$  GeV (upper right) as well as  $Q = 300$  GeV with  $\Lambda_m = 1$  GeV (lower left) and  $\Lambda_m = 3$  GeV (lower right). The blue solid line depicts the result of the analytical computation while the red squares represent the data points from the parton shower simulation.

the analytic relation (5.50). The centers of the red squares are the data points obtained from the parton shower simulations.

From Figure 5.4 we deduce a good agreement between the analytical prediction and the parton shower simulations from the dipole shower formalism. Hence, our results coincide with the findings of [9].

To conclude, we can say that the dependence of the peak position from parton shower simulations, using the dipole shower algorithm, matches the prediction from the analytical computations. Thus, the relation (5.50), derived from SCET and the coherent branching formalism, is not only valid for angular ordered parton showers but also for parton showers based on the Catani–Seymour dipole formalism.



## **Part 3**

# **UV Subtraction Terms for Self-Energy Corrections**





## CHAPTER 6

# UV Subtraction Terms at One-Loop

## Contents

---

<b>6.1. Motivation and a Toy Example</b>	<b>88</b>
6.1.1. A Simple Toy Example	91
<b>6.2. Subtraction Terms for <math>\phi^3</math>-Theory</b>	<b>93</b>
6.2.1. Setting up the Requirements	93
6.2.2. Constructing the Counterterm	96
6.2.3. Computation of Residues	99
<b>6.3. Subtraction Terms for QCD</b>	<b>101</b>
6.3.1. Light Quarks	102
6.3.2. Heavy Quarks	103
6.3.3. Gluons	104

---

In the last chapters, we discussed parton showers, the top quark mass, and the cutoff dependence of the top mass parameter in parton shower simulations. Next, we focus on the hard scattering part of modelling collider events, namely fixed-order calculations and some implications that come along with NNLO computations.

In Section 2.5 we discussed the renormalization of QCD to cancel UV divergences that arise when calculating loop diagrams. This is achieved by introducing counterterms into the Lagrangian. We demonstrated this renormalization, using the example of the quark self-energy contribution at one-loop order.

When going to higher orders in perturbation theory, we encounter diagrams with corresponding Feynman integrals that contain propagators with exponents bigger than one. In the following, we refer to propagators with this property as raised propagators. The higher powers of the raised propagators originate from the insertion of a self-energy on an internal line, i.e. on a particle line inside the exterior loop.

One ingredient, that is needed for calculations in the so-called loop-tree duality approach [110–122], is the residue of the integrand, when a raised propagator goes on-shell. In this chapter, we show that in the on-shell scheme, it is possible to find a counterterm at the integrand level that makes the residue vanish. Additionally, we provide a possible form of these counterterms for scalar  $\phi^3$ -theory and QCD at one-loop order as published in [11].

### 6.1. MOTIVATION AND A TOY EXAMPLE

In Chapter 3, we explained the structure and importance of NLO computations to make theoretical predictions for collider experiments. A special requirement for these calculations is the possibility to automatize them in a computer program. This is especially desirable for the case with more than two final-state particles involved.

However, due to the constantly increasing precision from the experimental side, the search for automatable methods using NNLO precision becomes indispensable for many  $2 \rightarrow n$  processes with  $n \geq 2$ . There exist two promising numerical methods to attack this problem. Here, we want to focus on numerical loop integration [123–135] combined with loop-tree duality [110–122]. Also, methods based on numerical unitarity [136–140] provide a possible way to a solution of the problem.

Starting at NNLO, i.e. at two-loop order, one encounters raised propagators coming from self-energy insertions in the main loop. Figure 6.1 shows an example for a self-energy insertion in a scalar theory. For some integrals, containing raised propagators, it is possible to calculate them analytically. In this case, the integral is reduced to master integrals using integration-by-parts identities [141]. The master integrals themselves may contain raised propagators and are calculable analytically.

However, we are interested in numerical approaches that can be automated. Although our focus is on the combination of loop-tree duality with numerical loop integration, our results are also useful for numerical unitarity based methods. In these approaches, the residue of the integrand has to be calculated for the case that a raised propagator goes on-shell. Let us consider a function  $f(z)$  that depends on the complex variable  $z$ . If this function has a pole of order  $\nu$  at  $z_0$ ,

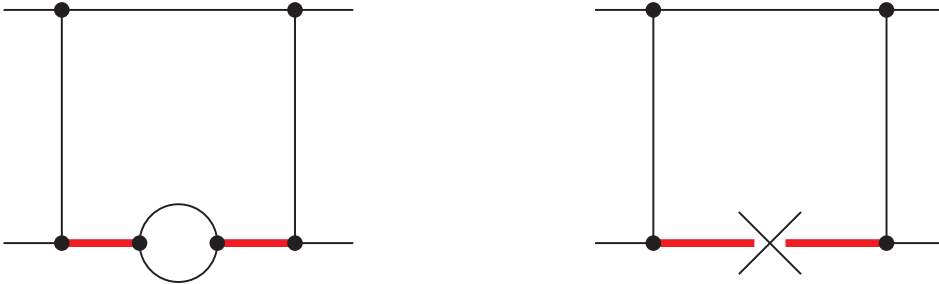


FIGURE 6.1. A two-loop diagram involving a self-energy insertion (left) and the corresponding diagram with a counterterm (right). The red line marks the raised propagator. [11]

the residue at  $z_0$  can be calculated using

$$(6.1) \quad \text{res}(f, z_0) = \frac{1}{(\nu - 1)!} \left( \frac{\partial}{\partial z} \right)^{\nu-1} [(z - z_0)^\nu f(z)] \Big|_{z=z_0}.$$

A generalization of this one-dimensional formula to multivariate residues can be found in [142]. In general, the calculation of the residues can be carried out for each individual integrand. However, this procedure is very troublesome and depends on the considered process. Hence, it is not well suited for automation. Another approach, proposed in [112], suggests to use integration-by-parts relations for the reduction of integrals containing raised propagators to Feynman integrals with no higher powers in the propagators. This procedure is manageable but also depends on the underlying process.

In loop-tree duality an  $l$ -loop contribution is cut exactly  $l$  times. In this approach it is desirable to isolate the part of the  $l$ -loop contribution that contains the problem, i.e. the internal line with the self-energy insertion, to a small part that does not depend on the underlying process. One way to do this is to not only consider the diagram with the self-energy insertion on a specific line, but taking all diagrams into account that contribute to this self-energy insertion. This means, particularly, to look at the diagram with a renormalization counterterm, corresponding to the self-energy insertion on this specific internal line.

It is possible to calculate the self-energy and the corresponding term analytically in the on-shell scheme. Here, the counterterm is the second order Taylor expansion of the self-energy around its on-shell value. Doing this calculation, the double pole is canceled and the residue is zero. However, this method is not practicable when it comes to automation because the solution of the analytic calculation is a transcendental function. To work numerically, as we have to do for automated computations, all functions have to be rational.

Therefore, we show that it is possible to find counterterms on an integrand level that lead to vanishing residues. Since we have to find a proper counterterm, the integral and its UV-behavior are fixed. It should be local in loop momentum space and its on-shell behavior is fixed by our requirement that the residue has to vanish. For the last requirement to hold we set the condition

$$(6.2) \quad \lim_{k^2 \rightarrow m^2} (\text{self-energy integrand}) = \mathcal{O}\left((E - E^b)^2\right).$$

By  $E^b$  we denote the energy flowing through the raised propagator in the on-shell limit. In words, the condition states that the whole integrand has to vanish quadratically in the case where the external momenta of the self-energy are on-shell. When (6.2) is fulfilled, the poles from the propagators are cancelled and the residue will vanish. Note that the small amount of requirements on the counterterms leads to the situation that they are not unique.

In this chapter, we present a method to obtain counterterms with the desired behavior. Additionally, we construct these counterterms for  $\phi^3$ -theory and QCD at one-loop order. These counterterms can be used to make the residues vanish that are encountered when calculating integrals for two-loop diagrams with a self-energy insertion on an internal line. The main advantage of our method is that the counterterms work on an integrand level. Hence, all functions are rational and, therefore, applicable for automated calculations.

It may be conspicuous that the counterterms also contain raised propagators. This means that for the calculation of the residues, there are also derivatives that have to be calculated (cf. (6.1)). However, since we isolated the problem of raised propagators into the self-energy insertion part, it became process-independent. Therefore, the residues can be calculated once and used for every diagram that contains self-energy insertions.

## 6.1.1. A Simple Toy Example

Before we move on to our method for physical theories, namely  $\phi^3$ -theory and QCD, let us examine the procedure using a simple toy example from complex analysis. We inspect the local residues of the rational function  $R$ , which serves as our integrand. In our case it is given by

$$(6.3) \quad R = \frac{1}{D_1 D_2^2 D_6},$$

with the polynomials, i.e. the propagators,

$$(6.4) \quad D_1 = z_1 + \frac{1}{2}z_2 + 1, \quad D_2 = z_2, \quad D_6 = z_1 - \frac{1}{2}z_2 - 1,$$

where the two complex variables  $z_1$  and  $z_2$  could be considered as energy variables in a quantum field theoretical context. The locations of the residues are at

$$(6.5) \quad (z_1, z_2) \in \{(-1, 0), (1, 0), (0, -2)\},$$

with double poles, coming from  $D_2^2$ , at  $P_1 = (-1, 0)$  and  $P_2 = (1, 0)$ . The left image of Figure 6.2 shows the location of the residues in the  $(z_1, z_2)$ -plane.

Let us first calculate the residue at  $P_1$ , using (6.1) iteratively

$$(6.6) \quad \text{res}(\text{res}(R, z_2 = 0), z_1 = -1) = \frac{1}{4}.$$

The residue, corresponding to  $P_2$ , is calculated analogously and we obtain

$$(6.7) \quad \text{res}(R, P_1) = \frac{1}{4}, \quad \text{res}(R, P_2) = -\frac{1}{4}.$$

The task is, to find a counterterm  $R_{\text{CT}}$  such that the residues at  $P_1$  and  $P_2$  of the sum  $R + R_{\text{CT}}$  vanish. In quantum field theory, we define the on-shell projections of the propagators  $D_1$  and  $D_6$  by setting  $z_2 = 0$ :

$$(6.8) \quad D_1^b = z_1 + 1, \quad D_6^b = z_1 - 1.$$

To find the counterterm  $R_{\text{CT}}$ , let us first consider a general form of rational functions that only has poles along  $D_1^b$ ,  $D_2$  and  $D_6^b$

$$(6.9) \quad R_{\text{general}} = \frac{P(z_1, z_2)}{(D_1^b)^{\nu_1} D_2^{\nu_2} (D_6^b)^{\nu_6}}.$$

Here, we have the exponents  $\nu_1, \nu_2, \nu_6 \in \mathbb{N}$  and  $P(z_1, z_2)$  is a polynomial of the variables  $z_1$  and  $z_2$ . This situation is shown in the right part of Figure 6.2.

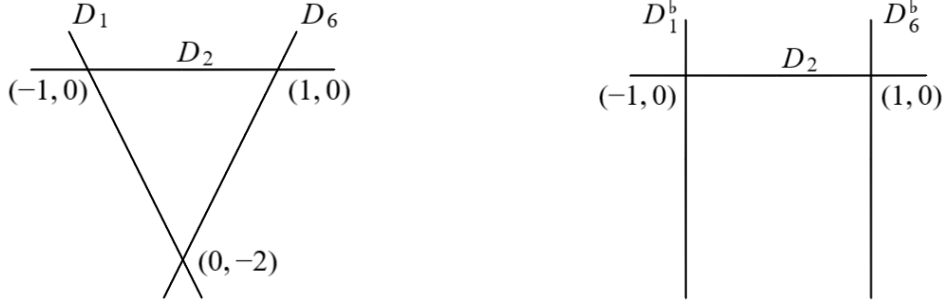


FIGURE 6.2. The location of the residues of the toy example in the  $(z_1, z_2)$ -plane (left) and the residues with the on-shell projections of the propagators (right).

The functions  $R_{\text{general}}$  have residues only at  $P_1$  and  $P_2$ . As a first guess of a counterterm for  $R$ , that cancels the residues at  $P_1$  and  $P_2$ , we try the simplest version of  $R_{\text{general}}$  with  $\nu_2 = 2$ ,

$$(6.10) \quad R_{\text{guess}} = \frac{1}{D_1^b D_2^2 D_6^b} = \frac{1}{(z_1 + 1) z_2^2 (z_1 - 1)}.$$

When calculating the residues of  $R_{\text{guess}}$  at  $P_1$  and  $P_2$ , we find that these vanish

$$(6.11) \quad \text{res}(R_{\text{guess}}, P_1) = \text{res}(R_{\text{guess}}, P_2) = 0.$$

Hence,  $R_{\text{guess}}$  yields no suitable counterterm to  $R$ . A counterterm with the desired properties can be obtained by expanding  $R$  around the on-shell projections to second order in  $z_2$ .

Let us define  $f(D) := 1/D$ . Then, the Taylor expansion of  $f$  around the on-shell projection of the propagator, i.e. around  $D^b$ , is given by

$$(6.12) \quad T_N f(D; D^b) = \sum_{n=0}^N (-1)^n \frac{(D - D^b)^n}{(D^b)^{n+1}}.$$

The expansion of  $R$  around the on-shell projections  $D_1^b$  and  $D_6^b$  can be written as a product of the individual expansions

$$(6.13) \quad R \approx \frac{1}{D_2^2} \left[ \sum_{n_1=0}^N (-1)^{n_1} \frac{(D_1 - D_1^b)^{n_1}}{(D_1^b)^{n_1+1}} \right] \times \left[ \sum_{n_2=0}^N (-1)^{n_2} \frac{(D_6 - D_6^b)^{n_2}}{(D_6^b)^{n_2+1}} \right].$$

Applying the expansion up to terms of order  $z_2$  yields

$$(6.14) \quad R_{\text{CT}} = -\frac{1}{D_1^b D_2^2 D_6^b} \left( 1 - \frac{z_2}{2D_1^b} + \frac{z_2}{2D_6^b} \right).$$

The residues of  $R_{\text{CT}}$  at  $P_1$  and  $P_2$  are

$$(6.15) \quad \text{res}(R_{\text{CT}}, P_1) = -\frac{1}{4}, \quad \text{res}(R_{\text{CT}}, P_2) = \frac{1}{4},$$

and, therefore, the residues of the sum  $R + R_{\text{CT}}$  at  $P_1$  and  $P_2$  vanish

$$(6.16) \quad \text{res}(R + R_{\text{CT}}, P_1) = \text{res}(R + R_{\text{CT}}, P_2) = 0.$$

Thus, the expansion of  $R$  around the on-shell projections provides a suitable counterterm that cancels the residues at the points where we encounter a pole in the raised propagator.

## 6.2. SUBTRACTION TERMS FOR $\phi^3$ -THEORY

In this section, we take the lessons we learned from the toy example to set up requirements on the counterterm. These conditions are given in a universal, process-independent way, such that the resulting counterterms can be used in every two-loop calculation featuring a self-energy insertion. As a first physical example, we construct a suitable counterterm for the self-energy calculation in  $\phi^3$ -theory.

### 6.2.1. *Setting up the Requirements*

To set up the required conditions and construct a suitable counterterm in  $\phi^3$ -theory, let us first recall the corresponding Lagrangian of (2.27)

$$(6.17) \quad \mathcal{L} = \frac{1}{2}(\partial_\mu \phi)(\partial^\mu \phi) - \frac{1}{2}m^2 \phi^2 + \frac{1}{3!}\lambda^{(D)}\phi^3 + \mathcal{L}_{\text{CT}}.$$

Here, we imply that all quantities are already renormalized. By  $\mathcal{L}_{\text{CT}}$  we denote the counterterm part of the Lagrangian. The superscript of the coupling  $\lambda^{(D)}$  contains the information of dimensional regularization, with  $D = 4 - 2\epsilon$ . Its relation to  $\lambda$  is given by

$$(6.18) \quad \lambda^{(D)} = \mu^\epsilon S_\epsilon^{-\frac{1}{2}} \lambda,$$

where the factor  $S_\epsilon^{-\frac{1}{2}} = (4\pi)^\epsilon \exp(-\epsilon\gamma_E)$  and the scale  $\mu$  come from dimensional regularization.

The counterterm part of the Lagrangian reads

$$(6.19) \quad \mathcal{L}_{\text{CT}} = -\frac{1}{2}(Z_\phi - 1)\phi\Box\phi - \frac{1}{2}(Z_\phi Z_m^2 - 1)m^2\phi^2 + \frac{1}{3!}\left(Z_\phi^{\frac{3}{2}}Z_\lambda - 1\right)\lambda^{(D)}\phi^3,$$

where the series expansion of the renormalization constants (cf. (2.54)) is given by

$$(6.20) \quad Z_a = 1 + \sum_{n=1}^{\infty} Z_a^{(n)} \left( \frac{\lambda^2}{(4\pi)^2} \right)^n, \quad a \in \{\phi, m, \lambda\}.$$

The bare quantities are related to the renormalized quantities by

$$(6.21) \quad \phi_0 = Z_\phi^{\frac{1}{2}}\phi, \quad \lambda_0 = Z_\lambda\lambda^{(D)}, \quad m_0 = Z_m m.$$

Recalling Section 2.5, the renormalization constants needed for the self-energy are  $Z_\phi^{(1)}$  and  $Z_m^{(1)}$ . In the on-shell scheme they read

$$(6.22) \quad \begin{aligned} Z_\phi^{(1)} &= \frac{2-\epsilon}{6m^2} B_0(m^2, m^2, m^2) - \frac{1-\epsilon}{3m^4} A_0(m^2), \\ Z_m^{(1)} &= \frac{1}{4m^2} B_0(m^2, m^2, m^2), \end{aligned}$$

with the scalar one-loop integrals

$$(6.23) \quad \begin{aligned} A_0(m^2) &= C_\epsilon \int \frac{d^D k}{i(2\pi)^D} \frac{1}{k^2 - m^2}, \\ B_0(p^2, m_1^2, m_2^2) &= C_\epsilon \int \frac{d^D k}{i(2\pi)^D} \frac{1}{[(k + \frac{1}{2}p)^2 - m_1^2][(k - \frac{1}{2}p)^2 - m_2^2]}. \end{aligned}$$

The prefactor is defined by  $C_\epsilon := 16\pi^2 S_\epsilon^{-1} \mu^{2\epsilon}$ . Note that we use a definition of the momenta inside the self-energy loop that differs from the common conventions (cf. Section 2.5). Our convention is shown in Figure 6.3.

The type of diagrams, we are interested in, are two-loop diagrams with a self-energy insertion, as the left diagram in Figure 6.1.

The propagators are defined by

$$(6.24) \quad D_j = k_j^2 - m^2 + i\epsilon,$$

using the numbering of the propagators and the directions of the momenta depicted in Figure 6.4. The integral, corresponding to this two-loop diagram,



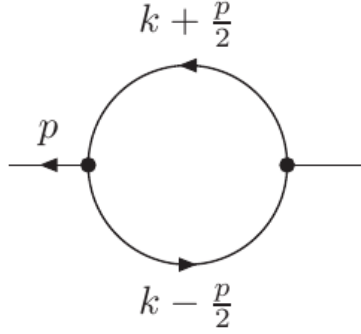


FIGURE 6.3. The scalar self-energy diagram. [11]

dropping one prefactor of  $\mu^{2\epsilon} S_\epsilon^{-1}$ , reads

$$(6.25) \quad I_{(2)} = i\lambda^6 \mu^{4\epsilon} S_\epsilon^{-2} \int \frac{d^D k_1}{(2\pi)^D} \int \frac{d^D k_2}{(2\pi)^D} R_{(2)}(k_1, k_2),$$

where the integrand is defined as

$$(6.26) \quad R_{(2)}(k_1, k_2) := \frac{1}{2D_1 D_2^2 D_3 D_4 D_5 D_6}.$$

Note that  $R_{(2)}(k_1, k_2)$  is a rational function in  $k_1$  and  $k_2$ .

Additional to the integral, corresponding to the full diagram, we need to consider the integral for the counterterm contribution in Figure 6.1. It is given by

$$(6.27) \quad I_{(2),\text{CT}} = -\frac{\lambda^6}{(4\pi)^2} \mu^{2\epsilon} S_\epsilon^{-1} \int \frac{d^D k_2}{(2\pi)^D} \frac{[Z_\phi^{(1)} k_2^2 - (Z_\phi^{(1)} + 2Z_m^{(1)}) m^2]}{D_2^2 D_3 D_4 D_5}.$$

There also exists an integral representation of this counterterm, involving an integration over the loop momentum of the self-energy insertion

$$(6.28) \quad I_{(2),\text{CT}} = i\lambda^6 \mu^{4\epsilon} S_\epsilon^{-2} \int \frac{d^D k_1}{(2\pi)^D} \int \frac{d^D k_2}{(2\pi)^D} R_{(2),\text{CT}}(k_1, k_2).$$

To implement this form of the counterterm within numerical calculations, the counterterm integrand  $R_{(2),\text{CT}}(k_1, k_2)$  must be a rational function in the energies  $E_1$  and  $E_2$ . To be a local counterterm for the UV divergence, coming from the self-energy graph, it has to fulfill the following statements:

- (1) Integrating (6.28) over  $k_1$  yields (6.27).

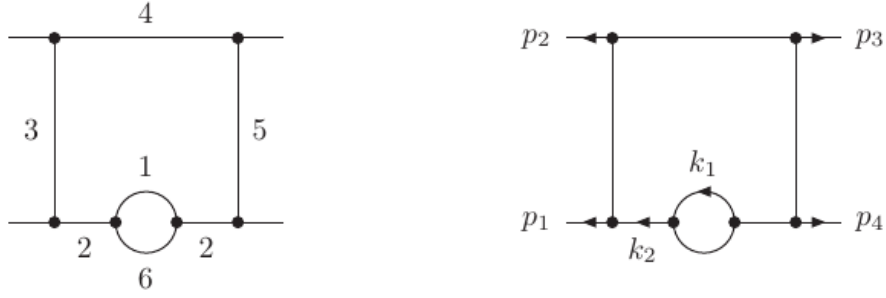


FIGURE 6.4. Our numbering of the propagators (left) and the labeling of the momenta (right). [11]

- (2) When  $|k_1|$  goes to infinity, the sum of  $R_{(2)}$  and  $R_{(2),\text{CT}}$  falls off as  $|k_1|^{-5}$ , i.e.

$$(6.29) \quad \lim_{|k_1| \rightarrow \infty} (R_{(2)}(k_1, k_2) + R_{(2),\text{CT}}(k_1, k_2)) = \mathcal{O}(|k_1|^{-5}).$$

Additionally, we require  $R_{(2),\text{CT}}$  to have such a form that the residue coming from  $D_2 \rightarrow 0$  vanishes (cf. 6.2):

- (3) When  $k_2$  goes on-shell, the sum of  $R_{(2)}$  and  $R_{(2),\text{CT}}$  has to vanish quadratically, i.e.

$$(6.30) \quad \lim_{k_2^2 \rightarrow m^2} (R_{(2)}(k_1, k_2) + R_{(2),\text{CT}}(k_1, k_2)) = \mathcal{O}((E - E^b)^2).$$

As a last requirement, we want to ensure that  $R_{(2),\text{CT}}$  receives no contributions coming from the cut, where both of the internal lines of the self-energy loop are cut. This is achieved by the condition:

- (4)  $R_{(2),\text{CT}}$  must not depend on the energy  $E_2$ .

We stress that all of the four requirements on the counterterm  $R_{(2),\text{CT}}$  do not refer to the full diagram, but only to the self-energy diagram that is inserted into the outer loop. Hence, all of the conditions are universal and do not depend on the underlying process.

### 6.2.2. Constructing the Counterterm

For the one-loop self-energy in  $\phi^3$ -theory (cf. Figure 6.3) we have

$$(6.31) \quad -i\Sigma_{(1)} = \lambda^2 \mu^{2\epsilon} S_\epsilon^{-1} \int \frac{d^D k}{(2\pi)^D} R_{(1)}.$$

With the propagators

$$(6.32) \quad D_1 = \left(k + \frac{1}{2}p\right)^2 - m^2, \quad D_2 = \left(k - \frac{1}{2}p\right)^2 - m^2,$$

the one-loop integrand is given by

$$(6.33) \quad R_{(1)} = \frac{1}{2D_1 D_2}.$$

From the external momentum  $p = (E, \vec{p})$ , we define  $p^b$  as

$$(6.34) \quad p^b := \left(\text{sign}(E)\sqrt{\vec{p}^2 + m^2}, \vec{p}\right).$$

Note that  $p^b$  does only depend on the sign of the energy  $E$ , not on its actual value. Additionally,  $p^b$  is on-shell,

$$(6.35) \quad (p^b)^2 = m^2.$$

Defining the four-vector  $n = (1, 0, 0, 0)$  we can write  $p^b$  in the form

$$(6.36) \quad p^b = p - cn,$$

where  $c$  is given by

$$(6.37) \quad c := \frac{1}{2n^2} \left(2p \cdot n - \text{sign}(2p \cdot n)\sqrt{(2p \cdot n)^2 - 4n^2(p^2 - m^2)}\right).$$

Now, we construct a counterterm  $R_{(1),\text{CT}}$ , on the integrand level that satisfies all four conditions set up above.

The counterterm corresponding to the self-energy diagram can be written as

$$(6.38) \quad -i\Sigma_{(1),\text{CT}} = \lambda^2 \mu^{2\epsilon} S_\epsilon^{-1} \int \frac{d^D k}{(2\pi)^D} R_{(1),\text{CT}}.$$

The only singularities of  $R_{(1),\text{CT}}$  shall arise from the on-shell projections of the propagators, i.e. the propagators  $D_1$  and  $D_2$  under the transformation  $p \rightarrow p^b$ . They are given by

$$(6.39) \quad D_1^b = \left(k + \frac{1}{2}p^b\right)^2 - m^2, \quad D_2 = \left(k - \frac{1}{2}p^b\right)^2 - m^2.$$

Recalling the method we applied for the toy example, we expand  $R_{(1)}$  around the on-shell kinematics up to first order in the momenta (cf. (6.13)). Thus, we

obtain

(6.40)

$$R_{(1),\text{expansion}} = -\frac{1}{2D_1^b D_2^b} \times \left[ 1 - \frac{4k \cdot (p - p^b) + p^2 - m^2}{4D_1^b} + \frac{4k \cdot (p - p^b) - p^2 + m^2}{4D_2^b} \right].$$

When summing  $R_{(1)}$  and  $R_{(1),\text{expansion}}$  we find that the difference is of order  $\mathcal{O}((p^2 - m^2)^2)$  and, hence, condition (3) is fulfilled. Additionally, the sum of  $R_{(1)}$  and  $R_{(1),\text{expansion}}$  falls off as  $|k|^{-5}$ . Thus,  $R_{(1),\text{expansion}}$  acts as a local UV counterterm to  $R_{(1)}$  and respects requirement (2). Following our definition of the on-shell momentum  $p^b$  in (6.34), that does not depend on the energy, condition (4) is also satisfied.

As a last step, we have to make sure that integrating the counterterm over  $k$  leads to the right expression (6.27)

$$(6.41) \quad \lambda^2 \mu^{2\epsilon} S_\epsilon^{-1} \int \frac{d^D k}{(2\pi)^D} R_{(1),\text{CT}} \stackrel{!}{=} \frac{\lambda^2}{(4\pi)^2} i \left[ Z_\phi^{(1)} p^2 - \left( Z_\phi^{(1)} + 2Z_m^{(1)} \right) m^2 \right],$$

with the renormalization constants from (6.22). To do that, we can add terms that do not spoil the conditions (2) to (4) but lead to the appropriate form of the integral. Taking this into account, we find a suitable form for the counterterm,

$$(6.42) \quad R_{(1),\text{CT}} = -\frac{1}{2D_1^b D_2^b} \times \left[ 1 - \frac{4k \cdot (p - p^b) + p^2 - m^2}{4D_1^b} + \frac{4k \cdot (p - p^b) - p^2 + m^2}{4D_2^b} \right] + \frac{(p - p^b)^2}{8m^2} \left( \frac{2}{D_1^b D_2^b} - \frac{1}{(D_1^b)^2} - \frac{1}{(D_2^b)^2} \right).$$

Note that the required on-shell behavior is given by the fact that, in the on-shell limit,  $(p - p^b)^2$  vanishes quadratically. Furthermore, the last factor, i.e. the three terms in brackets, ensure the correct UV behavior since they fall off

as  $\mathcal{O}(|k|)^{-6}$ :

$$(6.43) \quad \begin{aligned} \frac{2}{D_1^b D_2^b} - \frac{1}{(D_1^b)^2} - \frac{1}{(D_2^b)^2} &= -\frac{(D_1^b - D_2^b)^2}{(D_1^b)^2 (D_2^b)^2} \\ &= -\frac{4k^2 (p^b)^2}{(D_1^b)^2 (D_2^b)^2} \sim \mathcal{O}(|k|^{-6}). \end{aligned}$$

### 6.2.3. Computation of Residues

After having constructed a suitable counterterm at the integrand level, we are now left with the calculation of the residues. We can see from (6.42) that the counterterm  $R_{(1),\text{CT}}$  is a rational function of the energy  $E_k$  and has double poles in this variable. However, our four requirements are set up in such a way that the residues can be calculated once and, then, be used in every calculation involving a self-energy insertion.

As an example, let us calculate the residue at

$$(6.44) \quad E_{k,D_1^b} = -\frac{1}{2}E_{p^b} + E_1,$$

with

$$(6.45) \quad E_1 := \sqrt{\left(\vec{k} + \frac{1}{2}\vec{p}\right)^2 + m^2}.$$

Calculating the residue at  $k = (E_{k,D_1^b}, \vec{k})$  yields

$$(6.46) \quad \begin{aligned} \text{res} \left( R_{(1),\text{CT}}, E_k = E_{k,D_1^b} \right) &= -\frac{1}{4E_1 D_2^b} + \frac{(E_p - E_{p^b})^2}{8E_1 m^2 D_2^b} \\ &+ \frac{(E_p - E_{p^b})^2}{32E_1^3 m^2} - \frac{(E_p - E_{p^b})^2}{32E_1^3 D_2^b} \\ &- \frac{(E_1 - E_{p^b})(E_p - E_{p^b})}{2E_1 (D_2^b)^2} \\ &+ \frac{E_{p^b} (E_p - E_{p^b})^2}{16E_1^2 (D_2^b)^2} \Bigg|_{k=(E_{k,D_1^b}, \vec{k})}. \end{aligned}$$

The integrand of the one-loop calculation  $R_{(1)}$  only has single poles in the energy  $E_k$ . The location of the pole corresponding to the residue at (6.44) of the

counterterm lies at

$$(6.47) \quad E_{k,D_1} = -\frac{1}{2}E_p + E_1.$$

For the residue at  $k = (E_{k,D_1}, \vec{k})$  we obtain

$$(6.48) \quad \text{res} \left( R_{(1)}, E_k = E_{k,D_1} \right) = \frac{1}{4E_1 D_2} \Big|_{k=(E_{k,D_1}, \vec{k})}.$$

Adding the two residues (6.48) and (6.46), we find

$$(6.49) \quad \begin{aligned} \text{res} \left( R_{(1)}, E_k = E_{k,D_1} \right) + \text{res} \left( R_{(1),\text{CT}}, E_k = E_{k,D_1^b} \right) = \\ \frac{1}{4E_1} \left[ \frac{1}{D_2} - \frac{1}{D_2^b} - \frac{2(E_1 - E_{p^b})(E_p - E_{p^b})}{(D_2^b)^2} \right] \\ + \frac{(E_p - E_{p^b})^2}{8E_1 m^2 D_2^b} + \frac{(E_p - E_{p^b})^2}{32E_1^3 m^2} \\ - \frac{(E_p - E_{p^b})^2}{32E_1^3 D_2^b} + \frac{E_{p^b}(E_p - E_{p^b})^2}{16E_1^2 (D_2^b)^2}. \end{aligned}$$

It is obvious that the last four terms vanish quadratically in the on-shell limit. However, the term in the squared brackets is also of order  $\mathcal{O}((E_p - E_{p^b})^2)$ , when the propagators  $D_2$  and  $D_2^b$  are evaluated at  $k = (E_{k,D_1}, \vec{k})$  and  $k = (E_{k,D_1^b}, \vec{k})$ , respectively.

Let us shortly summarize what we gained in this section:

We constructed an integral representation for the counterterm of the self-energy diagram in  $\phi^3$ -theory in Figure 6.3. A benefit of our construction is that the counterterm satisfies all four requirements set up in the last section. In particular, it makes the residue of the sum of the counterterm and the self-energy integrand vanish in the on-shell limit.

This special property becomes useful when calculating two-loop integrals that contain a self-energy insertion, as the left diagram in Figure 6.1. In this case, the counterterm (6.42) can be used for a two-loop integral representation of the counterterm diagram in the right image of Figure 6.1. Within the loop-tree duality method the sum of both diagrams can be evaluated by applying cuts to two of the propagators, i.e. taking residues in the two energy integrations.

Our choice of the integrand of the counterterm (6.42) makes sure that the residue from the cut (1, 2) will vanish. For the cut (1, 6) we can say that there is no

residue coming from the counterterm diagram but only from the full two-loop contribution. This, we made sure by setting up condition (4) on the counterterm. All other cuts that can be applied are unproblematic, since they do not require taking residues of raised propagators.

### 6.3. SUBTRACTION TERMS FOR QCD

Next, we construct counterterms for the different one-loop self-energy contributions in QCD. By  $n_f$  and  $n_Q$ , we denote the number of massless and massive quarks, respectively. The QCD Lagrangian, including the counterterm contributions, is given in (2.53). The series expansion of the renormalization constants reads (2.54)

$$(6.50) \quad Z_a = 1 + \sum_{n=1}^{\infty} Z_a^{(n)} \left( \frac{\alpha_s}{4\pi} \right)^n.$$

For constructing the counterterms, we need the renormalization constants at one-loop order for a massless ( $Z_2$ ) and a massive ( $Z_{2,Q}$ ) quark field, the gluon field ( $Z_3$ ) and the mass  $m$  of the heavy quark ( $Z_m$ ). Additionally, we split up the renormalization constant for the gluon field into  $Z_{3,l}^{(1)}$  and  $Z_{3,Q}^{(1)}$  for the contributions, coming from the massless partons or the massive quark inside the loop, respectively

$$(6.51) \quad Z_3^{(1)} = Z_{3,l}^{(1)} + Z_{3,Q}^{(1)}.$$

At one-loop order and in the on-shell scheme the required renormalization constants are given by

$$(6.52) \quad \begin{aligned} Z_2^{(1)} &= 0, \\ Z_{2,Q}^{(1)} &= -(3 - 2\epsilon) C_F B_0(m^2, m^2, 0), \\ Z_m^{(1)} &= -(3 - 2\epsilon) C_F B_0(m^2, m^2, 0), \\ Z_{3,l}^{(1)} &= 0, \\ Z_{3,Q}^{(1)} &= -\frac{4}{3} T_R n_Q B_0(m^2, m^2, 0). \end{aligned}$$

Note that we only consider the case where all heavy quarks have the same mass  $m$  and we suppress all Kronecker deltas in color space. The counterterms are

then given by (2.55)

$$(6.53) \quad \delta_a := \frac{\alpha_s}{4\pi} Z_a^{(1)}.$$

### 6.3.1. Light Quarks

For the self-energy of a light quark, we consider the self-energy graph for a quark (cf. Figure 2.3) with the labeling of the momenta as in Figure 6.3. With

$$(6.54) \quad D_1 = \left(k + \frac{1}{2}p\right)^2, \quad D_2 = \left(k - \frac{1}{2}p\right)^2,$$

we find for the corresponding integral

$$(6.55) \quad -i\Sigma_{(1)} = g_s^2 \mu^{2\epsilon} S_\epsilon^{-1} \int \frac{d^D k}{(2\pi)^D} R_{(1)},$$

where the one-loop integrand is given by

$$(6.56) \quad R_{(1)} = C_F \frac{2(1-\epsilon) \not{k} + \frac{1}{2}\not{p}}{D_1 D_2}.$$

Then, the counterterm can be written as

$$(6.57) \quad -i\Sigma_{(1),\text{CT}} = g_s^2 \mu^{2\epsilon} S_\epsilon^{-1} \int \frac{d^D k}{(2\pi)^D} R_{(1),\text{CT}} \stackrel{!}{=} i\delta_2 \not{p} = 0.$$

The on-shell projections of the propagators are given by

$$(6.58) \quad D_1^b = \left(k + \frac{1}{2}p^b\right)^2, \quad D_2^b = \left(k - \frac{1}{2}p^b\right)^2.$$

Expanding  $R_{(1)}$  around the on-shell kinematics yields a suitable form for the counterterm integrand

$$(6.59) \quad R_{(1),\text{CT}} = -C_F \frac{2(1-\epsilon) \not{k} + \frac{1}{2}\not{p}}{D_1^b D_2^b} \times \left[ 1 - \frac{4k \cdot (p - p^b) + p^2}{4D_1^b} + \frac{4k \cdot (p - p^b) - p^2}{4D_2^b} \right].$$

Carrying out the integration over  $R_{(1),\text{CT}}$  shows that the integral vanishes in dimensional regularization. Hence, we do not need to add additional terms to satisfy condition (1), i.e. Equation (6.57).



## 6.3.2. Heavy Quarks

For heavy quarks, the situation is a bit more involved. With our labeling of the momenta, we have

$$(6.60) \quad D_1 = \left(k + \frac{1}{2}p\right)^2 - m^2, \quad D_2 = \left(k - \frac{1}{2}p\right)^2.$$

The self-energy integral is given by

$$(6.61) \quad -i\Sigma_{(1)} = g_s^2 \mu^{2\epsilon} S_\epsilon^{-1} \int \frac{d^D k}{(2\pi)^D} R_{(1)},$$

with the integrand

$$(6.62) \quad R_{(1)} = C_F \frac{2(1-\epsilon) \left(k + \frac{1}{2}p\right) - 4(1-\frac{1}{2}\epsilon)m}{D_1 D_2}.$$

In the massive case, the counterterm integral can be written as

$$(6.63) \quad \begin{aligned} -i\Sigma_{(1),\text{CT}} &= g_s^2 \mu^{2\epsilon} S_\epsilon^{-1} \int \frac{d^D k}{(2\pi)^D} R_{(1),\text{CT}} \\ &\stackrel{!}{=} i \left[ \delta_{2,Q} \not{p} - (\delta_{2,Q} + \delta_m) m \right]. \end{aligned}$$

The on-shell projections, we need to expand around, are

$$(6.64) \quad D_1^b = \left(k + \frac{1}{2}p^b\right)^2 - m^2, \quad D_2^b = \left(k - \frac{1}{2}p^b\right)^2$$

In the massless case, the expansion of  $R_{(1)}$  around  $D_1^b$  and  $D_2^b$  provided a sufficient form for the counterterm. However, it only yields the correct on-shell and UV behavior. For the massive case, we have to add terms that do not spoil this behavior and also give the desired result (6.63) when integrated over. Taking

all this into account, we find

$$\begin{aligned}
(6.65) \quad \frac{1}{C_F} R_{(1),\text{CT}} = & -\frac{2(1-\epsilon)(\not{k} + \frac{1}{2}\not{p}^b) - 4(1-\frac{1}{2}\epsilon)m}{D_1^b D_2^b} \\
& \times \left[ 1 - \frac{4k \cdot (p - p^b) + p^2 - m^2}{4D_1^b} + \frac{4k \cdot (p - p^b) - p^2 + m^2}{4D_2^b} \right] \\
& - \frac{(1-\epsilon)(\not{p} - \not{p}^b)}{D_1^b D_2^b} - \frac{\epsilon m (p - p^b)^2}{2(D_1^b)^2 D_2^b} \\
& - \frac{1}{4} (\not{p}^b - m) (p^2 - m^2) \frac{D_1^b - D_2^b + 4m^2}{(D_1^b)^2 (D_2^b)^2} \\
& + \frac{m (p - p^b)^2 (D_1^b - D_2^b) (D_1^b - D_2^b + 2m^2)}{4m^2 (D_1^b)^2 (D_2^b)^2} \\
& + \frac{(\not{p}^b - m) [p^b \cdot (p - p^b)] (D_1^b - D_2^b) (D_1^b - D_2^b + \frac{3}{2}m^2)}{m^2 (D_1^b)^2 (D_2^b)^2} \\
& + \frac{[2(\not{p} - m)m^2 - m(p^2 - m^2)] (D_1^b - D_2^b) (2D_1^b + D_2^b)}{2m^2 (D_1^b)^2 (D_2^b)^2}
\end{aligned}$$

as a suitable form for the counterterm. Note that the last five terms vanish in the on-shell and in the UV limit. As an example, the UV behavior of the last term is of order  $\mathcal{O}(|k|^{-5})$ . To see its behavior in the on-shell limit, one can show that

$$(6.66) \quad 2(\not{p} - m)m^2 - m(p^2 - m^2) = -m(\not{p} - m)(\not{p} - m).$$

Thus, (6.65) is a possible choice for the counterterm for the heavy quark self-energy that satisfies all four desired conditions.

### 6.3.3. Gluons

For the computation of the gluon self-energy we have to sum up four different diagrams. They differ in the particles in the loop. The first diagram in Figure 6.5 shows the case of a quark loop. The second and third diagrams show a gluon loop involving the three-gluon vertex and the four-gluon vertex, respectively. In the last diagram in Figure 6.5 we have to take the ghost loop into account (cf. Section 2.5).

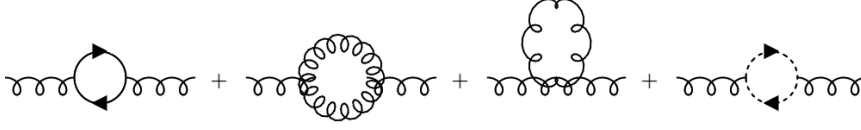


FIGURE 6.5. All Feynman diagrams that contribute to the gluon self-energy.

Additionally, we differentiate between two cases. First, we construct the counterterm for the case where the particles in the loop are massless, i.e. massless quarks, gluons and ghosts. Secondly, we construct a counterterm for the diagram with massive quarks in the loop.

For the gluon self-energy, we encounter the problem of tensor integrals. Let us denote the self-energy integral at one-loop by  $-i\Pi_{(1)}^{\mu\nu}$ . This is a tensor of second order. A commonly used technique for reducing tensor integrals to scalar integrals is the Passarino–Veltmann reduction [143]. In  $-i\Pi_{(1)}^{\mu\nu}$ , only the tensors  $g^{\mu\nu}$  and  $p^\mu p^\nu$  can appear. Hence, we may write

$$(6.67) \quad -i\Pi_{(1)}^{\mu\nu} = i(p^2 g^{\mu\nu} - p^\mu p^\nu) \Pi_{(1)}(p^2).$$

Expanding the scalar function  $\Pi_{(1)}(p^2)$  around the on-shell value  $p^2 = 0$  yields

$$(6.68) \quad \Pi_{(1)}(p^2) = \Pi_{(1)}(0) + \mathcal{O}(p^2).$$

This defines us the counterterm at one-loop order, using the definition of (2.55)

$$(6.69) \quad \delta_3 := \frac{\alpha_s}{4\pi} Z_3^{(1)} = \Pi_{(1)}(0).$$

The tensor structure of the counterterm, then, reads

$$(6.70) \quad -i\Pi_{(1),\text{CT}}^{\mu\nu} = -i(p^2 g^{\mu\nu} - p^\mu p^\nu) \delta_3,$$

and we find

$$(6.71) \quad -i\left(\Pi_{(1)}^{\mu\nu} + \Pi_{(1),\text{CT}}^{\mu\nu}\right) = i(p^2 g^{\mu\nu} - p^\mu p^\nu) \cdot \mathcal{O}(p^2).$$

We want to stress that this remnant vanishes in the on-shell limit, i.e. there is no residue to be calculated. For the first term on the right-hand-side, proportional to  $g^{\mu\nu}$ , we have a factor of  $(p^2)^2$ , which cancels a double pole from the propagators. The second term, coming with a factor  $p^2$ , cancels only one pole. Hence, there is still a residue coming from a single pole in the propagators. However, the contribution from this residue can be neglected because we can

contract  $p^\mu p^\nu$  with an on-shell momentum  $p_\mu$  or  $p_\nu$ . In this case the contribution will vanish.

### *Massless Case*

In the massless case we have to take all diagrams in Figure 6.5 into account. For the diagram with the quark loop, we only consider light quarks. With  $D_1$  and  $D_2$  defined as in (6.54), we have for the gluon self-energy, with only massless particles in the loop,

$$(6.72) \quad -i\Pi_{(1)}^{\mu\nu} = g_s^2 \mu^{2\epsilon} S_\epsilon^{-1} \int \frac{d^D k}{(2\pi)^D} R_{(1)}.$$

The integrand is given by

$$(6.73) \quad R_{(1)} = \frac{C_{\text{massless}}}{D_1 D_2},$$

where we introduced the abbreviation

$$(6.74) \quad \begin{aligned} C_{\text{massless}} := & \\ & -2C_A \left[ -p^2 g^{\mu\nu} + p^\mu p^\nu - 2(1-\epsilon) k^\mu k^\nu + \frac{1}{2}(1-\epsilon) g^{\mu\nu} (D_1 + D_2) \right] \\ & -2T_R n_f \left[ p^2 g^{\mu\nu} - p^\mu p^\nu + 4k^\mu k^\nu - g^{\mu\nu} (D_1 + D_2) \right]. \end{aligned}$$

The first term on the right-hand-side is obtained from the contributions of the gluons and the ghosts in the loop. The second term comes from the quark loop. The integral of the counterterm yields

$$(6.75) \quad \begin{aligned} -i\Pi_{(1),\text{CT}}^{\mu\nu} &= g_s^2 \mu^{2\epsilon} S_\epsilon^{-1} \int \frac{d^D k}{(2\pi)^D} R_{(1),\text{CT}} \\ &\stackrel{!}{=} -i (p^2 g^{\mu\nu} - p^\mu p^\nu) \delta_{3,l} = 0. \end{aligned}$$

For the massless case, we have the same on-shell kinematics as for the light quark self-energy

$$(6.76) \quad D_1^b = \left( k + \frac{1}{2} p^b \right)^2, \quad D_2^b = \left( k - \frac{1}{2} p^b \right)^2.$$

A form of the counterterm integrand  $R_{(1)}$  featuring the desired properties is given by

$$(6.77) \quad R_{(1),\text{CT}} = -\frac{C_{\text{massless}}}{D_1^b D_2^b} \left[ 1 - \frac{4k \cdot (p - p^b) + p^2}{4D_1^b} + \frac{4k \cdot (p - p^b) - p^2}{4D_2^b} \right] - C_{\text{massless}} \frac{(k \cdot (p - p^b))^2}{D_1^b D_2^b} \left( \frac{1}{(D_1^b)^2} + \frac{1}{(D_2^b)^2} - \frac{1}{D_1^b D_2^b} \right).$$

*Massive Case*

For the massive case, we only have to consider the left diagram in Figure 6.5 with heavy quarks in the loop. Assuming that both quarks carry the mass  $m$ , the propagators read

$$(6.78) \quad D_1 = \left( k + \frac{1}{2}p \right)^2 - m^2, \quad D_2 = \left( k - \frac{1}{2}p \right)^2 - m^2.$$

For the integral of the massive quark contribution, we have

$$(6.79) \quad -i\Pi_{(1)}^{\mu\nu} = g_s^2 \mu^{2\epsilon} S_\epsilon^{-1} \int \frac{d^D k}{(2\pi)^D} R_{(1)},$$

with the integrand

$$(6.80) \quad R_{(1)} = -2T_{\text{R}} n_Q \frac{p^2 g^{\mu\nu} - p^\mu p^\nu + 4k^\mu k^\nu - g^{\mu\nu} (D_1 + D_2)}{D_1 D_2}.$$

The integral of the counterterm is given by

$$(6.81) \quad -i\Pi_{(1),\text{CT}}^{\mu\nu} = g_s^2 \mu^{2\epsilon} S_\epsilon^{-1} \int \frac{d^D k}{(2\pi)^D} R_{(1),\text{CT}} \\ \stackrel{!}{=} -i (p^2 g^{\mu\nu} - p^\mu p^\nu) \delta_{3,Q}.$$

We can write the on-shell projections of  $D_1$  and  $D_2$  as

$$(6.82) \quad D_1^b = \left( k + \frac{1}{2}p^b \right)^2 - m^2, \quad D_2^b = \left( k - \frac{1}{2}p^b \right)^2 - m^2,$$

in the massive case.

Similar to the case of the heavy quark self-energy counterterm, we have to add several terms to the expansion of  $R_{(1)}$  to obtain the correct result, when  $R_{(1),\text{CT}}$  is integrated. Before we give our choice for the counterterm  $R_{(1),\text{CT}}$ , we want to recall the statements following (6.71): Although a term proportional to

$p^2 p^{b\mu} p^{b\nu}$  does not cancel a double pole in the propagators, it gives a vanishing contribution in the on-shell limit, when contracted with  $p_\mu^b$  or  $p_\nu^b$ .

Taking this into account, we find as a suitable form for the counterterm

$$\begin{aligned}
(6.83) \quad \frac{1}{T_{\text{R}} n_Q} R_{(1),\text{CT}} &= \frac{2(p^2 g^{\mu\nu} - p^\mu p^\nu)}{D_1^b D_2^b} \\
&\times \left[ 1 - \frac{4k \cdot (p - p^b) + p^2}{4D_1^b} + \frac{4k \cdot (p - p^b) - p^2}{4D_2^b} \right] \\
&+ \frac{[8k^\mu k^\nu - 2g^{\mu\nu} (D_1^b + D_2^b)]}{D_1^b D_2^b} \\
&\times \left[ 1 - \frac{4k \cdot (p - p^b) + p^2}{4D_1^b} + \frac{4k \cdot (p - p^b) - p^2}{4D_2^b} \right. \\
&\left. + (k \cdot (p - p^b))^2 \left( \frac{1}{(D_1^b)^2} + \frac{1}{(D_2^b)^2} - \frac{1}{D_1^b D_2^b} \right) \right] - \frac{p^2 g^{\mu\nu}}{D_1^b D_2^b} \\
&- \frac{3(p^b \cdot (p - p^b))^2 p^{b\mu} p^{b\nu}}{14 (D_1^b)^2 (D_2^b)^2} \\
&+ \left[ \left( \frac{1}{3} p^b \cdot (p - p^b) - \frac{p^2}{2} \right) (p - p^b)^\mu (p - p^b)^\nu \right. \\
&+ \left( \frac{2}{15} p^b \cdot (p - p^b) - \frac{p^2}{2} \right) \left( (p - p^b)^\mu p^{b\nu} + p^{b\mu} (p - p^b)^\nu \right) \\
&- \frac{1}{6} (p - p^b)^2 p^{b\mu} p^{b\nu} + \frac{2}{5} (p^b \cdot (p - p^b))^2 g^{\mu\nu} \\
&\left. + \frac{1}{6} \left( (p - p^b)^2 + 2p^2 \right) p^2 g^{\mu\nu} - \frac{4}{15} p^2 p^{b\mu} p^{b\nu} \right] \frac{D_1^b + D_2^b}{(D_1^b)^2 (D_2^b)^2}
\end{aligned}$$

Note that the terms in the lines six to ten had to be added to obtain the correct result, when integrating  $R_{(1),\text{CT}}$ . The other terms ensure the right behavior in the on-shell and UV limit.

## **Part 4**

# **Conclusions and Outlook**





## CHAPTER 7

### Conclusions and Outlook

In this thesis, we discussed several aspects of theoretical computations and predictions in high energy physics. It is apparent that the constantly increasing precision of experimental measurements also requires the theoretical predictions to become more accurate. Therefore, we focused on two different aspects of theoretical predictions that help to make a step forward on this path.

In the first part of the thesis, we gave a general introduction to the modelling of the event structure inside a collider experiment. Additionally, we recapitulated the basics of quantum chromodynamics (QCD), the theory of the strong interaction between quarks and gluons.

Let us shortly summarize, which are the constituents of the modelling of a collider event to make theoretical predictions:

Usually, we start from the hard scattering event that can be calculated perturbatively. What we obtain is the result for a scattering process with a limited number of final-state particles. Next, we apply a parton shower to the final-state configuration of the hard event. The parton shower evolves from the scale of the hard scattering down to a cutoff scale. In this way, the particle multiplicity is increased significantly.

The cutoff represents a separation between the perturbative regime of the parton shower and the non-perturbative region, where hadronization has to be applied. Thus, the next step in modelling an event is the application of a hadronization model that clusters the color charged partons into hadrons. Lastly, the decay of the final-state particles has to be modelled. Additionally, the particles can form jets, which is accounted for by applying a jet algorithm.

There exist computer programs that model all these steps required for event generation. They are called Monte Carlo (MC) event generators.

In the second part of this thesis, we focused on the role of the parton shower, particularly concerning the determination of the top quark mass. The top quark is by far the heaviest elementary particle and, hence, the exact knowledge of its

properties plays a crucial role in our understanding of the Standard Model (SM). However, it is still not exactly clear, how the top quark mass from event generators is related to a quantum field theoretical top quark mass inside a certain renormalization scheme. The mass inside the event generator is often referred to as MC mass.

To make a step forward in understanding this relation, it is natural to ask, how the MC mass depends on certain parameters inside the event generator, particularly inside the parton shower simulation. One step in this direction was made in the second part of this thesis.

In Chapter 3 we started from the general structure of next-to-leading order (NLO) computations to arrive at the dipole subtraction scheme. In this scheme, we encounter so-called dipole splitting functions. These splitting functions form the basis of the dipole parton shower algorithm that is described in Chapter 4. This shower algorithm is our preferred choice for the analysis carried out in Chapter 5.

In Chapter 5 we discussed some general aspects of the top mass determination and reviewed some recent work on quantifying the relation between the MC mass and a theoretically well-defined mass scheme.

The main part of this chapter is centered around the dependence of the top quark mass on the cutoff parameter  $Q_0$  of the parton shower. For this, we summarized the results of the analytical computations in [9]. There, they used two different theoretical approaches to quantify the relation of the peak position of the thrust distribution on the cutoff parameter  $Q_0$ . Thrust is an observable that is highly sensitive to the value of top quark mass.

The two ways to compute the thrust distribution are calculations in soft-collinear effective theory (SCET) and the coherent branching formalism. It is shown that both approaches lead to the same relation of the thrust peak position  $\tau_{\text{peak}}$  on the cutoff parameter  $Q_0$ . For the case of massless final-state particles this relation reads

$$(7.1) \quad \tau_{\text{peak}}(Q_0) = \tau_{\text{peak}}(Q'_0) - \frac{16}{Q} \int_{Q'_0}^{Q_0} dR \frac{\alpha_s(R) C_F}{4\pi}.$$

Here,  $\tau_{\text{peak}}(Q'_0)$  denotes the peak position at a reference value  $Q'_0$ ,  $Q$  is the center-of-mass energy of the hard event and  $\alpha_s$  is the strong coupling.

In [9], the analytic relation (7.1) is validated by using parton shower simulations from the general-purpose event generator HERWIG. We stress that the use of HERWIG implies an angular-ordered parton shower algorithm that is based on the coherent branching formalism. Since relation (7.1) is also derived within the coherent branching algorithm, the question arises, if it also holds for other shower algorithms, i.e. the dipole shower algorithm of Section 4.2.

This question was addressed by our analysis in Section 5.3. There, we presented our results for the cutoff dependence of the peak position of the thrust distribution obtained from parton shower simulations, using the dipole shower algorithm.

For this, we generated events for the process  $e^+e^- \rightarrow q\bar{q}$  with two different center-of-mass energies,  $Q = 91$  GeV and  $Q = 300$  GeV. For each center-of-mass energy we applied different cutoff scales  $Q_0$  in the range from 0.4 GeV to 2.0 GeV in steps of 0.2 GeV. We generated  $10^7$  events for each combination of  $Q$  and  $Q_0$ . The resulting distribution was obtained as a histogram with a bin size of  $\Delta\tau = 10^{-3}$ .

To obtain the correct distribution, the partonic thrust distribution had to be convolved with the soft model shape function  $S_{\text{mod}}$  according to

$$(7.2) \quad \frac{d\sigma}{d\tau}(\tau, Q) = \int_0^{Q\tau} d\ell \frac{d\hat{\sigma}_s}{d\tau} \left( \tau - \frac{\ell}{Q}, Q \right) S_{\text{mod}}(\ell).$$

The soft model shape function models hadronization effects. Since we were only interested in the relative dependence of the peak position on  $Q_0$ , the exact form of  $S_{\text{mod}}$  is not pivotal. For our analysis we adopted the soft model shape function used in [9], namely

$$(7.3) \quad S_{\text{mod}}(\ell) = \frac{128}{3} \frac{\ell^3}{\Lambda_m} \exp\left(-\frac{4\ell}{\Lambda_m}\right),$$

where  $\Lambda_m$  is a smearing parameter that we varied between 1 and 3 GeV.

Our analysis shows a good agreement between the dependence of  $\tau_{\text{peak}}$  on the cutoff  $Q_0$  inside our parton shower simulations and the relation in (7.1). As an example, the cutoff dependence for  $Q = 91$  GeV and  $\Lambda_m = 1$  GeV is shown in Figure 7.1. The centers of the red squares give the results of our analysis while the blue line depicts the analytic relation. For the reference value  $\tau_{\text{peak}}(Q'_0)$ , we chose the value obtained from the parton shower simulations at  $Q'_0 = 1.2$  GeV.

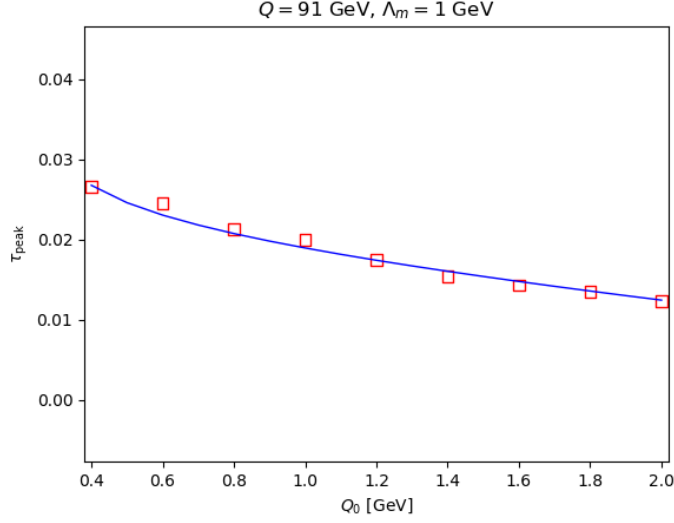


FIGURE 7.1. Cutoff dependence of  $\tau_{\text{peak}}$  for  $Q = 91$  GeV and  $\Lambda_m = 1$  GeV. The centers of the red squares give the data from shower simulations. The blue line comes from the analytical result.

Our results show that the analytically derived relation is not only valid for angular-ordered showers algorithms, but also for shower simulations that are based on the dipole formalism. We emphasize that our analysis is only carried out for massless final-state partons. To have better predictions on the dependence of the top quark mass on the cutoff, it is also desirable to examine the massive case. Additionally, there are many ways to further investigate the interplay between the shower parameters and observables. For example, the procedure could be used for other observables and different parameters in the shower. These tasks are left as future projects.

The third part of this thesis is dedicated to the topic of scattering amplitudes. To reach next-to-next-to-leading order (NNLO) accuracy in perturbative calculations, it is necessary to find ways to automate the computation of two-loop diagrams with more than two particles in the final state.

One promising approach to this task is found in loop-tree duality combined with numerical loop integration. In loop-tree duality at two-loop order, one encounters diagrams that have a self-energy insertion on one of the internal lines. This leads to propagators in the loop integral that have exponents bigger than one. These are referred to as raised propagators.

For calculations in loop-tree duality, the residues of the raised propagators have to be calculated for the case of these propagators going on-shell. However, the calculation of the residue involves the computation of derivatives. This makes it process-dependent and, hence, not well suited for automation.

In Chapter 6, we showed that it is possible to find a counterterm for the self-energy insertion on an integrand level in the on-shell scheme that makes the residue vanish. This counterterm has the correct UV and on-shell behavior and leads to a vanishing residue, when combined with the self-energy insertion. However, the form of the counterterm is not unique.

We started from a toy model and extended our method to scalar  $\phi^3$ -theory and QCD. Not only did we show that counterterms with the desired properties exist but we also provided explicit forms for the counterterms in  $\phi^3$ -theory and QCD. Let us add that the resulting counterterms contain higher powers in the propagators as well. However, by constructing the counterterms we isolated the problem of raised propagators into a process-independent part. Therefore, the residues involving the raised propagators can be calculated once and, then, be used in every two-loop calculation involving a self-energy insertion.

The counterterms we provided are for self-energy graphs at one-loop order. Since in the foreseeable future, theoretical considerations might reach an accuracy that requires three-loop computations, it is natural to ask, if our method can be extended to self-energy insertions at two loops or more. We expect that this is indeed possible. The search for an answer to this essential question is left as a future project.

As a final conclusion, let us say that although many big steps have been made on the way to understanding the world of elementary particles and their interactions, there is still a lot of work to do. We hope, the research and results of this thesis contribute to the search for an answer to the question, already raised in Goethe's Faust, of "whatever binds the world's innermost core together".



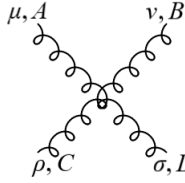
**Part 5**

**Appendix**



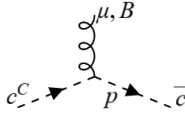






$$\begin{aligned}
&= -ig_s^2 [f^{ABE} f^{CDE} (g^{\mu\rho} g^{\nu\sigma} - g^{\mu\sigma} g^{\nu\rho}) \\
&\quad + f^{ACE} f^{BDE} (g^{\mu\nu} g^{\rho\sigma} - g^{\mu\sigma} g^{\nu\rho}) \\
&\quad + f^{ADE} f^{BCE} (g^{\mu\nu} g^{\rho\sigma} - g^{\mu\rho} g^{\nu\sigma})]
\end{aligned}$$

Finally, we have for the ghost-gluon vertex:



$$= -g_s f^{ABC} p^\mu$$

## A.2. FORMULAE FOR THE IMPLEMENTATION OF $\alpha_s$

For the implementation of  $\alpha_s$ , using a reference value  $\alpha_s(\mu_0)$  at a given scale  $\mu_0$ , different formulae can be used. The expansion around this value up to order  $\alpha_s^3$  reads [13]

$$\begin{aligned}
\alpha_s(\mu) &= \alpha_s(\mu_0) - \frac{\alpha_s^2(\mu_0)}{2\pi} \beta_0 \log\left(\frac{\mu}{\mu_0}\right) \\
&+ \frac{\alpha_s^3(\mu_0)}{8\pi^2} \left[ -\beta_1 \log\left(\frac{\mu}{\mu_0}\right) + 2\beta_0^2 \log^2\left(\frac{\mu}{\mu_0}\right) \right] + \mathcal{O}(\alpha_s^4(\mu_0)),
\end{aligned}
\tag{A.1}$$

where  $\beta_0$  and  $\beta_1$  are the first two coefficients of the QCD beta function (2.41). A second way to implement the strong coupling is to use the following formulae, at one-loop order

$$\alpha_s^{(1)}(\mu) = \frac{\alpha_s(\mu_0)}{1 + \frac{\alpha_s(\mu_0)}{2\pi} \beta_0 \log\left(\frac{\mu}{\mu_0}\right)}.
\tag{A.2}$$

It is obtained by solving the RGE of  $\alpha_s$  at first order

$$\frac{d\alpha_s}{d \log(\mu)} = -\frac{\alpha_s^2}{2\pi} \beta_0,
\tag{A.3}$$

by separation of variables and integration from  $\mu_0$  to  $\mu$ .

A similar approach at two-loop order, including a resummation of logarithms

as  $\log(\mu_0/\mu)$ , yields [144]

$$(A.4) \quad \alpha_s^{(2)}(\mu) = \frac{\alpha_s(\mu_0)}{w} \left[ 1 - \frac{\beta_1}{\beta_0} \alpha_s(\mu_0) \frac{\log(w)}{w} \right],$$

with

$$(A.5) \quad w := 1 + \beta_0 \alpha_s(\mu_0) \log \left( \frac{\mu}{\mu_0} \right).$$



## APPENDIX B

### Parton Showers

#### B.1. LORENTZ TRANSFORMATIONS

Here, we present the explicit form of the Lorentz transformations used to obtain the momenta of the partons  $i$ ,  $j$  and  $k$  after the branching in the dipole shower formalism of Section 4.2.

Let  $P$  and  $q$  be two arbitrary four momenta and  $|P| = \sqrt{p^2}$  as usual. Let us additionally assume that  $p^2 \neq 0$ . The Lorentz boost that transforms  $q$  into the rest frame of  $P$  is given by

$$(B.1) \quad \Lambda^b(\hat{P})q = \left[ \frac{E_P}{|P|} E_q - \frac{\vec{P} \cdot \vec{q}}{|P|}, \vec{q} + \left( \frac{\vec{P} \cdot \vec{q}}{|P|(E_P + |P|)} - \frac{E_q}{|P|} \right) \vec{P} \right].$$

The parity operation on a four-vector  $x$  is defined as  $\hat{x} := (x^0, -\vec{x})$ .

The boost back to the original frame is given by

$$(B.2) \quad \Lambda^b(P)q = \left[ \frac{E_P}{|P|} E_q + \frac{\vec{P} \cdot \vec{q}}{|P|}, \vec{q} + \left( \frac{\vec{P} \cdot \vec{q}}{|P|(E_P + |P|)} + \frac{E_q}{|P|} \right) \vec{P} \right].$$

The matrix that defines the rotation around the  $z$ -axis by the angle  $\phi_z$  reads

$$(B.3) \quad \Lambda_z^r(\phi_z) = \begin{pmatrix} 1 & 0 & 0 & 0 \\ 0 & \cos(\phi_x) & -\sin(\phi_x) & 0 \\ 0 & \sin(\phi_x) & \cos(\phi_x) & 0 \\ 0 & 0 & 0 & 1 \end{pmatrix},$$

while the rotation around the  $y$ -axis by the angle  $\theta_y$  is given by

$$(B.4) \quad \Lambda_y^r(\theta_y) = \begin{pmatrix} 1 & 0 & 0 & 0 \\ 0 & \cos(\theta_y) & 0 & \sin(\theta_y) \\ 0 & 0 & 1 & 0 \\ 0 & -\sin(\theta_y) & 0 & \cos(\theta_y) \end{pmatrix}.$$



## Bibliography

- [1] G. Corcella, I. G. Knowles, G. Marchesini, S. Moretti, K. Odagiri, P. Richardson, M. H. Seymour, and B. R. Webber, “HERWIG 6: An Event generator for hadron emission reactions with interfering gluons (including supersymmetric processes)”, *JHEP* **01**, 010 (2001), arXiv:hep-ph/0011363 [hep-ph].
- [2] M. Bahr et al., “Herwig++ Physics and Manual”, *Eur. Phys. J.* **C58**, 639–707 (2008), arXiv:0803.0883 [hep-ph].
- [3] J. Bellm et al., “Herwig 7.0/Herwig++ 3.0 release note”, *Eur. Phys. J.* **C76**, 196 (2016), arXiv:1512.01178 [hep-ph].
- [4] J. Bellm et al., “Herwig 7.1 Release Note”, (2017), arXiv:1705.06919 [hep-ph].
- [5] T. Sjostrand, S. Mrenna, and P. Z. Skands, “PYTHIA 6.4 Physics and Manual”, *JHEP* **05**, 026 (2006), arXiv:hep-ph/0603175 [hep-ph].
- [6] T. Sjöstrand, S. Ask, J. R. Christiansen, R. Corke, N. Desai, P. Ilten, S. Mrenna, S. Prestel, C. O. Rasmussen, and P. Z. Skands, “An Introduction to PYTHIA 8.2”, *Comput. Phys. Commun.* **191**, 159–177 (2015), arXiv:1410.3012 [hep-ph].
- [7] T. Gleisberg, S. Hoeche, F. Krauss, M. Schonherr, S. Schumann, F. Siegert, and J. Winter, “Event generation with SHERPA 1.1”, *JHEP* **02**, 007 (2009), arXiv:0811.4622 [hep-ph].
- [8] E. Bothmann et al., “Event Generation with Sherpa 2.2”, *SciPost Phys.* **7**, 034 (2019), arXiv:1905.09127 [hep-ph].
- [9] A. H. Hoang, S. Plätzer, and D. Samitz, “On the Cutoff Dependence of the Quark Mass Parameter in Angular Ordered Parton Showers”, (2018), arXiv:1807.06617 [hep-ph].
- [10] M. Dinsdale, M. Ternick, and S. Weinzierl, “Parton showers from the dipole formalism”, *Phys. Rev.* **D76**, 094003 (2007), arXiv:0709.1026 [hep-ph].

- [11] R. Baumeister, D. Mediger, J. Pečovnik, and S. Weinzierl, “Vanishing of certain cuts or residues of loop integrals with higher powers of the propagators”, *Phys. Rev.* **D99**, 096023 (2019), arXiv:1903.02286 [hep-ph].
- [12] R. K. Ellis, W. J. Stirling, and B. R. Webber, “QCD and collider physics”, *Camb. Monogr. Part. Phys. Nucl. Phys. Cosmol.* **8**, 1–435 (1996).
- [13] M. D. Schwartz, *Quantum Field Theory and the Standard Model* (Cambridge University Press, 2014).
- [14] M. E. Peskin and D. V. Schroeder, *An Introduction to quantum field theory* (Addison-Wesley, Reading, USA, 1995).
- [15] M. Tanabashi et al. (Particle Data Group), “Review of Particle Physics”, *Phys. Rev.* **D98**, 030001 (2018).
- [16] S. Weinzierl, “Tales of 1001 Gluons”, *Phys. Rept.* **676**, 1–101 (2017), arXiv:1610.05318 [hep-th].
- [17] H. D. Politzer, “Reliable Perturbative Results for Strong Interactions?”, *Phys. Rev. Lett.* **30**, 1346–1349 (1973).
- [18] D. J. Gross and F. Wilczek, “Ultraviolet Behavior of Nonabelian Gauge Theories”, *Phys. Rev. Lett.* **30**, 1343–1346 (1973).
- [19] D. J. Gross and F. Wilczek, “Asymptotically Free Gauge Theories - I”, *Phys. Rev.* **D8**, 3633–3652 (1973).
- [20] T. van Ritbergen, J. A. M. Vermaseren, and S. A. Larin, “The Four loop beta function in quantum chromodynamics”, *Phys. Lett.* **B400**, 379–384 (1997), arXiv:hep-ph/9701390 [hep-ph].
- [21] M. Czakon, “The Four-loop QCD beta-function and anomalous dimensions”, *Nucl. Phys.* **B710**, 485–498 (2005), arXiv:hep-ph/0411261 [hep-ph].
- [22] P. A. Baikov, K. G. Chetyrkin, and J. H. Kühn, “Five-Loop Running of the QCD coupling constant”, *Phys. Rev. Lett.* **118**, 082002 (2017), arXiv:1606.08659 [hep-ph].
- [23] T. Luthe, A. Maier, P. Marquard, and Y. Schroder, “Complete renormalization of QCD at five loops”, *JHEP* **03**, 020 (2017), arXiv:1701.07068 [hep-ph].
- [24] F. Herzog, B. Ruijl, T. Ueda, J. A. M. Vermaseren, and A. Vogt, “The five-loop beta function of Yang-Mills theory with fermions”, *JHEP* **02**, 090 (2017), arXiv:1701.01404 [hep-ph].



- [25] I. I. Y. Bigi, M. A. Shifman, N. G. Uraltsev, and A. I. Vainshtein, “The Pole mass of the heavy quark. Perturbation theory and beyond”, *Phys. Rev.* **D50**, 2234–2246 (1994), arXiv:hep-ph/9402360 [hep-ph].
- [26] M. Beneke, “More on ambiguities in the pole mass”, *Phys. Lett.* **B344**, 341–347 (1995), arXiv:hep-ph/9408380 [hep-ph].
- [27] M. Beneke and V. M. Braun, “Heavy quark effective theory beyond perturbation theory: Renormalons, the pole mass and the residual mass term”, *Nucl. Phys.* **B426**, 301–343 (1994), arXiv:hep-ph/9402364 [hep-ph].
- [28] M. Beneke, “Renormalons”, *Phys. Rept.* **317**, 1–142 (1999), arXiv:hep-ph/9807443 [hep-ph].
- [29] M. Beneke, P. Marquard, P. Nason, and M. Steinhauser, “On the ultimate uncertainty of the top quark pole mass”, *Phys. Lett.* **B775**, 63–70 (2017), arXiv:1605.03609 [hep-ph].
- [30] A. H. Hoang, A. Jain, I. Scimemi, and I. W. Stewart, “Infrared Renormalization Group Flow for Heavy Quark Masses”, *Phys. Rev. Lett.* **101**, 151602 (2008), arXiv:0803.4214 [hep-ph].
- [31] A. H. Hoang, A. Jain, C. Lepenik, V. Mateu, M. Preisser, I. Scimemi, and I. W. Stewart, “The MSR Mass and the  $\mathcal{O}(\Lambda_{QCD})$  Renormalon Sum Rule”, (2017), arXiv:1704.01580 [hep-ph].
- [32] W. T. Giele and E. W. N. Glover, “Higher order corrections to jet cross-sections in  $e^+ e^-$  annihilation”, *Phys. Rev.* **D46**, 1980–2010 (1992).
- [33] W. T. Giele, E. W. N. Glover, and D. A. Kosower, “Higher order corrections to jet cross-sections in hadron colliders”, *Nucl. Phys.* **B403**, 633–670 (1993), arXiv:hep-ph/9302225 [hep-ph].
- [34] S. Keller and E. Laenen, “Next-to-leading order cross-sections for tagged reactions”, *Phys. Rev.* **D59**, 114004 (1999), arXiv:hep-ph/9812415 [hep-ph].
- [35] B. W. Harris and J. F. Owens, “The Two cutoff phase space slicing method”, *Phys. Rev.* **D65**, 094032 (2002), arXiv:hep-ph/0102128 [hep-ph].
- [36] J. Gao, C. S. Li, and H. X. Zhu, “Top Quark Decay at Next-to-Next-to Leading Order in QCD”, *Phys. Rev. Lett.* **110**, 042001 (2013), arXiv:1210.2808 [hep-ph].

- [37] R. Boughezal, C. Focke, X. Liu, and F. Petriello, “ $W$ -boson production in association with a jet at next-to-next-to-leading order in perturbative QCD”, *Phys. Rev. Lett.* **115**, 062002 (2015), arXiv:1504.02131 [hep-ph].
- [38] J. Gaunt, M. Stahlhofen, F. J. Tackmann, and J. R. Walsh, “N-jettiness Subtractions for NNLO QCD Calculations”, *JHEP* **09**, 058 (2015), arXiv:1505.04794 [hep-ph].
- [39] Z. Kunszt, A. Signer, and Z. Trocsanyi, “Singular terms of helicity amplitudes at one loop in QCD and the soft limit of the cross-sections of multiparton processes”, *Nucl. Phys.* **B420**, 550–564 (1994), arXiv:hep-ph/9401294 [hep-ph].
- [40] S. Frixione, Z. Kunszt, and A. Signer, “Three jet cross-sections to next-to-leading order”, *Nucl. Phys.* **B467**, 399–442 (1996), arXiv:hep-ph/9512328 [hep-ph].
- [41] S. Frixione, “A General approach to jet cross-sections in QCD”, *Nucl. Phys.* **B507**, 295–314 (1997), arXiv:hep-ph/9706545 [hep-ph].
- [42] S. Catani and M. H. Seymour, “A General algorithm for calculating jet cross-sections in NLO QCD”, *Nucl. Phys.* **B485**, [Erratum: *Nucl. Phys.* **B510**, 503(1998)], 291–419 (1997), arXiv:hep-ph/9605323 [hep-ph].
- [43] L. Phaf and S. Weinzierl, “Dipole formalism with heavy fermions”, *JHEP* **04**, 006 (2001), arXiv:hep-ph/0102207 [hep-ph].
- [44] S. Catani, S. Dittmaier, M. H. Seymour, and Z. Trocsanyi, “The Dipole formalism for next-to-leading order QCD calculations with massive partons”, *Nucl. Phys.* **B627**, 189–265 (2002), arXiv:hep-ph/0201036 [hep-ph].
- [45] S. Dittmaier, “A General approach to photon radiation off fermions”, *Nucl. Phys.* **B565**, 69–122 (2000), arXiv:hep-ph/9904440 [hep-ph].
- [46] S. Weinzierl, “Automated computation of spin- and colour-correlated Born matrix elements”, *Eur. Phys. J.* **C45**, 745–757 (2006), arXiv:hep-ph/0510157 [hep-ph].
- [47] R. Frederix, S. Frixione, F. Maltoni, and T. Stelzer, “Automation of next-to-leading order computations in QCD: The FKS subtraction”, *JHEP* **10**, 003 (2009), arXiv:0908.4272 [hep-ph].
- [48] S. Frixione, “Colourful FKS subtraction”, *JHEP* **09**, 091 (2011), arXiv:1106.0155 [hep-ph].

- [49] D. A. Kosower, “Antenna factorization of gauge theory amplitudes”, *Phys. Rev.* **D57**, 5410–5416 (1998), arXiv:hep-ph/9710213 [hep-ph].
- [50] J. M. Campbell, M. A. Cullen, and E. W. N. Glover, “Four jet event shapes in electron - positron annihilation”, *Eur. Phys. J.* **C9**, 245–265 (1999), arXiv:hep-ph/9809429 [hep-ph].
- [51] A. Gehrmann-De Ridder, T. Gehrmann, and E. W. N. Glover, “Antenna subtraction at NNLO”, *JHEP* **09**, 056 (2005), arXiv:hep-ph/0505111 [hep-ph].
- [52] A. Daleo, T. Gehrmann, and D. Maitre, “Antenna subtraction with hadronic initial states”, *JHEP* **04**, 016 (2007), arXiv:hep-ph/0612257 [hep-ph].
- [53] G. Somogyi and Z. Trocsanyi, “A New subtraction scheme for computing QCD jet cross sections at next-to-leading order accuracy”, (2006), arXiv:hep-ph/0609041 [hep-ph].
- [54] C. H. Chung, M. Kramer, and T. Robens, “An alternative subtraction scheme for next-to-leading order QCD calculations”, *JHEP* **06**, 144 (2011), arXiv:1012.4948 [hep-ph].
- [55] S. Dittmaier, A. Kabelschacht, and T. Kasprzik, “Polarized QED splittings of massive fermions and dipole subtraction for non-collinear-safe observables”, *Nucl. Phys.* **B800**, 146–189 (2008), arXiv:0802.1405 [hep-ph].
- [56] M. Czakon, C. G. Papadopoulos, and M. Worek, “Polarizing the Dipoles”, *JHEP* **08**, 085 (2009), arXiv:0905.0883 [hep-ph].
- [57] D. Goetz, C. Schwan, and S. Weinzierl, “Random Polarizations of the Dipoles”, *Phys. Rev.* **D85**, 116011 (2012), arXiv:1205.4109 [hep-ph].
- [58] G. Bevilacqua, M. Czakon, M. Kubocz, and M. Worek, “Complete Nagy-Soper subtraction for next-to-leading order calculations in QCD”, *JHEP* **10**, 204 (2013), arXiv:1308.5605 [hep-ph].
- [59] T. Kinoshita, “Mass singularities of Feynman amplitudes”, *J. Math. Phys.* **3**, 650–677 (1962).
- [60] T. D. Lee and M. Nauenberg, “Degenerate Systems and Mass Singularities”, *Phys. Rev.* **133**, [25(1964)], B1549–B1562 (1964).
- [61] S. Frixione, P. Nason, and C. Oleari, “Matching NLO QCD computations with Parton Shower simulations: the POWHEG method”, *JHEP* **11**, 070 (2007), arXiv:0709.2092 [hep-ph].

- [62] G. Altarelli and G. Parisi, “Asymptotic Freedom in Parton Language”, Nucl. Phys. **B126**, 298–318 (1977).
- [63] Y. L. Dokshitzer, “Calculation of the Structure Functions for Deep Inelastic Scattering and  $e^+ e^-$  Annihilation by Perturbation Theory in Quantum Chromodynamics.”, Sov. Phys. JETP **46**, [Zh. Eksp. Teor. Fiz.73,1216(1977)], 641–653 (1977).
- [64] V. N. Gribov and L. N. Lipatov, “Deep inelastic  $e p$  scattering in perturbation theory”, Sov. J. Nucl. Phys. **15**, [Yad. Fiz.15,781(1972)], 438–450 (1972).
- [65] G. C. Fox and S. Wolfram, “A Model for Parton Showers in QCD”, Nucl. Phys. **B168**, 285–295 (1980).
- [66] A. Buckley et al., “General-purpose event generators for LHC physics”, Phys. Rept. **504**, 145–233 (2011), arXiv:1101.2599 [hep-ph].
- [67] S. Höche, “Introduction to parton-shower event generators”, in Proceedings, Theoretical Advanced Study Institute in Elementary Particle Physics: Journeys Through the Precision Frontier: Amplitudes for Colliders (TASI 2014): Boulder, Colorado, June 2-27, 2014 (2015), pp. 235–295, arXiv:1411.4085 [hep-ph].
- [68] Z. Nagy and D. E. Soper, “Matching parton showers to NLO computations”, JHEP **10**, 024 (2005), arXiv:hep-ph/0503053 [hep-ph].
- [69] Z. Nagy and D. E. Soper, “A New parton shower algorithm: Shower evolution, matching at leading and next-to-leading order level”, in Proceedings, Ringberg Workshop on New Trends in HERA Physics 2005: Ringberg Castle, Tegernsee, Germany, October 2-7, 2005 (2006), pp. 101–123, arXiv:hep-ph/0601021 [hep-ph].
- [70] S. Schumann and F. Krauss, “A Parton shower algorithm based on Catani-Seymour dipole factorisation”, JHEP **03**, 038 (2008), arXiv:0709.1027 [hep-ph].
- [71] P. Richardson and S. Webster, “Spin Correlations in Parton Shower Simulations”, Eur. Phys. J. **C80**, 83 (2020), arXiv:1807.01955 [hep-ph].
- [72] P. Nason, “A New method for combining NLO QCD with shower Monte Carlo algorithms”, JHEP **11**, 040 (2004), arXiv:hep-ph/0409146 [hep-ph].
- [73] S. Alioli, P. Nason, C. Oleari, and E. Re, “A general framework for implementing NLO calculations in shower Monte Carlo programs: the POWHEG BOX”, JHEP **06**, 043 (2010), arXiv:1002.2581 [hep-ph].

- [74] S. Frixione and B. R. Webber, “Matching NLO QCD computations and parton shower simulations”, *JHEP* **06**, 029 (2002), arXiv:hep-ph/0204244 [hep-ph].
- [75] V. Khachatryan et al. (CMS), “Measurement of the top quark mass using proton-proton data at  $\sqrt{s} = 7$  and 8 TeV”, *Phys. Rev.* **D93**, 072004 (2016), arXiv:1509.04044 [hep-ex].
- [76] M. Aaboud et al. (ATLAS), “Measurement of the top quark mass in the  $t\bar{t} \rightarrow$  dilepton channel from  $\sqrt{s} = 8$  TeV ATLAS data”, *Phys. Lett.* **B761**, 350–371 (2016), arXiv:1606.02179 [hep-ex].
- [77] T. E. W. Group (CDF, D0), “Combination of CDF and D0 Results on the Mass of the Top Quark using up to  $9.7 \text{ fb}^{-1}$  at the Tevatron”, (2014), arXiv:1407.2682 [hep-ex].
- [78] E. Eichten and B. R. Hill, “An Effective Field Theory for the Calculation of Matrix Elements Involving Heavy Quarks”, *Phys. Lett.* **B234**, 511–516 (1990).
- [79] H. Georgi, “An Effective Field Theory for Heavy Quarks at Low-energies”, *Phys. Lett.* **B240**, 447–450 (1990).
- [80] S. Fleming, A. H. Hoang, S. Mantry, and I. W. Stewart, “Jets from massive unstable particles: Top-mass determination”, *Phys. Rev.* **D77**, 074010 (2008), arXiv:hep-ph/0703207 [hep-ph].
- [81] S. Fleming, A. H. Hoang, S. Mantry, and I. W. Stewart, “Top Jets in the Peak Region: Factorization Analysis with NLL Resummation”, *Phys. Rev.* **D77**, 114003 (2008), arXiv:0711.2079 [hep-ph].
- [82] A. H. Hoang and I. W. Stewart, “Top Mass Measurements from Jets and the Tevatron Top-Quark Mass”, *Nucl. Phys. Proc. Suppl.* **185**, 220–226 (2008), arXiv:0808.0222 [hep-ph].
- [83] A. H. Hoang, “The Top Mass: Interpretation and Theoretical Uncertainties”, in *Proceedings, 7th International Workshop on Top Quark Physics (TOP2014): Cannes, France, September 28-October 3, 2014* (2014), arXiv:1412.3649 [hep-ph].
- [84] P. Nason, “The Top Mass in Hadronic Collisions”, in *From my vast repertoire ...: guido altarelli’s legacy*, edited by A. Levy, S. Forte, and G. Ridolfi (2019), pp. 123–151, arXiv:1712.02796 [hep-ph].

- [85] G. Corcella, R. Franceschini, and D. Kim, “Fragmentation Uncertainties in Hadronic Observables for Top-quark Mass Measurements”, *Nucl. Phys.* **B929**, 485–526 (2018), arXiv:1712.05801 [hep-ph].
- [86] G. Heinrich, A. Maier, R. Nisius, J. Schlenk, M. Schulze, L. Scyboz, and J. Winter, “NLO and off-shell effects in top quark mass determinations”, *JHEP* **07**, 129 (2018), arXiv:1709.08615 [hep-ph].
- [87] S. Ferrario Ravasio, T. Ježo, P. Nason, and C. Oleari, “A theoretical study of top-mass measurements at the LHC using NLO+PS generators of increasing accuracy”, *Eur. Phys. J.* **C78**, 458 (2018), arXiv:1801.03944 [hep-ph].
- [88] M. Neubert, “Heavy quark symmetry”, *Phys. Rept.* **245**, 259–396 (1994), arXiv:hep-ph/9306320 [hep-ph].
- [89] A. V. Manohar and M. B. Wise, “Heavy quark physics”, *Camb. Monogr. Part. Phys. Nucl. Phys. Cosmol.* **10**, 1–191 (2000).
- [90] J. Kieseler, K. Lipka, and S.-O. Moch, “Calibration of the Top-Quark Monte Carlo Mass”, *Phys. Rev. Lett.* **116**, 162001 (2016), arXiv:1511.00841 [hep-ph].
- [91] M. Butenschoen, B. Dehnadi, A. H. Hoang, V. Mateu, M. Preisser, and I. W. Stewart, “Top Quark Mass Calibration for Monte Carlo Event Generators”, *Phys. Rev. Lett.* **117**, 232001 (2016), arXiv:1608.01318 [hep-ph].
- [92] A. H. Hoang, S. Mantry, A. Pathak, and I. W. Stewart, “Extracting a Short Distance Top Mass with Light Grooming”, (2017), arXiv:1708.02586 [hep-ph].
- [93] I. W. Stewart, F. J. Tackmann, and W. J. Waalewijn, “N-Jettiness: An Inclusive Event Shape to Veto Jets”, *Phys. Rev. Lett.* **105**, 092002 (2010), arXiv:1004.2489 [hep-ph].
- [94] M. Dasgupta, A. Fregoso, S. Marzani, and G. P. Salam, “Towards an understanding of jet substructure”, *JHEP* **09**, 029 (2013), arXiv:1307.0007 [hep-ph].
- [95] A. J. Larkoski, S. Marzani, G. Soyez, and J. Thaler, “Soft Drop”, *JHEP* **05**, 146 (2014), arXiv:1402.2657 [hep-ph].
- [96] S. Adomeit, “Top-quark mass measurements: Alternative techniques (LHC + Tevatron)”, in *Proceedings, 7th International Workshop on Top Quark*

- Physics (TOP2014): Cannes, France, September 28–October 3, 2014 (2014), arXiv:1411.7917 [hep-ex].
- [97] M. Vos (ATLAS, CMS), “Top-quark mass measurements at the LHC: alternative methods”, PoS **TOP2015**, 035 (2016), arXiv:1602.00428 [hep-ex].
- [98] J. H. Kim (CMS), “Alternative methods for top quark mass measurements at the CMS”, EPJ Web Conf. **141**, 08006 (2017).
- [99] T. Becher, A. Broggio, and A. Ferroglia, “Introduction to Soft-Collinear Effective Theory”, Lect. Notes Phys. **896**, pp.1–206 (2015), arXiv:1410.1892 [hep-ph].
- [100] E. Farhi, “A QCD Test for Jets”, Phys. Rev. Lett. **39**, 1587–1588 (1977).
- [101] R. Abbate, M. Fickinger, A. H. Hoang, V. Mateu, and I. W. Stewart, “Thrust at N<sup>3</sup>LL with Power Corrections and a Precision Global Fit for  $\alpha_s(m_Z)$ ”, Phys. Rev. **D83**, 074021 (2011), arXiv:1006.3080 [hep-ph].
- [102] C. F. Berger, T. Kucs, and G. F. Sterman, “Event shape / energy flow correlations”, Phys. Rev. **D68**, 014012 (2003), arXiv:hep-ph/0303051 [hep-ph].
- [103] M. D. Schwartz, “Resummation and NLO matching of event shapes with effective field theory”, Phys. Rev. **D77**, 014026 (2008), arXiv:0709.2709 [hep-ph].
- [104] T. Becher and M. D. Schwartz, “A precise determination of  $\alpha_s$  from LEP thrust data using effective field theory”, JHEP **07**, 034 (2008), arXiv:0803.0342 [hep-ph].
- [105] S. Catani, B. R. Webber, and G. Marchesini, “QCD coherent branching and semiinclusive processes at large  $x$ ”, Nucl. Phys. **B349**, 635–654 (1991).
- [106] S. Catani, L. Trentadue, G. Turnock, and B. R. Webber, “Resummation of large logarithms in  $e^+e^-$  event shape distributions”, Nucl. Phys. **B407**, 3–42 (1993).
- [107] A. H. Hoang and I. W. Stewart, “Designing gapped soft functions for jet production”, Phys. Lett. **B660**, 483–493 (2008), arXiv:0709.3519 [hep-ph].

- [108] R. Kleiss, W. J. Stirling, and S. D. Ellis, “A New Monte Carlo Treatment of Multiparticle Phase Space at High-energies”, *Comput. Phys. Commun.* **40**, 359 (1986).
- [109] S. Weinzierl, “Introduction to Monte Carlo methods”, (2000), arXiv:hep-ph/0006269 [hep-ph].
- [110] S. Catani, T. Gleisberg, F. Krauss, G. Rodrigo, and J.-C. Winter, “From loops to trees by-passing Feynman’s theorem”, *JHEP* **09**, 065 (2008), arXiv:0804.3170 [hep-ph].
- [111] I. Bierenbaum, S. Catani, P. Draggiotis, and G. Rodrigo, “A Tree-Loop Duality Relation at Two Loops and Beyond”, *JHEP* **10**, 073 (2010), arXiv:1007.0194 [hep-ph].
- [112] I. Bierenbaum, S. Buchta, P. Draggiotis, I. Malamos, and G. Rodrigo, “Tree-Loop Duality Relation beyond simple poles”, *JHEP* **03**, 025 (2013), arXiv:1211.5048 [hep-ph].
- [113] S. Buchta, G. Chachamis, P. Draggiotis, I. Malamos, and G. Rodrigo, “On the singular behaviour of scattering amplitudes in quantum field theory”, *JHEP* **11**, 014 (2014), arXiv:1405.7850 [hep-ph].
- [114] R. J. Hernandez-Pinto, G. F. R. Sborlini, and G. Rodrigo, “Towards gauge theories in four dimensions”, *JHEP* **02**, 044 (2016), arXiv:1506.04617 [hep-ph].
- [115] S. Buchta, G. Chachamis, P. Draggiotis, and G. Rodrigo, “Numerical implementation of the loop–tree duality method”, *Eur. Phys. J.* **C77**, 274 (2017), arXiv:1510.00187 [hep-ph].
- [116] G. F. R. Sborlini, F. Driencourt-Mangin, R. Hernandez-Pinto, and G. Rodrigo, “Four-dimensional unsubtraction from the loop-tree duality”, *JHEP* **08**, 160 (2016), arXiv:1604.06699 [hep-ph].
- [117] F. Driencourt-Mangin, G. Rodrigo, and G. F. R. Sborlini, “Universal dual amplitudes and asymptotic expansions for  $gg \rightarrow H$  and  $H \rightarrow \gamma\gamma$  in four dimensions”, *Eur. Phys. J.* **C78**, 231 (2018), arXiv:1702.07581 [hep-ph].
- [118] F. Driencourt-Mangin, G. Rodrigo, G. F. R. Sborlini, and W. J. Torres Bobadilla, “Universal four-dimensional representation of  $H \rightarrow \gamma\gamma$  at two loops through the Loop-Tree Duality”, *JHEP* **02**, 143 (2019), arXiv:1901.09853 [hep-ph].



- [119] R. Runkel, Z. Szőr, J. P. Vesga, and S. Weinzierl, “Causality and loop-tree duality at higher loops”, *Phys. Rev. Lett.* **122**, [Erratum: *Phys. Rev. Lett.* **123**, no. 5, 059902 (2019)], 111603 (2019), arXiv:1902.02135 [hep-ph].
- [120] J. J. Aguilera-Verdugo, F. Driencourt-Mangin, J. Plenter, S. Ramírez-Uribe, G. Rodrigo, G. F. R. Sborlini, W. J. Torres Bobadilla, and S. Tracz, “Causality, unitarity thresholds, anomalous thresholds and infrared singularities from the loop-tree duality at higher orders”, (2019), arXiv:1904.08389 [hep-ph].
- [121] R. Runkel, Z. Szőr, J. P. Vesga, and S. Weinzierl, “Integrands of loop amplitudes”, (2019), arXiv:1906.02218 [hep-ph].
- [122] Z. Capatti, V. Hirschi, D. Kermanschah, and B. Ruijl, “Loop-Tree Duality for Multiloop Numerical Integration”, *Phys. Rev. Lett.* **123**, 151602 (2019), arXiv:1906.06138 [hep-ph].
- [123] D. E. Soper, “QCD calculations by numerical integration”, *Phys. Rev. Lett.* **81**, 2638–2641 (1998), arXiv:hep-ph/9804454 [hep-ph].
- [124] D. E. Soper, “Techniques for QCD calculations by numerical integration”, *Phys. Rev.* **D62**, 014009 (2000), arXiv:hep-ph/9910292 [hep-ph].
- [125] Z. Nagy and D. E. Soper, “General subtraction method for numerical calculation of one loop QCD matrix elements”, *JHEP* **09**, 055 (2003), arXiv:hep-ph/0308127 [hep-ph].
- [126] W. Gong, Z. Nagy, and D. E. Soper, “Direct numerical integration of one-loop Feynman diagrams for N-photon amplitudes”, *Phys. Rev.* **D79**, 033005 (2009), arXiv:0812.3686 [hep-ph].
- [127] M. Assadsolimani, S. Becker, and S. Weinzierl, “A Simple formula for the infrared singular part of the integrand of one-loop QCD amplitudes”, *Phys. Rev.* **D81**, 094002 (2010), arXiv:0912.1680 [hep-ph].
- [128] M. Assadsolimani, S. Becker, C. Reuschle, and S. Weinzierl, “Infrared singularities in one-loop amplitudes”, *Nucl. Phys. Proc. Suppl.* **205-206**, 224–229 (2010), arXiv:1006.4609 [hep-ph].
- [129] S. Becker, C. Reuschle, and S. Weinzierl, “Numerical NLO QCD calculations”, *JHEP* **12**, 013 (2010), arXiv:1010.4187 [hep-ph].
- [130] S. Becker, D. Goetz, C. Reuschle, C. Schwan, and S. Weinzierl, “NLO results for five, six and seven jets in electron-positron annihilation”, *Phys. Rev. Lett.* **108**, 032005 (2012), arXiv:1111.1733 [hep-ph].

- [131] S. Becker, C. Reuschle, and S. Weinzierl, “Efficiency Improvements for the Numerical Computation of NLO Corrections”, *JHEP* **07**, 090 (2012), arXiv:1205.2096 [hep-ph].
- [132] S. Becker and S. Weinzierl, “Direct contour deformation with arbitrary masses in the loop”, *Phys. Rev.* **D86**, 074009 (2012), arXiv:1208.4088 [hep-ph].
- [133] S. Becker and S. Weinzierl, “Direct numerical integration for multi-loop integrals”, *Eur. Phys. J.* **C73**, 2321 (2013), arXiv:1211.0509 [hep-ph].
- [134] D. Götz, C. Reuschle, C. Schwan, and S. Weinzierl, “NLO corrections to Z production in association with several jets”, *PoS* **LL2014**, 009 (2014), arXiv:1407.0203 [hep-ph].
- [135] S. Seth and S. Weinzierl, “Numerical integration of subtraction terms”, *Phys. Rev.* **D93**, 114031 (2016), arXiv:1605.06646 [hep-ph].
- [136] H. Ita, “Two-loop Integrand Decomposition into Master Integrals and Surface Terms”, *Phys. Rev.* **D94**, 116015 (2016), arXiv:1510.05626 [hep-th].
- [137] S. Abreu, F. Febres Cordero, H. Ita, M. Jaquier, and B. Page, “Subleading Poles in the Numerical Unitarity Method at Two Loops”, *Phys. Rev.* **D95**, 096011 (2017), arXiv:1703.05255 [hep-ph].
- [138] S. Abreu, F. Febres Cordero, H. Ita, M. Jaquier, B. Page, and M. Zeng, “Two-Loop Four-Gluon Amplitudes from Numerical Unitarity”, *Phys. Rev. Lett.* **119**, 142001 (2017), arXiv:1703.05273 [hep-ph].
- [139] S. Abreu, F. Febres Cordero, H. Ita, B. Page, and M. Zeng, “Planar Two-Loop Five-Gluon Amplitudes from Numerical Unitarity”, *Phys. Rev.* **D97**, 116014 (2018), arXiv:1712.03946 [hep-ph].
- [140] S. Abreu, F. Febres Cordero, H. Ita, B. Page, and V. Sotnikov, “Planar Two-Loop Five-Parton Amplitudes from Numerical Unitarity”, *JHEP* **11**, 116 (2018), arXiv:1809.09067 [hep-ph].
- [141] K. G. Chetyrkin and F. V. Tkachov, “Integration by Parts: The Algorithm to Calculate beta Functions in 4 Loops”, *Nucl. Phys.* **B192**, 159–204 (1981).
- [142] M. Sogaard and Y. Zhang, “Unitarity Cuts of Integrals with Doubled Propagators”, *JHEP* **07**, 112 (2014), arXiv:1403.2463 [hep-th].

- [143] G. Passarino and M. J. G. Veltman, “One Loop Corrections for  $e^+ e^-$  Annihilation Into  $\mu^+ \mu^-$  in the Weinberg Model”, Nucl. Phys. **B160**, 151–207 (1979).
- [144] G. Dissertori, “The Determination of the Strong Coupling Constant”, Adv. Ser. Direct. High Energy Phys. **26**, 113–128 (2016), arXiv:1506.05407 [hep-ex].